Adv Polym Sci (2013) 258: 43–116
DOI: 10.1007/12_2013_220

Published online: 26 September 2013

Syndiotactic Polypropylene: Discovery, Development, and Industrialization via Bridged Metallocene Catalysts

Abbas Razavi

Abstract This chapter covers the discovery that enabled, for the first time, the manufacturing of high molecular weight, highly stereoregular syndiotactic polypropylene polymers with narrow molecular weight distribution via the new class of metallocene molecules with bridged cyclopentadienyl-fluorenyl ligands. First, the salient crystal structural features of the neutral metallocene molecules and the crystal structure of the corresponding mono-alkyl-zirconocenium cation is introduced. Then, by employing the structural and geometrical data, a realistic working model for the active site precursor is developed and presented. The stereochemistry of the catalytic propylene poly-insertion reaction and the formation of syndiotactic polypropylene according to the enantiomorphic site control mechanism at the enantiotopic cationic active sites, formed after the activation of the prochiral metallocene dichloride with methylaluminoxane, MAO, is reviewed and further delineated. In the following sections, the impact of the introduction of substituents with proper size and composition at some selected positions of the ligand is discussed and the methods for increasing the molecular weight and stereoregularity of syndiotactic polypropylene polymers are elaborated. With the aid of computational calculations on real and hypothetical catalyst systems with substitutionally altered ligand structures, it is shown that the degree of enantioselectivity of syndiospecific catalyst systems can be determined and/or predicted for these systems quantitatively and with high precision. The calculations confirm that the introduction of substituent(s) reinforcing the preferential conformational orientation of the polymer chain enhances the overall enantioselectivity of the active site, and to certain extends stereoselectivity in general, by affecting the site epimerization processes. The computational calculations reveal that to account correctly for the frequency of the site epimerization-dependent m-type stereo-errors it is essential to include the counter-ion, as an integrated part of the

A. Razavi (✉)
35 Domaine de la Brisee, 7034 Obourg, Belgium
e-mail: abbasrazavi@skynet.be

catalyst system, into the calculations. The relevance of the symmetry and stereorigidity of the metallocene structure for the syndiospecificity of the final catalyst is debated by presenting a few "non-conforming" catalyst examples.

Finally, the challenges involved in the manufacture of syndiotactic polypropylene in commercial scale continuous production processes are highlighted as well as the polymer's unique structural, physical, mechanical and rheological properties.

Keywords Counter-anion effects · C_s symmetric zirconocene catalyst · Enantioselectivity · Enantiomeric mis-insertion · Heterogenization · Site epimerization · Syndiotactic polypropylene

Contents

1 Introduction

Syndiotactic polypropylene was first isolated by Natta and coworkers as a minor by-product of an isotactic polypropylene (i-PP) produced with a $TiCl_3$-based Ziegler–Natta (ZN) catalyst, $TiCl_3/Et_2AlCl$ [1–9]. The nature of the active sites and the mechanism of formation of this polymer (discovered more than half a century ago) are not very well known and still a matter of much debate. It is, however, believed that they are formed on catalytic sites with C_2 symmetry and of low chlorine coordination (Fig. 1) via a chain-end controlled mechanism. Later, Zambelli and coworkers produced syndiotactic polypropylene (s-PP) directly, at subzero polymerization temperatures, using a vanadium-based catalyst. In this case, more is known about the nature of the active site (Fig. 1) and the mechanism of the polymerization has been elucidated satisfactorily [10–17]. It is assumed that the polymer chains are formed at low temperatures at the homogeneous active sites according to a mechanism that is controlled by the chirality of the last inserted monomer unit located at the metal-end of the growing polymer chain. No single-crystal X-ray structure of the catalyst precursor is available due to the very temperature-sensitive nature of the catalytic species and its precursor.

After discovery of the bridged cyclopentadienyl-fluorenyl metallocene-based syndiotactic-specific catalyst systems and the resulting s-PP polymers [18–27] it was possible for the first time to make ever more accurate statements about the nature of the syndiospecific active site and the mechanism of the polymerization of these fascinating yet very complex systems. By studying the available X-ray structural data of the metallocene molecules and their stabilized alkylmetallocenium cation [19–21] (as the immediate active site precursor), it has become possible to make reasonable deductions on the nature of the active sites and their mode of functioning during the different stages of the polymerization, i.e., monomer coordination, activation, insertion, and propagation. On the other hand, the facile availability of large syndiotactic polymer samples, prepared at different and precise polymerization temperatures/conditions, and statistical analysis of the data extracted from their high-resolution ^{13}C NMR spectra, provided the means for accurate statements on the mechanism of the polymerization and the relationship between catalyst structure and polymer microstructure. The bridged cyclopentadienyl-fluorenyl ligand-based metallocene structure proved to be a very versatile precatalyst system. Depending on the substitutional modifications performed on different parts of the organic ligand, the bridge,

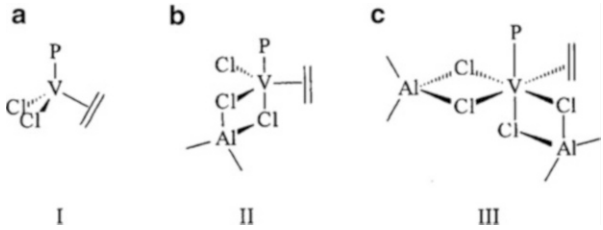

Fig. 1 (**a**–**c**) Zambelli's models (*I*–*III*) for hypothetical active sites in VCl_4-based catalysts

fluorenyl, and/or cylopentadienyl moieties it is possible to create new catalysts systems that can produce s-PP polymers with increased molecular weights, stereoregularities, and melting points. The ligand modifications can bring about, in certain cases, even a change in the tactic behavior of the resulting catalysts, leading to the development of a whole range of new polypropylene macromolecules whose chain tacticities include hemi-isotactic and stereoblock in addition to syndiotactic and isotactic [28–34].

2 Bridged Cyclopentadienyl-Fluorenyl Metallocene Molecules

In late 1987, a simple coupling reaction between the reagent 6,6-dimethylfuvene and the fluorenyl anion in tetrahydrofuran (THF) led to the formation of 2-cyclopentadienyl-2-fluorenyl-propane, a new bi-functional ligand whose double deprotonation with an alkyl lithium, and subsequent reaction with MCl_4 (M = Zr, Hf) resulted in the successful synthesis of two bridged metallocene molecules, (η^5-C_5H_4-μ-CMe_2-η^5-$C_{13}H_8$) MCl_2, where M = Zr (**1**) or M = Hf (**2**). Complexes **1** and **2**, after their activation with methylaluminoxane (MAO), become very active catalysts for olefin polymerization. More importantly, they promote the catalytic polymerization of propylene to highly syndiotactic polypropylene. Complexes **1** and **2** have been characterized by single-crystal X-ray diffraction methods and NMR spectroscopy [19, 20]. Figure 2 presents two different perspective views of the molecular structures of **1** and **2** as determined by single-crystal X-ray diffraction. The structural characteristics of these two complexes were discussed at length soon after their discovery in a series of publications [18–27, 28–34]. However, some of the prominent structural features that are relevant to their catalytic performance with respect to stereoselective propylene polymerization are reiterated here with an emphasis on the zirconium-based complex **1** as an example.

The fact that the metallocene complexes **1** and **2** are active for olefin polymerization was, of course, of no surprise; Kaminsky and Sinn had discovered in the mid-1970s that MAO obtained from partial hydrolysis of tri-methylaluminum (TMA) could activate metallocene dichloride complexes to very efficient olefin

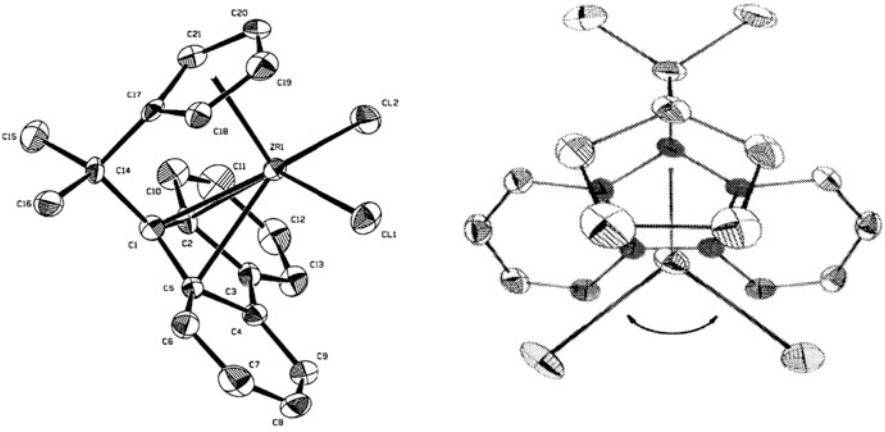

Fig. 2 Side (*left*) and top (*right*) views of the molecular structure of **(η^5-C_5H_4-μ-CMe_2-η^5-$C_{13}H_8$)MCl_2**; M = Zr (**1**), M = Hf (**2**)

polymerization catalysts [35–42]. The rationalization of the activation processes of the metallocene complexes with MAO and the mechanistic aspects of the their olefin polymerization (such as monomer coordination, activation, insertion, propagation, and possible pathways for chain termination) were in many ways identical or very similar, except for minor details, to catalyst systems that were discovered by Ziegler and Natta in 1953. Also, the fact that homotopic metallocene/MAO catalysts polymerize propylene to stereoregular crystalline polypropylene was already known. In the mid-1980s, after the discovery of the bridged chiral *ansa*-bis-indenyl metallocene complexes [43–45], it was shown, in a series of polymerization tests, that MAO activation of C_2 symmetric chirotopic bis-indenyl-based metallocene complexes very efficiently promotes the isospecific polymerization of propylene to highly stereoregular i-PP [46–55]. In this case, the rationalization for the nature and behavior of catalytically active species and the formation of i-PP was again very similar to the activation processes and mechanistic routes that had been proposed, and generally accepted, for stereospecific polymerization of propylene with heterogeneous ZN catalyst systems [56–63]. The polymerization mechanism involving the face-selective coordination of propylene, its activation, insertion, and stereoselective propagation at a C_2 symmetric active metal center could satisfactorily explain the formation of i-PP with these metallocene-based catalysts according to the same mechanism, and in a similar way, as proposed much earlier for the heterogeneous titanium trichloride-based ZN catalyst systems. With the exception of some minor differences, the enantio- and stereoselectivity as well as regioselectivity of the poly-insertion reaction and chain termination path ways were very similar to those processes that had been proposed for heterogeneous ZN catalysts [64–76].

What was unprecedented in the polymerization behavior of the newly discovered catalyst systems, however, was the fact that an initially nonchiral metallocene

(prochiral!) molecule, after activation with MAO, could provide an enantiotopically chiral catalyst that could produce a crystalline polypropylene with syndiotactic chain architecture according to a new mechanism that follows, in a rhythmic alternation, the *si*/*re* prochiral face-selective coordination and insertion of propylene molecules at its two available enantiotopic coordination positions.

To understand the functioning mode of this catalyst system and the mechanistic aspects of the stereochemical events involved in the formation of s-PP chains, it is very important to first examine more closely the molecular structure and structural characteristics of the complex **1** (and/or **2**). The structural data can be then correlated to the information gleaned from different polymer analyses in order to determine the polymerization mechanism and the elementary steps involved in the formation of s-PP chains on the basis of the well-established principle of catalyst structure–polypropylene chain microstructure interrelationship.

2.1 *Molecular Structure of Isopropylidene(cyclopentadienyl-fluorenyl)MCl_2 (M = Zr, Hf): Bonding and Symmetry*

Two different views of the molecular structures of the metallocene complexes isopropylidene(cyclopentadienyl-fluorenyl)MCl_2, where M = Zr (**1**) or Hf (**2**), are depicted in Fig. 2. As evident from the molecular views presented in Fig. 2, the stereorigid metallocene molecule **1** (and **2**) possess, in the solid state, a bilateral symmetry (or a plane of symmetry, σ_v). Consequently, the left and right halves of the molecule, if bisected by the imaginary symmetry plane, would be mirror image related. Apart from this global observation, detailed examination of the structural data, particularly those concerning the Zr–C and C–C bond distances, reveals the following facts. Despite the presence of a relatively short bridge (basically a carbon atom) as the inter-annular tie between the two aromatic ring systems (the cyclopentadienyl and fluorenyl centroids), the bonding relationship of these rings to the zirconium metal is very strong and of a η^5 nature. The thermal stability of **1** (and **2**) also favors the notion of a doubly η^5-bonded centroid–M–centroid molecular structure. The observed variation in the bond distances with a progressive increase in the $Zr–C_{flu}$ bond distances from the bridge-head carbon to the proximal carbons, extending to the distal carbons, is believed to be caused by the nonbonding repulsive steric interaction between the two σ-bonded chloride ligands and the distal C–H groups of the two six-membered rings of the fluorenyl section [19]. Similar reasoning applies to the $Zr–C_{cp}$ bond distance variation due to different carbon atoms in the cyclopentadienyl moiety. The Zr–C bond distance lengthening, on average about 0.2 Å, due to nonbonded contact and repulsive interaction between the σ-ligands and the distal C–H groups of both aromatic systems is of prime importance for the stereoselectivity and the degree of enantioselectivity of the resulting catalysts (Sect. 2.4). The distal parts of cyclopentadienyl and fluorenyl moieties of the ligand are positioned exactly above and below the two

chloride groups, occupying the prospective coordination sites designated for future monomer coordination and polymer chain growth. By interacting with their substituents, they regulate and direct the orientation of the growing polymer chain, determine the *re* or *si* selective coordination of propylene, and govern the whole scenery of the stereospecific polymerization process.

For future discussions, it is also important to know that the fluorenyl–Zr–cyclopentadienyl bond angle in the zirconium complex **1** is 118.6° (119.4° for hafnium complex **2**) and deviates by about 10° from the ideal tetrahedral angle of 109.5° (tetrahedral formed around the bridging carbon and the bonds with its four substituents, two methyl groups plus fluorenyl and cyclopentadienyl groups) and a Cl–Zr–Cl bond angle of 98.2° (Cl–Hf–Cl = 97.5°).

2.2 *Crystal Structure of the Metallocenium–Monoalkyl Cation and the Structure of the Putative Active Site*

Before the discovery of the metallocene-based syndiospecific catalyst system there existed, thanks to intensive investigations by several research groups worldwide, sufficient evidence to assume that the active species involved in metallocene-based olefin polymerization catalysis are cationic in nature [77–96]. It is now widely accepted that the active site species are cationic metallocenium–monoalkyl complexes. They are formed generally during the activation step(s) when the catalyst precursor, the metallocene dichloride, is treated with the alkyl-aluminum co-catalysts/activators in a "two-step" alkylation and alkyl abstraction reaction (in reality the alkylation process comprises a rather complex multi-step halide/alkyl exchange with reversible and nonreversible reactions and side reactions leading to the final cationic species and some unspecified nonreactive or dormant species. See also [97] and the quoted references). Therefore it is reasonable to assume that similar cationic species are being formed during the activation stages of **1** (and **2**)/MAO catalyst systems with MAO or other alkylating, ionizing agents.

It was recognized that for mechanistic elucidation of the elementary steps involved in stereospecific propylene polymerization catalysis with **1** (and **2**)/MAO, access to the molecular structure of the corresponding zirconocenium–methyl cation of complex **1** would be very useful. Its molecular structure and X-ray determined interatomic parameters could help to design a practical and realistic model for the hypothetical active site at which the actual syndiospecific polymerization of propylene is actually taking place. The geometrical data for the cationic complex allow better visualization and insight into the immediate stereo-electronic environment of the hypothetical active site, and elaboration of its functioning.

The metallocenium complex **3**, $[(\eta^5\text{-}C_5H_4\text{-}\mu\text{-}CMe_2\text{-}\eta^5\text{-}C_{13}H_8)Zr^+Me][B(C_6F_5)_4]^-$, is prepared via the double methylation of complex **1** and the subsequent reaction of the di-methylated reaction product with an equivalent of the reagent trityl-tetrakis-pentaflurophenylborate, $(C_6H_5)_3C\text{-}B(C_6F_5)_4$, in toluene at room temperature.

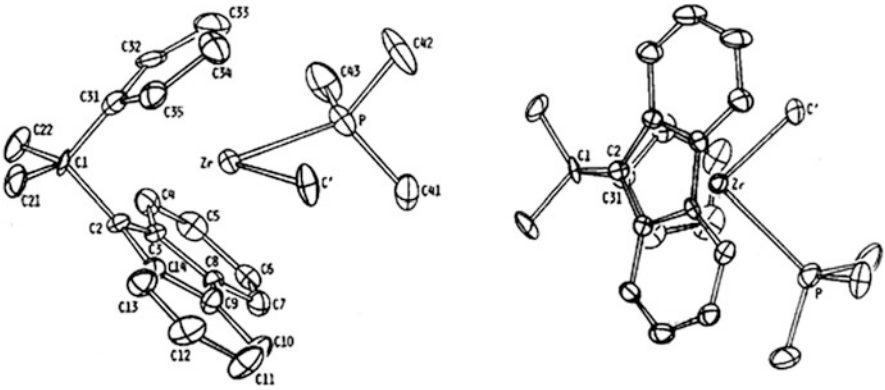

Fig. 3 Two different views of the molecular structure of $[(\eta^5\text{-}C_5H_4\text{-}\mu\text{-}CMe_2\text{-}\eta^5\text{-}C_{13}H_8)Zr^+Me(PMe)_3][^-B(C_6F_5)_4]$ as determined by X-ray single-crystal analysis. The anion is omitted for the sake of clarity

As expected, complex **3** is very active for catalytic polymerization of propylene to s-PP, and the microstructures and molecular weights of the s-PP polymers it produces are very close to the properties of syndiotactic polymers obtained with the complex **1**/MAO catalyst system, prepared under the same polymerization condition. All attempts to isolate the polymerization active cationic reaction intermediate, $[(\eta^5\text{-}C_5H_4\text{-}\mu\text{-}CMe_2\text{-}\eta^5\text{-}C_{13}H_8)Zr^+Me][B(C_6F_5)_4]$, in crystalline form for X-ray structure determination failed. However, it could be isolated, in its stabilized form, after the addition of one equivalent of the reagent tri-methyl-phosphine, PMe_3, to a solution of the catalytically active complex **3** in toluene. The resulting dark purple reaction product, complex **4**, $[(\eta^5\text{-}C_5H_4\text{-}\mu\text{-}CMe_2\text{-}\eta^5\text{-}C_{13}H_8)Zr^+Me(PMe_3)][^-B(C_6F_5)_4]$ could be crystallized out of the solution and was isolated in pure form and identified by its ^1H NMR spectrum and single-crystal X-ray structure determination [21] (see Fig. 3).

The general feature of the crystal structure of complex **4** is very similar to that of the X-ray structure of complex **1** (or **2**). The centroid–Zr–centroid bonds are η^5 in nature and, as for similar metallocene having a $C_5H_4CR_2C_{13}H_8$ ligand, the least squares planes defined by the two C_5 fragments in **4** are inclined towards the zirconium atom with respect to the C1–C2 and C1–C31 vectors (see Fig. 3 left). The effect is more pronounced for the cyclopentadienyl ring than for the fluorenyl group, with inclination angles of 15.5° and 11.8°, respectively. A noteworthy feature of this structure is the unusually small Me–Zr–PMe_3 angle of 88.4°. An α-agostic Zr–H–C interaction (vide infra) could be responsible for this phenomenon by forcing the Zr–C bond to move closer to the Zr–P bond. However, we have no experimental evidence for this, except the fact that the H–Zr distance for one of the three methyl hydrides seems to be spatially shorter than the other two H–Zr distances [21].

Table 1 Polymerization conditions and results with (**1** and **2**)/MAO

Metal	Temperature (°C)	Activity (kg/g)	M_w (×1,000)	rrrr (%)
Zr	60	180	90	82
Zr	40	120	138	86
Hf	60	2.7	778	73
Hf	40	0.2	1,322	64

Polymerization conditions: 1 L liquid propylene; 5 mL MAO (11 wt% in toluene); 60 min

Table 2 Presentation of the relevant ^{13}C NMR normalized spectroscopic stereo-sequence distributions (%) for syndiotactic polypropylene samples produced with (**1** and **2**)/MAO at different temperatures

Metal	Temperature (°C)	rrrr (%)	rrmr (%)	rmmr (%)	mmmm (%)
Zr	60	82	2.70	1.65	0
Zr	40	86	1.15	1.55	0
Hf	60	73	7.20	3.80	0.5
Hf	40	64	10.50	3.50	1.8

2.3 *Polymerization Behavior of 1/MAO and 2/MAO Catalyst Systems*

As mentioned above, the activation of the metallocene dichlorides **1** and **2** with MAO provides very efficient catalysts for polymerization of propylene to high molecular weight, highly crystalline s-PP polymers. Detailed propylene polymerization conditions, results, and polymer analysis with **1** and **2**/MAO catalyst systems are presented in Tables 1 and 2. Inspection of the data presented in Table 1 reveals, aside from the fact that all the produced polypropylene polymer samples are syndiotactic in nature (apparent from the large rrrr pentads), other important information.

The molecular weights (M_w) of s-PP polymers produced with **2**/MAO are much higher than those of the corresponding polymers produced with **1**/MAO, and the molecular weights of all the s-PP polymers produced with either one of the two catalysts systems decrease with increasing polymerization temperature. On the other hand, the polymers produced with **1**/MAO are much more stereoregular than the corresponding polymers produced with **2**/MAO. And, finally, for both (**1** and **2**)/MAO catalyst systems, the catalysts' stereoselectivity decreases with increasing polymerization temperature. The methyl region of the ^{13}C NMR spectra of the s-PP polymers produced with (**1** and **2**)/MAO at 60°C are depicted in Fig. 4. On the left hand side of the figure is shown the ^{13}C NMR spectrum of the s-PP produced with the Zr-based catalyst and on the right hand side of Fig. 4 is the ^{13}C NMR spectrum corresponding to the s-PP produced with Hf-based catalyst. The ^{13}C NMR spectra reveal that the basic architectures of the two sets of polymers are basically the same (steric pentads, chemical shifts) [19]. It can be seen pictorially from these spectra that the polymer produced with (**1** and **2**)/MAO catalysts systems are highly syndiotactic, as evident from the predominant rrrr pentads signals with the chemical shift at 20.15 ppm. They represent long uninterrupted syndiotactic sequences of *racemic*

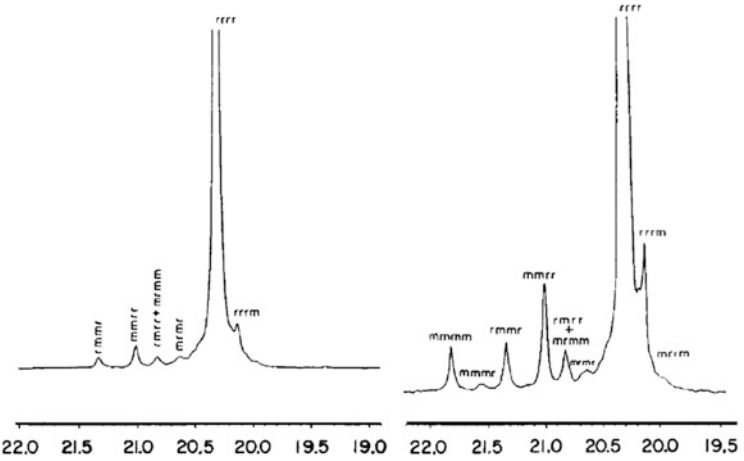

Fig. 4 The methyl region of ^{13}C NMR spectra of syndiotactic polypropylene produced with Zr- (*left*) and Hf-based (*right*) metallocene catalysts. The chemical shift scale is recorded in ppm downfield from tetramethylsilane signal with a 300 MHz spectrometer

dyads, r, in the backbone of the individual polymer chains. The ^{13}C NMR spectra also reveal the appearance of other small signals characteristic for stereodefects in the backbone syndiotactic polymer chains due to occasional errors made by the catalyst during the propylene enchainment process. The s-PP polymers produced with Zr-based catalyst have all the basic finger print microstructure . . .rrrrrrrrmmrrrrrrrmrrrrrrr. . .. The mm and m units seen in the backbone of the chain are the so-called isotactic *meso* triad and isotactic *meso* dyad characteristic stereo-defects ubiquitous in all s-PP chains produced with enantiotopic metallocene catalysts. The corresponding, less stereoregular, Hf-based s-PP polymer's microstructure . . .rrrrrrmmrrrrrrmrrrrmmmmrrr. . . exhibits, in addition to the two mentioned mm and m stereodefects, about 1.8% of short sequences of isotactic pentads, mmmm, centered at 21.65 ppm of the ^{13}C NMR spectrum (see Fig. 4, right spectrum, and Table 2). Table 2 presents the microtacticity variations in the s-PP chains occurring with the changes in polymerization temperature. As the stereoselectivity decreases with increasing polymerization temperature, so does the rrrr pentad concentration, due to the simultaneous increase in stereodefects in the related pentads, rmmr and rrmr. However, whereas the increase in rmmr stereodefect related pentads is very moderate to negligible, the rrmr stereo-defect related pentads increase much faster with increasing polymerization temperature for s-PPs produced with both catalyst systems. For polymers produced with the Zr-based **1**/MAO catalyst system they more than double for every 20°C increase in the polymerization temperature.

In spite of their almost identical structures [19], catalyst systems prepared with complexes **1**/MAO and **2**/MAO, show substantial differences in their catalytic behavior and polymerization performance. The mechanism of propylene polymerization with (**1** and **2**)/MAO catalyst systems will be discussed further in some length. For now, it should be just mentioned that since the polymerization proceeds

in both cases according to the same basic mechanism and they both produce similar s-PP chains, it could be reasonably assumed that the even the isotactic stereodefects (mmmm) in the backbone of polymer chains formed with (**1** and **2**)/MAO catalyst systems are also generated following the same basic mechanism, operating only with slightly less efficiency in the case of **2**/MAO. As for the substantial differences related to the activities of the two catalysts and molecular weights of their polymers, different kinetic behavior for **1**/MAO and **2**/MAO catalyst systems is suspected.

2.4 Mechanism of Syndiospecific Polymerization

In order to describe correctly the mechanism of the syndiospecific polymerization with (**1** and **2**)/MAO catalyst systems, as mentioned before, access to a realistic model representing the active site is of utmost importance. The information extracted from the molecular structures of complexes **1** and **4** provides all necessary elements required to construct such a "realistic" active site model. From the discussion in Sects. 2.1 and 2.2, it can be reasonably assumed that the structure of the actual active centers, at least during the π-complex formation, are very similar and close to the structures of complex **4** depicted in Fig. 3. All is needed is to imagine the PMe_3 molecule as removed and replaced by a propylene molecule. In this form, it can be used to describe the different stereochemical events, step by step, during different stages of polymerization, activation, monomer selection/coordination, monomer insertion, chain propagation and chain termination responsible for the formation of s-PP with the microstructure ...rrrrrrmmrrrrmrrr... with complex **1**/MAO:

1. The stereorigid bridged metallocene dichloride **1**, as depicted in Fig. 2, is a prochiral molecule and possesses bilateral symmetry. The activation of metallocene dichloride **1** leads to the formation of enantiomeric metallocenium–monoalkyl cationic species that are both electron-deficient and coordinatively unsaturated and structurally very similar to the enantiomeric molecule depicted in Fig. 3. These enantiomeric metallocenium–monoalkyl species have the necessary vacant coordination position and energetically low lying, accessible empty fragment orbitals to be used for coordination and activation of incoming propylene molecules via interaction with their available π orbitals.
2. The cationic metallocenium–monoalkyl species [21] are composed of equal numbers of *R* and *S* mirror-image related enantiomers and have monomer *re*/*si* π-face selective properties (Fig. 5).
3. The *re* or *si* face-selectivity is induced by the unique steric arrangement of the chelating ancillary ligand engulfing the resident chiral transition metal center via a delicately balanced, cooperative and nonbonded steric interactions between different parts of the "active" catalytic species, ligand, polymer chain, and coordinating monomer. The nonbonded steric interactions govern the whole scenery of the syndiospecific polymerization process during all its individual steps.

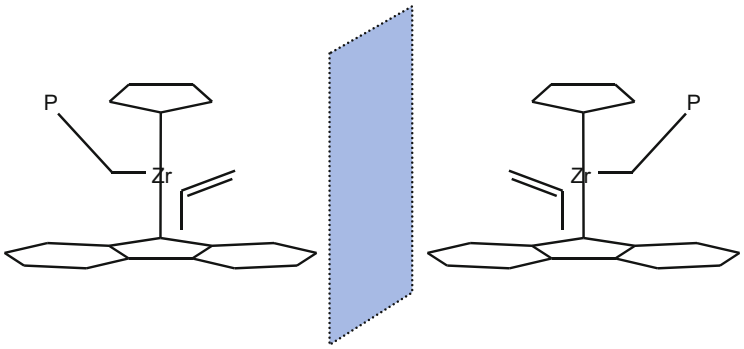

Fig. 5 The hypothetical *re*/*si* propylene face-selective *R* and *S* enantiomeric active species formed after activation of the metallocene molecule

4. Since according to this mechanism each enantiomer *R* or *S*, independently, would produce isotactic chains, and yet exclusively syndiotactic polymer chains are formed, it has to be concluded that the active enantiomeric species "enantiomerize" via an intramolecular mechanism and interconvert individually after each monomer insertion.
5. The systematic transformation of the *R* and *S* antipodes into one another implies that the relative positions of at least two of the four ligands or ligand moieties surrounding the transition metal center must be changed systematically.
6. Since the η^5-bonded aromatic ligands are tied together by a structural bridge and their rearrangement is impossible and excluded, such a reversible interconversion can take place only when the alkyl group (polymer chain) and the coordinating monomer exchange their positions uninterruptedly and systematically after each insertion; i.e., chain migratory insertion! [64–76].
7. The *meso* triad-based, enantiomorphic site control type of stereochemical errors, mm, are formed whenever the said balanced nonbonded steric interaction is perturbed, and the correct alignment of the substituents of the three main participants (ligand, polymer chain and monomer) is not materialized perfectly. In such a case, a monomer with "wrong face" is inserted and a unit with inverted configuration is enchained. The ability of occasional reverse face selectivity emanates from the inherent structural factors of the metallocene-based catalyst. It is independent of monomer concentration and counter-ion pairing nature; however, it is dependent on polymerization temperature.
8. The *meso* dyad-based stereo-errors, m, arise from occasional back migration of the polymer chain before the insertion of the next monomer unit. As a consequence of this active site epimerization (see Fig. 6), a double monomer insertion at the same enantiotopic coordination site will takes place and units of two monomers with identical stereogenic centers (m) are enchained (vide infra).

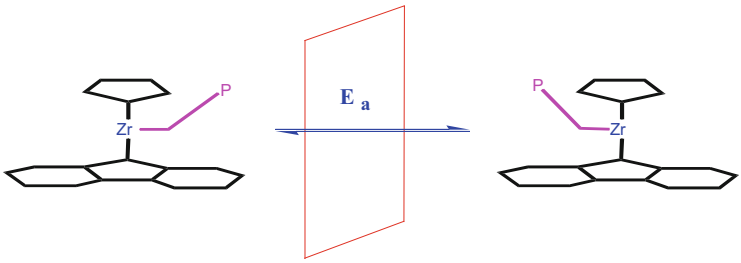

Fig. 6 Representation of the endothermic active site epimerization (chain migration without insertion) process. E_a activation energy

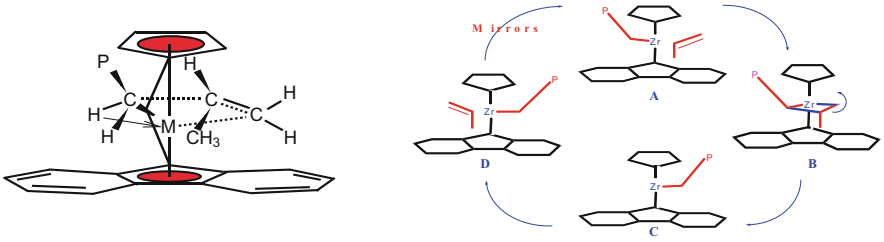

Fig. 7 The syndiospecific transition state structure (*left*). Representation of the syndio-insertion catalytic cycle (*right*); the bridge is omitted for the sake of clarity. (*A*) Large substituted cyclopentadienyl group, the fluorenyl group, and a smaller unsubstituted cyclopentadienyl group are tied together by an isopropylidene bridge. (*B*) Steric interaction with the fluorenyl ligand forces the growing polymer chain to orientate towards the free space left or right of the unsubstituted cyclopentadienyl moiety. (*C*) Trioordinated polymeryl-Zironocenium cation. (*D*) Incoming monomer orients itself with its methyl group *trans* to the growing polymer chain

2.5 *Syndiospecific Transition State Structure and Syndio-Insertion Catalytic Cycle*

To delineate how these many factors operate in a concerted manner to provide the necessary and sufficient conditions for the syndiospecificity of the catalytic site created with complex **1**, we can now employ the constructed molecular model to devise a transition state structure that explains in a plausible manner the behavior of this very complex system and the important steps involved in the catalytic cycles.

Figure 7 (left) represents the hypothetical active site transition state structure for syndiospecific polymerization of propylene to polypropylene. The model is constructed on the basis of data obtained from the X-ray structure of complex **1** and **4**; it is further refined to include an α-agostic bond between the transition metal and the alky group, representing the growing polymer chain, and a coordinated propylene monomer. On the right-hand side of Fig. 7 a syndioselective insertion cycle is shown involving the cationic active site and a migratory inserting polymer chain. The hypothetical transition state geometry reveals the relative importance of

the nonbonded steric interactions operating on different parts of the catalytic species and on the polymerization active participants, the aromatic ligand, the polymer chain, and the coordinating monomer in the following order. The organic ligand consists of a large substituted cyclopentadienyl group, the fluorenyl group, and a smaller, sterically less challenging, unsubstituted cyclopentadienyl group tied together with an isopropylidene bridge. The steric interaction between the flat and spatially extended fluorenyl ligand forces the growing polymer chain, during the polymerization, to adopt the conformation that permits its orientation towards the free space left (or right) of the unsubstituted cyclopentadienyl moiety of the ligand. The incoming monomer in turn (to avoid an excessive repulsive steric exposure) orients itself in a manner such that its methyl group is "trans" positioned with respect to the growing polymer chain (alkyl group).

The system thus reaches its minimum energy during the formation of the metalacyclobutane transition state. In this coordination mode, the coordinated monomer points with its methyl group head-down into the empty space in the central region of the fluorenyl ligand with little or no direct interaction with the ligand. The importance of the "head-down" orientation of the monomer with respect to the "upward" orientation of the chain during the π-complex formation and transition state was recognized and proposed early on after extensive molecular mechanics and force field calculations performed by Corradini and coworkers [64, 69, 71, 73–75]. The model underwent later additional refinement and took its current form after experiments conducted by several research groups supported the idea of the formation of an α-hydride agostic Zr bond assisting and stabilizing the chain conformation orientation in the metalacyclobutane transition state geometry, before the actual propylene insertion [98–106]. It implies that the insertion transition state relies on the formation of an α-agostic bond between either one of the two available hydrides on the last carbon (α-C) of the growing polymer chain and the transition metal center. This agnostic interaction provokes the rotation of the highly directional sp^3 orbital of the α carbon towards the π orbital of the 1,2-coordinated propylene monomer, allowing for larger orbital overlapping and contributing to the stabilization of the insertion transition state and thus affecting profoundly the stereochemistry of insertion; selection of one or the other α-hydride for agostic interaction could bring the growing polymer chain either into the congested quadrant of the ancillary ligand or its free quadrant left or right of the cyclopentadienyl group [99].

After insertion of the first monomer, the alkyl group (polymer chain), now enlarged by one monomer, is moved to the coordination side that has become vacant after the monomer insertion and is replaced itself by a new incoming propylene monomer presenting a different face. Thus, another cycle begins with another monomer face at the other enantiotopic coordination site (see Fig. 7, right). The systematic and repetitious cycles would then lead to the formation of polypropylene chains with alternatively inverted stereogenic centers. The systematic transformation of the two *S* and *R* enantiomorphic antipodes into one another, after each olefin insertion, ensures that the relative positions of the σ-and π-bonded ligands in the equatorial plane of the transition metal are exchanged and that monomers with

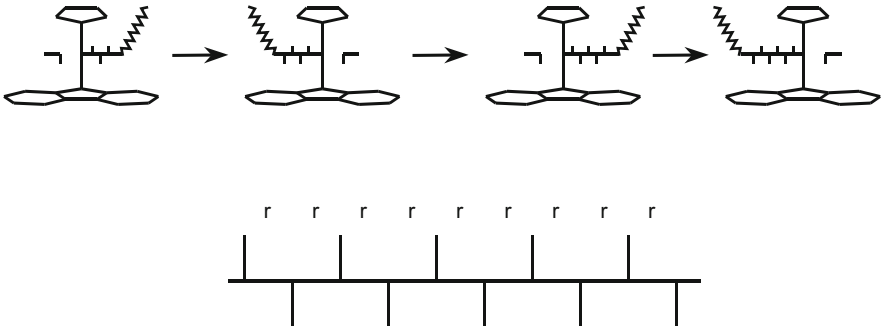

Fig. 8 Representation of mechanism of syndiospecific polymerization and formation of syndiotactic polypropylene (*top*). Fischer projection of a perfect syndiotactic chain sequence (*bottom*)

alternative faces are coordinated and inserted, resulting in the formation of sequences of monomer units with alternating relative configuration, i.e., formation of syndiotactic chains (Fig. 8).

The description involving an enantiotopic, cationic active species combined with the chain migratory insertion mechanism is perfectly fit to explain the formation of s-PP polymers. According to the scheme shown in Fig. 8, reproducing several catalytic cycles, the regularly alternating enantio-facial preference for the *re* and *si* prochiral faces of the monomer arises from the propylene insertion taking place at regularly alternating sides (enantiotopic coordination site) of the pseudo-tetrahedral geometry of the active site.

The working hypothesis, active site model, and the transition state structure discussed in the preceding paragraphs not only account for the syndiospecificity of the catalysts and formation of the s-PP chain but they also warrant the formation of microstructural chain defects or stereo-errors due to monomer misplacements in the backbone of the syndiotactic polymer chains, as shown pictorially in Fig. 9.

From the two types of stereo-errors, the *meso* triads (mm) and *meso* dyads (m), encountered in the backbone microstructure of the syndiotactic polymer chains, the formation mechanism of the so-called enantiomorphic site control type errors (mm) is straightforward and well understood. They could be produced at the step A (or D) in the cycle shown in Fig. 7 whenever the chain/monomer arrangement is not in *trans* mode configuration, and either the growing polymer chain or the propylene is mis-oriented with respect to the ligand and to each other (Fig. 9, top). These types of stereo-errors have been detected and were explained in connection with isotactic polymers prepared with the classical $TiCl_3$-based ZN catalyst systems [56–63, 64–76]. They are also ubiquitous in the backbone of the i-PP formed with isotactic-specific metallocene catalysts. Formation of the *meso* dyad (m) stereo-errors, unique to s-PP chains, are related to the epimerization of the active center and can take place in step C of the catalytic cycle (see Figs. 7 and 9) whenever the polymer chain migrates, without inserting a propylene monomer, to the other coordination position of the active site before arrival of the next propylene

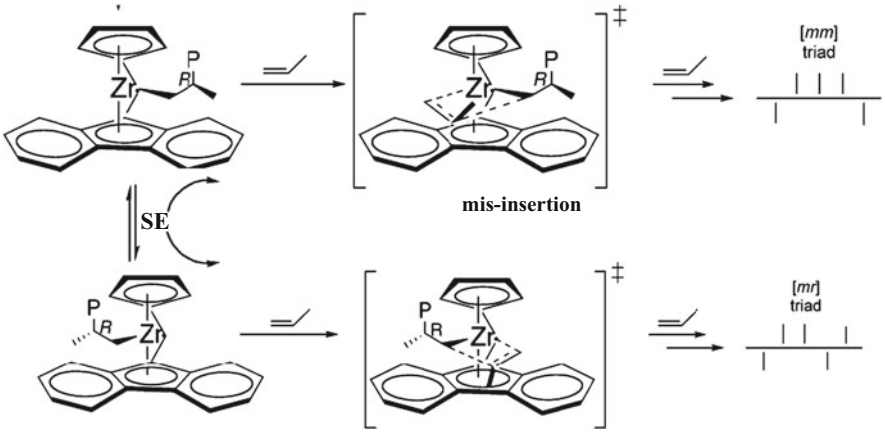

Fig. 9 Mechanisms of the enantiofacial mis-insertion and of the site epimerization (SE), and their corresponding signature pentad distributions

monomer. Their formation will be discussed in some detail later. The mechanism of the enantio-facial mis-insertion and site epimerization are presented more explicitly in Fig. 9 (bottom).

To summarize the above points, it can be generally stated that in order to form highly syndiotactic polypropylene chains with **1**/MAO or any other enantiotopic metallocene-based catalyst system, it is required that the chain assumes a dual responsibility. Whereas its "static" or steric interactions with the ligand and the monomer substituents are crucial for the degree of enantioselectivity, its dynamic behavior of regular and systematic, back and forth, migrations determine the frequency of site epimerization and the overall stereoselectivity. A "malfunctioning" of the latter leads to an increasing amount of m-type stereodefects and, in extreme cases, could even lead to a reversal of stereospecificity, from syndio- to isospecificity [28–34]. Whenever the chain plays both roles efficiently, the inherently enantiotopic catalyst produces s-PP with high stereoregularity. Its dysfunctioning in fulfilling one of these two roles can cause a lowering in the degree of enantio- or stereospecificity, leading to lower stereoregularity of the resulting s-PP.

3 Structural Modifications to Enhance the Syndiospecific Catalytic Performance

The s-PP samples produced with **1**/MAO catalyst system all have long enough chain lengths and high enough stereoregularities and melting points to provide polymeric materials with crystallinities and mechanical properties sufficient for general purpose applications. However, to enlarge the field of s-PP polymer resin applications for broader usage, it is necessary to further widen the range of melting points and molecular weights of the industrially produced s-PP polymers.

In order to increase the melting point of the semicrystalline s-PP polymers, it is necessary to increase the stereoregularity of the individual polymer chains. This in turn requires the suppression of the concentration of both types of stereodefects (m and mm) in the backbone of the polymer chains, whose combined numbers determine the crystallinity, melting point, and most of the physical properties, such as crystallization rate, optics, etc.

In the following sections, a few examples are presented as case studies to show how these substitutional modifications are realized and in what way they bring about the desired improvements. The discussion starts with the topic of modification of the bridge and bridge substituents to increase the syndiotactic polymer's molecular weight. We continues with the subject of structural modifications for improving the stereoselectivity of the catalyst and the stereoregularity of the resulting s-PP.

Before entering the discussions, it should be noted from the onset that there exist only limited options for substitutional modifications with the aim of increasing molecular weight and/or improving the enantioselectivity of the **1**/MAO catalyst system without tampering with its salient syndiospecific characteristics. Therefore, for these investigations, only limited substitution modification patterns have been selected that can bring about the desired improvement but otherwise leave the syndiotactic selective behavior of the system intact.

3.1 Modification of the Bridge and Syndiotactic Polymer Molecular Weight

The importance of the bridge in *ansa*-metallocene catalysts was recognized early on during the development of chiral metallocene catalysts for olefin polymerization [43–45]. Its existence is the prerequisite for stereorigidity of the metallocene structure, designed to prevent the free rotation of the aromatic ring(s) and to maintain the appropriate chirality of the corresponding cationic active species during the initial stages and the entire process of the polymerization. Later, it was recognized that the size of the bridge connecting the two aromatic rings could be additionally used as a regulating tool for modifying the active site's bite angle. For example, by replacing a one-carbon bridge such as $=CR_2$ with a two-carbon bridge like –RC–CR– or a silicon bridge like $=SiR_2$ it is possible to decrease the opening around, and control the monomer accessibility to, the transition metal center and thus influence the activity of the catalyst [107, 108, 109–112].

Based on a series of molecular mechanic calculations and polymerization experiments performed with a number of *ansa*-bis-(fluorenyl)zirconium dichloride complexes, Alt et al. [109–112] demonstrated that the size of the bridging unit plays an important role in the final catalytic activity of these complexes towards ethylene polymerization. A bigger bite angle, i.e., bigger opening around the active site, is supposed to increase the catalytic activity because of a less-hindered monomer

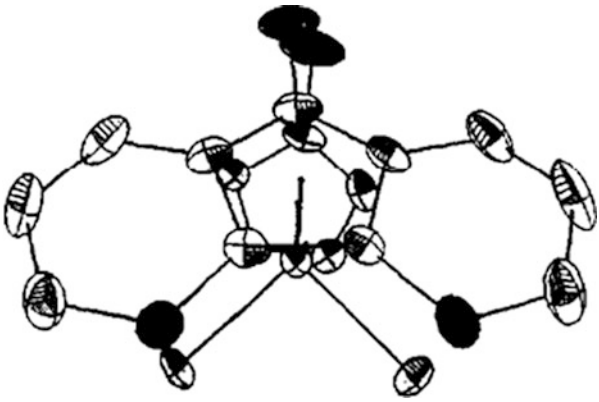

Fig. 10 Top view of the molecular structure of complex (η^5-C_5H_4-μ-Et-η^5-$C_{13}H_8$)$ZrCl_2$, **5**

approach as it passes through a wider entrance. However, the authors note that in addition to the "purely" steric effect, some degree of electronic influence has also to be taken into consideration to account for the overall change in catalyst behavior. Naturally, a large opening also translates into better incorporation of higher α-olefins and better comonomer incorporation in copolymerization reactions involving larger comonomers.

Little was known about the influence of the bridge and bridge substituent(s) on the catalytic performance with respect to the molecular weight of the resulting polymer until the advent of the syndiotactic-selective metallocene catalyst systems. The following two sections describe the modifications of the size and substituents of the inter-annular bridge in complex **1** and their impact on the catalytic performance and resulting s-PP.

3.2 Bridge Size Modification: 1,2-Ethano-Bridge Versus 2,2-Propano-Bridge

Syndiotactic-selective precatalyst complexes **1** and **2** have a ligand system in which the inter-annular bridge, connecting the two aromatic rings together, is the single carbon atom of the isopropylidene, or 2,2-dimethyl-propano group. It appeared intriguing to know what would be the effect on the polymerization behavior of the resulting catalyst of an increase in the number of carbon atoms of the bridge (i.e., an increase in the size) by one additional carbon atom. To answer this question, a review of the polymerization behavior of the complex [1,2-(cyclopentadienyl-fluorenyl)ethane]$ZrCl_2$, **5**, whose single-crystal X-ray structure is depicted in Fig. 10, is very helpful [34, 113]. As revealed by the molecular structure shown in Fig. 10, and similar to complex **1**, the molecule in complex **5** is prochiral and can be divided into two almost equivalent halves by a symmetry plane, σ_v, bisecting the Cl–Zr–Cl angle (only the two carbon atoms in the bridge lie on a skew line with respect to the mirror plane and are not symmetry related (cf. Fig. 10). Consequently,

Table 3 Polymerization conditions, results, and polymer analyses with 5

Temperature (°C)	Activity (kg/g)	M_w (×1,000)	MWD	rrrr (%)	Melting point (°C)
20	25	491	4.7	84.30	133
40	35	248	3.4	82.90	125
60	50	171	3.7	74.31	111
80	35	71	2.7	56.71	–

Polymerization conditions: 1 L liquid propylene, 10 mL MAO 10% in toluene

Table 4 Presentation of the relevant ^{13}C NMR normalized spectroscopic stereosequence distributions (%) for syndiotactic polypropylene samples produced with **5**/MAO at different polymerization temperatures

Temperature (°C)	rrrr (%)	rrrm (%)	rrmr (%)	rmmr (%)
20	84.30	4.15	4.62	1.63
40	82.90	5.95	4.29	1.98
60	74.31	8.94	6.91	2.48
80	56.71	13.54	13.49	2.91

the catalyst prepared from **5** and MAO bears close resemblance to **1**/MAO catalyst system and behaves accordingly by efficiently polymerizing propylene to s-PP after its activation.

The polymerization conditions, results, and polymer analyses for the **5**/MAO catalyst system and the corresponding s-PP polymers are presented in Tables 3 and 4. A comparison of the data listed in Tables 3 and 4 with the data listed in Tables 1 and 2 reveals that the catalyst derived from **5**/MAO produces, as expected, s-PP chains but with higher molecular weight (almost double in size). The data also show that the ethano-bridged catalyst system is less active and less stereoselective (cf. the percentage of rrrr, rmmr, and rrmr pentads!) than the corresponding propano-bridged catalyst system made with **1**/MAO, at all polymerization temperatures tested. Interestingly and surprisingly, all the polymers produced with **5**/MAO, particularly those produced at lower polymerization temperatures, exhibit broad molecular weight distribution (MWD, 4–5), which is very unusual for polymers produced with single-site catalysts. However, analysis of the methyl signal pattern and pentad intensity distributions obtained from the ^{13}C NMR spectra of syndiotactic polymers produced with **5**/MAO at different polymerization temperatures (see Table 4) show that they are, in general, architecturally and microstructurally very similar to the polymers produced with the **1**/MAO catalyst system [34, 113]. These macromolecules also exhibit all the chain microtacticity fine structures ...rrrrrrrrrmmrrrrmrrr... with two types of configurational defects; *meso* triad (mm) and *meso* dyad (m).

Table 4 presents the variation in steric pentad distributions with the polymerization temperature. The precipitous decrease in rrrr steric pentads concomitant with a rapid increase in rrmr pentad sequences and a moderate but noticeable increase in rmmr pentads with increasing polymerization temperature (particularly for the temperature range between 40°C and 60°C and higher) is also reminiscent of the microstructure–temperature interdependence of s-PP polymers formed with

1/MAO. It is an indication of a rampant site epimerization setting in faster and faster with increasing polymerization temperature. The concentrations of the site epimerization related rrmr pentads in the syndiotactic polymers produced with the **5**/MAO catalyst system have, however, almost triple the size of corresponding rrmr pentads found in polymers produced with **1**/MAO. The enantioselectivity related (rmmr) pentad concentrations in s-PP chains produced at the same polymerization temperature with both catalyst systems are less different in size and do not change as dramatically with the change in polymerization temperature, within the range tested (see data on related pentads in Table 4).

The observed general similarities in catalytic behavior between **5**/MAO and **1**/MAO catalyst systems corroborate the molecular structural resemblance of **1** and **5** but are in contradiction with the displayed discrepancies regarding larger polydispersity, higher molecular weight, and lower stereoregularity. The complete interpretation of the polymerization data can, however, be given in an elegant and convincing way, as least with respect to larger polydispersity, by close inspection of the single-crystal X-ray structure and associated data [34, 113] (similar results have been reported by Kim et al. [114]) and by inspecting more closely the impact of the bridge as the potential source of behavioral dissimilarity.

Let us first start the discussion with the polydispersity and focus on the reasons for a relatively large molecular weight distribution (up to 4.7) observed for s-PP polymers produced with **5**/MAO catalyst systems. It follows from the theory [115] that for polymers produced with single-site type catalysts the expected molecular weight distributions should have a value of 2. Accordingly, values of 2 (or close to 2) have been measured generally for all polymers produced in homogeneous olefin polymerization catalysis with activated metallocenes under controlled polymerization conditions. Large deviations from this value are generally indicative of the presence of diffusion phenomena or temperature variations during the polymerization process. In the absence of the said factors, broader molecular weight distribution reflect, unambiguously, the presence of more than one population of active species in the polymerization medium. Closer inspection of the crystal structure data for **5** confirms this fact and provides the clue for this apparently rather unusual phenomenon.

The in-depth examinations of the X-ray data for **5** by Atwood and colleagues [113] revealed that the unit cell of the crystalline lattice of **5** accommodates two types of molecules, i.e., two different conformers. The formation of two conformers arises from the fact that the ligand structure of complex **5** contains a two-carbon atom unit in its ethano-based bridge that has a fluxional character. The ethano ($–CH_2–CH_2–$) group can assume two different spatial arrangements with respect to the aromatic rings, being able to oscillate about the center of inertia lying mid-way between the two CH_2 groups. These arrangements give rise to two energetically identical, stable, but different conformers, δ and λ, whose structures are presented in Fig. 11. The two independent molecules populate equally the unit cells of the crystalline lattice in the solid state.

These conformers, as neutral molecules, interconvert very quickly in solution at room temperature and are indistinguishable (in a temperature range measured from −80°C to 90°C) in the ^{1}H NMR timescale [34]. The ^{1}H NMR spectrum of **5**

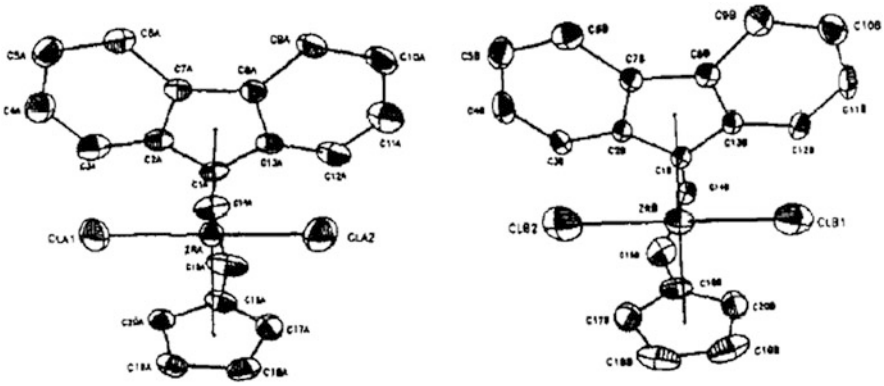

Fig. 11 The two δ/λ-(η^5-C_5H_4-μ-Et-η^5-$C_{13}H_8$)$ZrCl_2$ conformers of **5**

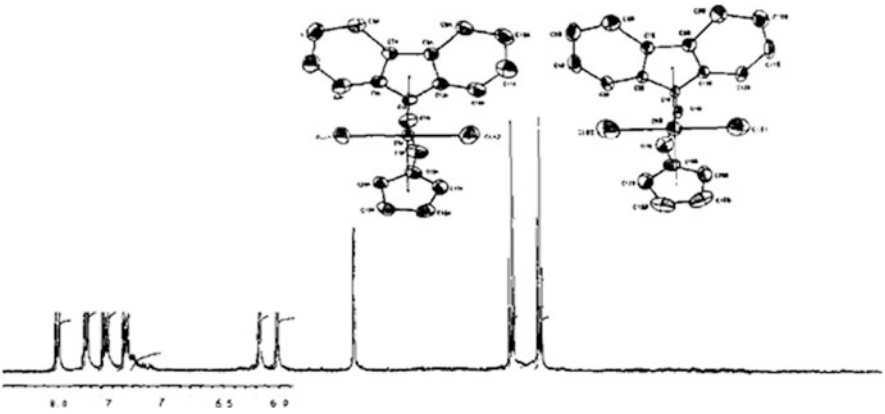

Fig. 12 ^{1}H NMR spectrum of δ/λ-**5** conformers in toluene at room temperature. Only aromatic proton chemical shifts are shown

(displayed in Fig. 12) reflects this fact by exhibiting for each proton pair of the two conformers only one time-averaged signal.

After the activation with MAO, the interconversion mobility of their cationic species seems to become severely restricted, probably due to the electronic differences between the cationic molecule and the neutral molecule and/or because of ion pairing dynamics between the cationic zirconium alkyl conformers and the MAO anion [34, 113]. Since the two conformers have different enough structural characteristics (two sets of bond angles and bond distances) they consequently behave differently as catalytic species after their activation and transformation to cationic species. The two cationic conformational species thus have slightly different catalytic properties and produce two different populations of active species, giving rise to two populations of polymer chains distinguishable by the difference in their polymer chain lengths. In this respect, the catalytic system generated with **5**/MAO resembles very much a dual-site catalyst system [116–121].

At higher polymerization temperatures, however, the energy for overcoming the interconversion barrier is apparently provided even for cationic systems and the polydispersity of the polymers begins to decrease with the gradually increasing polymerization temperature, as the difference between the two populations of active species vanishes due to very fast δ–λ interconversion. The two polymer chain populations coalesce around 80°C into one single population. At 90°C, the catalyst produces an amorphous polypropylene polymer that contains a large portion of atactic pentads but a narrow molecular weight distribution.

At higher temperatures, at the same time as the polydispersity decreases because of the rapid reversible δ–λ interconversion, the rigid structural integrity is also more and more compromised. The concentration of enantiomorphic site control related stereo-errors (rmmr) increases, but the rate of site epimerization and concentration of rrmr pentads increase much more dramatically, parallel to the increase in the conformational interconversion rate and the resulting molecular flexibility.

The explanation for the formation of the longer polymer chains with the **5**/MAO catalyst system requires a different approach and necessitates a comparative evaluation of the interatomic parameters for structures **5** and **1**, including some important bond angles and bond distances. It is apparent from structural data [113] that the substitution of one carbon atom (in the bridge of **1**) with two carbon atoms (in the bridge of **5**) provokes the increase in centroid–Zr–centroid angle (a smaller bite angle!) by several degrees (127.28°/127.08° versus 118.6° for **1**). The cyclopentadienyl and fluorenyl ring systems are forced to move closer and adopt a more parallel position. This new ring arrangement causes the increase in the average cyclopentadienyl Zr–centroid bond distance ($Zr–C_{cp}$ = 2.268 Å/2.285 Å for **5**, **5′** versus 2.170 Å for **1**) and the decrease in the average fluorenyl Zr–centroid bond distance ($Zr–C_{flu}$ = 2.196 Å/2.196 Å for **5**, **5′** versus 2.240 Å for **1**). The net effect is that under these conditions slightly more ligand coverage is provided for the transition metal's coordination sites. The increase in the centroid–Zr–centroid angle at the same time is accompanied by an increase in the frontier orbital energies and a change in the degree of their hybridization [107, 108, 122]. Furthermore, the increased steric congestion around the coordination sites increases the nonbonded steric contacts between the ligand and the growing chain substituents, preventing it from getting close enough to the Zr center for an adequate orbital overlapping between the metal fragment orbitals and hydrides for a meaningful α- or β-agostic exchange. The lower probability of the β-agostic approach favors the formation of a longer chain and, on the other hand, the lower probability of α-agostic interaction is favorable for enhanced conformational orientation of the chain and faster insertion/propagation steps, resulting in a lower degree of enantioselectivity and lower activity due to lower insertion rate (and also smaller bite angle!). Thus both from a steric and a valence orbital energetic point of view, the approach and subsequent orbital overlapping between chain-end hydride orbitals and transition metal fragment orbitals for a proper agostic interaction (of any kind) will be less favored for the new catalyst formed with **5** (similar results have been reported by Kim et al. [114]).

3.3 Bridge Substituents and Syndiotactic Polypropylene Molecular Weight

An increase in the size of the bridge, exemplified by replacement of the single-carbon isopropylidene inter-annular bridge with a two-carbon ethano-bridge, in syndiospecific catalyst system **5**/MAO provides the desired increase in the molecular weight of the s-PP polymer, but is unfortunately accompanied by some undesired side effects such as a decrease in the catalytic activity and stereospecificity and a lowering of the stereoregularity of the s-PP polymer. Other investigations related to the increase in the size of the bridge have also shown, for example, that the replacement of the carbon bridge with a silicon bridge has a similar deleterious effect on the enantioselectivity of the final catalysts [123, 124]. These findings are suggestive of the fact that any bridge modification with the purpose of improving the overall final catalyst properties must maintain the single-carbon arrangement of the bridge in the basic skeleton of complex **1**. This leaves only one remaining option for further consideration: modification of the bridge substituents.

The effect of the bridge substituents on the molecular weight of s-PP polymer was accidentally discovered during a systematic study of structural modifications for syndiospecific catalyst systems. The aim of the study was initially to perform substitutional modifications on the ligand without destroying the bilateral symmetry in the original metallocene molecule **1**. In the course of the study, by us and other research groups, the two methyl substituents of the bridge were exchanged individually or simultaneously for one or two phenyl groups, one or two hydride groups, and a series of other potential aliphatic or aromatic groups [125–127]. Of the many bridge substituent modifications, the effect of replacing the two methyl substituents of the bridge in **1** with two phenyl groups causes the most spectacular results with respect to increasing the molecular weight of s-PP and is discussed below in some detail.

3.4 Polymerization Behavior of Diphenylmethylidene (cyclopentadienyl-fluorenyl)MCl_2/MAO: Methyl Versus Phenyl Substituent in the Bridge

The replacement of the two methyl groups in the isopropylidene bridge of the complex **1** (and **2**) by two phenyl groups leads to the formation of two new complexes, diphenylmethylidene(cyclopentadienyl-fluorenyl)MCl_2 or (η^5-C_5H_4-CPh_2-η^5-$C_{13}H_8$)MCl_2; M = Zr, (**6**) or Hf (**7**). Complexes **6** and **7** can be prepared according to a method very similar to that used for the preparation of **1** and **2** (see Sect. 8).

Two different views of the molecular structure of **6** (and **7**) are portrayed in Fig. 13. From both a molecular symmetry point of view and from solid structural characteristics (bond distances and bond angles) point of view, complexes **6** and **7** appear almost indistinguishable from **1** and **2** [20]. It was, therefore, expected that

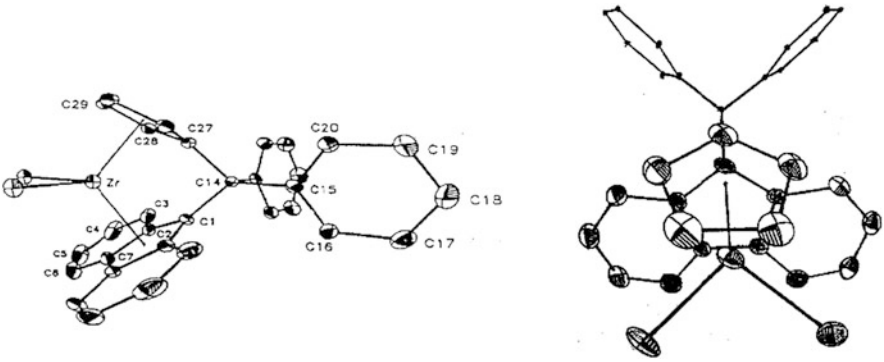

Fig. 13 Two different views of single-crystal X-ray molecular structure of complexes (η^5-C_5H_4-CPh_2-η^5-$C_{13}H_8$)MCl_2; M = Zr (**6**), Hf (**7**)

Table 5 Polymerization results and conditions for (**6** and **7**)/MAO

Complex	Temperature (°C)	Activity (g/g)	M_w (×1,000)	rrrr (%)	Melting point (°C)
Zr	20	11,800	1,243	145.60	91.04
Zr	40	26,000	785	89.74	144.45
Zr	60	138,000	478	86.78	133.40
Hf	40	17,500	2,863	76.60	103.81
Hf	60	27,500	1,950	7.03	102.17

Polymerization conditions: 1 L liquid propylene; 10 mL MAO (11 wt% in toluene); 60 min

Table 6 Presentation of ^{13}C NMR normalized spectroscopic stereosequence distributions (%) for syndiotactic polypropylene samples produced with (**6** and **7**)/MAO at different polymerization temperatures

Complex	Temperature (°C)	rrrr (%)	rrmr (%)	rmmr (%)	mmmm (%)
Zr	20	91.04	1.07	0.92	0.00
Zr	40	89.74	1.21	2.08	0.00
Zr	60	86.78	1.95	2.40	0.11
Hf	40	76.60	2.71	4.55	0.58
Hf	60	74.03	1.37	3.46	0.86

their activated forms as catalysts would produce very similar, if not identical, s-PP chains when polymerizing propylene. Correspondingly, after activation with MAO or other ethylating/ionizing agents, complexes **6** and **7** are transformed into excellent catalysts for promoting the polymerization of propylene to highly syndiotactic polypropylene. Table 5 presents the polymerization conditions, results, and polymer analysis for (**6** and **7**)/MAO catalyst systems. Table 6 compares the microtacticities of s-PP produced with catalyst systems (**6** and **7**)/MAO and (**1** and **2**)/MAO at different polymerization temperatures.

A cursory comparison of the data given in Table 5 for s-PP samples produced with complexes (**6** and **7**)/MAO and the data in Table 1 for complexes (**1** and **2**)/MAO

reveals that, under similar polymerization conditions, the catalyst systems **6**/MAO (and **7**/MAO) produce s-PP polymers with much higher molecular weights compared to polymers produced with **1**/MAO (and **2**/MAO) catalyst systems. On the other hand, for both systems the polymers' stereoregularities and microtacticities, as measured by the size of the related pentad (rmmr and rrmr) intensities, within the expected experimental errors, were very close.

The general model and mechanism that was discussed in Sect. 2.4 and proposed for the mechanism of the syndiospecific polymerization of propylene with the C_S symmetric metallocene catalyst system **1**/MAO vindicate the similar microtacticity and stereoregularity of the syndiotactic polymers perfectly, but does not in any way account for or rationalize, the polymerization behavior of catalyst system diphenylmethylidene-μ-(cyclopentadienyl-fluorenyl)zirconium dichloride **6**/MAO (**7**/MAO) with respect to the dramatic increases in the molecular weights of the resulting s-PP polymers.

The molecular structures of **1** and **6**, depicted in Figs. 2 and 13, expose their extraordinary overall resemblance and the reason for the production of s-PP chains with very similar microstructures. They do not, however, provide any clue as to why the molecular weights of their corresponding s-PP polymers are so different. A review of the solid state interatomic bond distances obtained from crystal structure data for complexes **1** and **6** [19, 20] also does not give, at the first sight, any indications that might justify the different catalytic performance in this respect. It seems that upon introduction of the phenyl groups in the bridge, the important Zr–C bond distances in the modified complex **6** have not undergone palpable changes. Both aromatic ring systems in complex **6** are η^5-bonded to the zirconium center and the observed slight variations in Zr–C and C–C bond distance are, in general, well within the expected experimental uncertainties.

However, closer inspection of the bond angles reveals some minor changes. The centroid–Zr–centroid (and Cl–Zr–Cl) bond angle in complex **6** is smaller than the corresponding bond angles for complex **1**.The angle has decreased from a value of 118.60° (and 98.20°) to a value of 117.60° (and 96.60°), i.e., by 1.00° (and 1.60°). These angular changes imply that in complex **6**, as a result of the repulsive interaction between the two aromatic phenyl substituents in the bridge, the external tetrahedral angle, i.e. the angle including the bridging carbon and the bonds connected to the two phenyl groups, is increased and as a direct consequence the internal tetrahedral angle, including the bridging carbon and its bonds to cyclopentadienyl and fluorenyl bridge-head carbon atoms, is decreased.[1] The smaller internal angle forces the transition metal Zr (Hf) to move slightly outward in order to fit better inside the ligand and to have a more efficient *d* orbitals overlapping with their aromatic ring π-systems.[2]

[1] (a) Tetrahedral formed by the bridging carbon and the four bonds connecting it to two phenyl groups, a cyclopentadienyl, and a fluorenyl group. (b) Interpretation of the X-ray data in [20] was given by Professor Jerry Atwood (private communication) with respect to Zr displacement.

[2] See footnote 1, part b.

A comparison of the ^{1}H NMR spectra [19, 20, 128] of complexes **1** and **6** reveals further that the structural differences may be more substantial in solution phase. Comparison of ^{1}H NMR spectra of the complexes **1** and **6** shows that for both molecules the proton signals related to the cyclopentadienyl groups of both catalyst systems have very similar chemical shift values and present the same coupling pattern (two virtual triplets) [20]. Examination of the fluorenyl's proton signals indicates that some of the protons belonging to the fluorenyl part of complex **6** have been subjected to major different shielding and deshielding forces, giving rise to completely different chemical shifts and signal patterns. Fluorenyl protons attached to carbons 3,3′ and 4,4′ (see Fig. 13 for numbering) closest to the bridge substituents, the phenyl groups, in complex **6** experience the most dramatic up-field shift. Their signals appear more than 1.5 and 0.5 ppm shifted to higher field, respectively, whereas the chemical shift variations for protons 5,5′ and 6,6′ (attached to carbon 5,5′ and 6,6′ in Fig. 13), more distant from the bridge, are negligible (see Sect. 8) [20, 129, 130]. Apparently, the introduction of the phenyl groups in the C1 bridge (vide supra) causes important changes in the electron density distribution of the aromatic π-system of the fluorenyl's six-membered rings. This in turn provokes a redistribution of the electron densities concentrated on the different C–H atom groups and their chemical shift repositioning [20, 129, 130]. It is also possible that the magnetic field anisotropy caused by the ring currents of the two phenyl substituents in the bridge is responsible for the observed differences in the chemical shifts and signal patterns for the said protons.

The slight outward repositioning of the metal center and dramatic differences in chemical shifts and signal pattern of the fluorenyl protons for compounds **1** and **6**, on the other hand, could be indicative of fact that the fluorenyl moieties of the ligands of these complexes are engaged in different bonding relationship or hapticities with the transition metal in the solution phase. In other words, the redistribution of the electron densities and changes in the Zr–C bonds in fluorenyl carbon atoms may be associated with, or a result of, an eventual hapticity change from η^5-bonding to η^3-bonding. It is in essence speculated that different Zr–C_{flu} bond hapticities, η^5 or η^3, (or even a η^1-type bonding) are at the origin of the different catalytic performances of (**1** and **2**)/MAO, and (**6** and **7**)/MAO catalyst systems [129, 130]. To prove the veracity of the hypothesis concerning different η-bonding in complexes **1** and **6** in solution phase, a hydrogenation experiment was undertaken that proved to be very revealing.

The aim of the hydrogenation experiment was, first, to verify the assumption that whether in either one of the complexes a η^3 Zr–C_{flu} is operative and, if so, to assign the correct Zr–C_{flu} centroid hapticities to each of the two metallocene complexes **1** and **6**. Theoretically, the η^3 nature of the five-membered ring of Zr–fluorenyl bond in one of the metallocenes would basically imply that the corresponding two six-membered rings are fully aromatic and not easily subject to hydrogenation. On the contrary, if in one of the metallocenes the Zr–C_{flu} centroid bond is η^5 in nature, then the fused six-membered rings are not "quite" aromatic and more hexadiene like in nature and therefore subject to facile hydrogenation. Figure 14 shows the hydrogenation scheme for the two metallocene complexes **1** and **6** and the formation

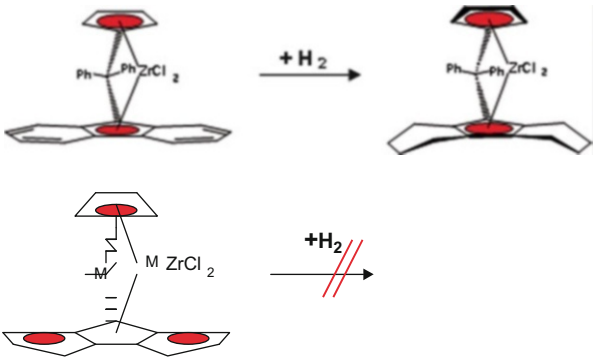

Fig. 14 Representation of **1** (*bottom left*) and **6** (*top left*) and the hydrogenation scheme. The structure of complex **8** is shown (*right*). The *solid areas* in the rings represent their aromatic nature

of the complex, diphenylmethylidene-μ-(cyclopentadienyl-octahydrofluorenyl)$ZrCl_2$, **8**, as the only hydrogenation product. Metallocene **8** was obtained from **6** under mild hydrogenation conditions [28, 30].

All attempts to hydrogenate metallocene **1** under similar and even more vigorous conditions failed. It can be therefore concluded that an η^3 bonding scenario represent the correct Zr–fluorenyl bond hapticity for complex **1** in solution phase and an η^5 bonding correctly describes the bonding of the Zr–fluorenyl centroid for complex **6** both in solution phase and solid state. The structures of complexes **1** and **6** with correct Zr–Centroid bonding for **1** and **6** are presented in Fig. 14. The solid areas in the rings reflect their aromatic nature in each case.

The hydrogenation experiment clearly shows that the complexes **1** and **6** are chemically different from each other in solution, at least with respect to the fluorenyl–Zr bond hapticities, despite their solid state apparent close resemblance.

The displacement of the transition metal towards the more open section of the ligand leads, at the same time, to a greater exposure of the transition metal and its protruding frontier orbitals in **6**. Even though it is difficult to establish a direct link between the hapticity of the $Zr–C_{flu}$ centroid bonds of the two catalyst systems and the molecular weights of their s-PPs, it is conceivable that the more exposed orbitals and the different electronic characteristics of the ligand changes the electrophilicity of the transition metal active site and its bond strength to carbon (of the polymer chain). The alteration of the shape, direction, and spatial extension of the frontier orbitals and the Lewis acidity of the transition metal of the metallocenium–monoalkyl cation can potentially influence the kinetics of the polymerization reaction by requiring new reaction pathways and different insertion transition state energies and chain transfer transition state energies. For the catalyst systems **1**/MAO and **6**/MAO it seems that the stereo-electronics in the former are conducive to a higher probability of β-hydride agostic interaction/transfer and formation of shorter chains, whereas the geometry in the latter is more prone to a rather frequent α-hydride agostic interaction and formation of longer chains.

4 Fluorenyl Substituents and Catalyst Enantioselectivity

As in the case of the bridge substituent modifications, this section describes the results of a systematic investigation involving fluorenyl substitution patterns. The investigations have shown that any modification of cyclopentadienyl substitution in complex **1** is at best ineffective [proximal position(s)] or completely disruptive [distal position(s)] to syndiospecificity of the final catalyst. As far as the fluorenyl substitution pattern is concerned, the combined substitutions at position 4 and 5 proved to be generally disruptive to enantioselectivity and had some adverse effects on polymer stereoregularity due to blockage of the central space in the frontal positions of the fluorenyl that accommodate the propylene methyl group [131–136]. By contrast, substitution at the 2 and 7 positions of the fluorenyl does not bring about any improvement in enantioselectivity of the parent complex **1**. On the other hand, double substitution involving positions 3 and 6 of the fluorenyl moiety of the ligand proved to bring about the desired improvements in catalyst stereoselectivity and in the resulting polymer's stereoregularity, melting point, and crystallinity. This will be discussed below as a successful case study. The study also shows that, as well as the position of the substituents, the size of the substituent is an important factor such that the larger the substituents, the more dramatic the effect they exert.

4.1 Stereoregularity Improvement and Frontal Substituents

The zirconocene complex (η^5-C_5H_4-μ-CPh_2-η^5-3,6-di-^{t}Bu-$C_{13}H_6$)$ZrCl_2$, **9**, can be synthesized according to a similar synthetic procedure that describes the synthesis of **6** (see Sect. 8 and [20]) with only difference being that, instead of the unsubstituted fluorene used for preparation of **6**, the 3,6-di-*tert*-butyl-substituted fluorene is employed for the synthesis of the ligand of complex **9**. The procedures for the aromatization of the ligand, its reaction with $ZrCl_4$, and isolation and identification of complex **9** all follow similar reaction procedures and work-up steps as for the preparation of **1** and **6** (see Sect. 8). Complex **9** is identified by its ^{1}H NMR spectrum and its single-crystal X-ray structure. The molecular structure of complex **9** is depicted in Fig. 15. As can be seen from molecular views, the metallocene molecule **9** projects the overall symmetry and bonding characteristics that were described for **6** except for the presence of two protruding *tert*-butyl substituents at positions 3 and 6 in its frontal section. When activated with MAO, complex **9** polymerizes propylene to highly syndiotactic polypropylene very efficiently. Catalyst prepared with the complex **9**/MAO is more active than the corresponding catalysts prepared with complexes **1** and **6** under the same polymerization conditions. Tables 7 and 8 present the polymerization conditions, results, and polymer analyses of the syndiotactic polymers produced with the **9**/MAO catalyst system at different polymerization temperatures [28–30]. A quick comparative

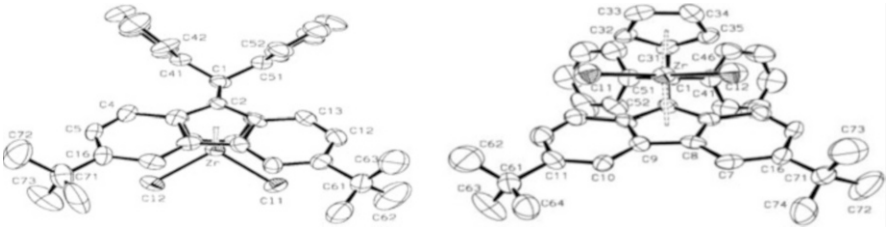

Fig. 15 Two perspective views of the single-crystal X-ray determined molecular structure of (η^5-C_5H_4-μ-CPh_2-η^5-3,6-di-^{t}Bu-$C_{13}H_6$)$ZrCl_2$, **9** [28–30]

Table 7 Polymerization results, polymer analysis, and stereodefects generated in the polymers produced with **9**/MAO at different polymerization temperatures

Temperature (°C)	M_W (kDa)	rrrr (%)	rmmr (%)	rrmr (%)	Melting point (°C)
40	766	91.0	0.73	0.93	150
60	590	88.5	0.85	1.65	143
80	443	79.0	1.06	3.79	128

Table 8 Comparison of ^{13}C NMR normalized spectroscopic stereosequence distributions (%) of syndiotactic polypropylene samples produced with **1**/MAO and **9**/MAO at different polymerization temperatures

	9/MAO catalyst system		**1**/MAO catalyst system	
Temperature (°C)	rmmr (%)	rrmr (%)	rmmr (%)	rrmr (%)
40	0.73	0.93	1.55	1.15
60	0.85	1.99	1.65	2.70
80	1.06	3.79	2.20	4.82

glance at the data given in Tables 1, 2, 7, and 8 reveals that the introduction of *tert*-butyl groups in positions 3 and 6 of the fluorenyl moiety of the ligand causes substantial improvements with respect to enantio- and stereoselectivity of the resulting catalysts **9**/MAO and the stereoregularity of the s-PP polymers it produces. The data presented in Table 8, compares the microtacticity variations of **1** and **9** under changing polymerization temperatures.

The data clearly shows, as anticipated, a substantial decrease in rmmr pentad concentrations related to *meso* triad (mm) stereoerrors in the backbone of syndiotactic polymer chains produced with **9**/MAO compared to the corresponding polymers produced with **1**/MAO at comparable polymerization temperatures. Interestingly, even the rrmr pentad concentrations in polymers produced with **9**/MAO, directly proportional to the catalyst's site epimerization frequency, are lower than the observed rrmr pentad concentration for polymers produced with **1** (and **6**). For syndiotactic polymers produced with both catalyst systems, the rrmr pentad concentrations almost double with every 20°C increase in polymerization temperature with the same rate. On the other hand, the enantiomorphic site control related rmmr pentad concentrations in syndiotactic polymers produced at different temperatures

with catalyst **9**/MAO are about half those of the corresponding rmmr pentad concentrations determined for polymers produced with catalysts of complexes (**1** and **6**)/MAO. Additionally, rmmr pentads in syndiotactic polymers produced with **9**/MAO show an even more moderate temperature dependency than the rmmr temperature dependency observed for polymers of (**1** and **6**)/MAO.

The improved enantioselectivity, reflected in lower percentage of rmmr pentads, for catalyst system **9**/MAO could be explained by the beneficial presence/action of the bulky *tert*-butyl substituents placed at positions 3 and 6 of the fluorenyl section of the ligand. These direct the polymer chain to the most preferred "upward" conformation away from fluorenyl part of the ligand and toward available quadrants left or right of the cyclopentadienyl group (see Sect. 3.2) and, at the same time, provide a more effective guidance for the preferred head-down propylene coordination mode (*anti* position with respect to the polymer chain via creation of a tighter "chiral pocket"). The explanation for the lower site epimerization related rrmr pentad concentration in polymers produced with **9**/MAO versus **1**/MAO, at the same polymerization temperature and monomer concentration is, however, less straightforward. It is most likely related to the steric bulk of the *tert*-butyl group's action in pushing the counter-ion (the anion) further away from the active cationic site, preventing a tight ion-pair formation and affecting the dynamic cation/anion association/dissociation processes [137, 138]. A cursory glance at the top and front views of the molecular structure of (η^5-C_5H_4-μ-CPh_2-η^5-3,6-di-^{t}Bu-$C_{13}H_6$)$ZrCl_2$, **9**, presented in Fig. 15, reveal the fact that due to substantial steric bulk of the *tert*-butyl substituents, the tight contact ion-pairing with MAO anion would be more difficult or harder for **9**/MAO systems than with the corresponding cations formed with (**1** and **6**)/MAO, rendering the site epimerization more difficult by forcing the anion to rearrange to the other coordination position after each insertion rather than associate back immediately. Thus, the immediate contact ion-pairing preventive effect of the *tert*-butyl substituents in **9** is an additional factor for the improved stereoselectivity of **9**/MAO as a result of slower active site epimerization. Most importantly, less tight ion-pairing is concomitant with higher activities due to easier availability of the coordination site to monomer coordination/insertion and chain propagation.

The two bulky *tert*-butyl groups in the fluorenyl moiety of the ligand affect the catalytic performance of **9**/MAO probably due to steric factors (interactions with polymer chain, monomer, and counter-ion as suggested above) rather than electronic factors. Use of a similar catalyst system in which the two *tert*-butyl substituents are placed at the 2 and 7 positions of the fluorenyl moiety of the ligand (η^5-C_5H_4-μ-CPh_2-η^5-2,7-di-^{t}Bu-$C_{13}H_6$)$ZrCl_2$/MAO [131–136] does not show any marked improvement in the enantioselectivity or stereoselectivity of the resulting syndiospecific catalyst or in the stereoregularity of its s-PP.

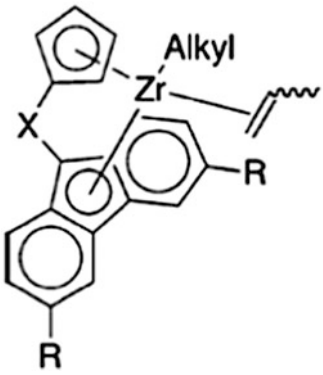

Scheme 1 C_s symmetric catalyst systems studied in computational investigation. R = H (system 1); R = methyl (system 2); R = *tert*-butyl (system 3); X = CMe_2; *Alkyl* = isobutyl

4.2 *Computational Calculations: Determination and/or Prediction of Enantioselectivity of Syndiospecific Catalyst Systems*

The experimental results concerning the effect of frontal substituent on the enantioselectivity of syndiotactic-specific metallocene catalysts can be further consolidated by computational calculations in a general and universal way. The computational calculations deliver the means for not only calculating the enantioselectivity of real and experimentally tested catalyst systems but also the ability to predict the enantioselectivity of hypothetical systems. In this section, the results of such computational calculations for three catalyst systems with a basic isopropylidene-bridged cyclopentadienyl-fluorenyl ligand skeleton are presented. The three chosen structures, for the reasons mentioned above, differ only by the gradually increasing size of the substituents located at positions 3 and 6 of their fluorenyl moieties. For the real catalyst systems, the catalysts **1**/MAO (system 1) and **9**/MAO (system 3) were selected. Additionally, a catalyst with a hypothetical structure, the isopropylidene(cyclopentadienyl-bis-3,6-dimethyl-fluorenyl)$ZrCl_2$, 3,6-dimethyfluorenyl-substituted version of complex **1** (system 2), is included for the calculation. The geometry of the model active sites for the three systems are depicted in Scheme 1 in which the bridge is represented by CMe_2, an isopropylidene group; R represents the substituents placed at positions 3 and 6 of the fluorenyl group, i.e., H, Me, and a *tert*-butyl group. The polymer chain is represented by an isobutyl group.

The basic system 1, with R = H, (fluorenyl without substituents), represent the catalysts system of complex **1** activated with MAO. It has been studied by many research groups including Angermund and colleagues [139–144] using a combination of density functional theory (DFT) functionals and a basis set very similar to the one chosen for this calculation by us [145–147]. The hypothetical system 2, is a modified version of complex **1** in which the ligand bears two methyl substituents in the 3 and 6 positions of its fluorenyl moiety. Furthermore, the insertion transition states are optimized for system 3 with two *tert*-butyl groups in the 3,6 positions of the fluorenyl ligand, representing catalysts system prepared with **9**/MAO [146].

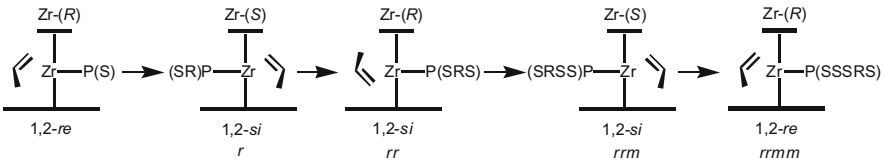

Scheme 2 Representation of the stereo-error sequence following an enantiomeric mis-insertion

It is commonly accepted that the syndiotactic-specific catalyst systems are highly regioselective (the regio-errors are either not present or very low in concentration and not easily detectable), and the single main source of the stereo-errors in the syndiospecific polymerization of propylene is enantiomeric mis-insertion, i.e., the insertion of a monomer unit with the "wrong" enantio-face. The "right" enantio-face would be the one that allows minimization of repulsive steric interactions between the olefin's side group and the growing polymer chain, as well as between the ligands and the growing polymer chain. This arrangement is best attained when the olefin's substituent and the alkyl (polymer) chain are in an "anti" relationship (versus a "syn" relationship), while at the same time the polymer (alkyl) chain is as far away as possible from the bulkier sections of the ligand. An enantiomeric mis-insertion event in the syndiospecific polymerization of propylene leads to the occurrence of a *meso* triad (mm) type stereo-error, as depicted in Scheme 2, whereas a perfect syndiotactic polymer is composed exclusively of *racemic* r dyads (Fig. 8). The preferred, dominant enantioselective enchainment sequence versus an enantiomeric mis-insertion event could be therefore presented schematically as in Scheme 2 (see also Fig. 9).

Each step in Scheme 2 represents a full catalytic cycle from the depicted π-complex to the one obtained after insertion, followed by uptake or coordination of the next monomer unit. At each step, the polymer chain is expected to be oriented away from the bulky fluorenyl ligand ("chain-away"). The four possible diastereomeric conformations are depicted in Fig. 16. In the most preferred stereochemical sequence, the methyl groups of propylene and the polymer chain are in an "anti" stereochemical relationship (the "chain-away/*anti*" diastereomeric conformation, (Fig. 16a) and one of the two faces of propylene, termed *re* or *si*, is inserted preferentially.[3] The 1,2-*si* enantiomeric mis-insertions take place either when the polymer chain points away from the fluorenyl group and the propylene's methyl group is "syn" oriented to it (diastereomeric conformation "chain-away/*syn*," Fig. 16c), or when the polymer chain points toward the fluorenyl group, while maintaining an "anti" relationship with the olefin substituent (diastereomeric

[3] For parent syndiospecific catalyst systems, the propylene π-complexes in which the Zr center has an *S* configuration insert the monomer in a 1,2-*si* fashion, and the configuration of the chiral center on the alkyl chain closest to the metal center is *R*. Alternatively, when the configuration of the Zr center is *R*, the closest chiral center on the chain is of *S* configuration and a 1,2-*re* insertion occurs. After each insertion, the alkyl chain "migrates" from one coordination site to the other. Due to the enantiotopic nature of the metallic active center, to have a complete picture it is sufficient to study only one of the two possibilities.

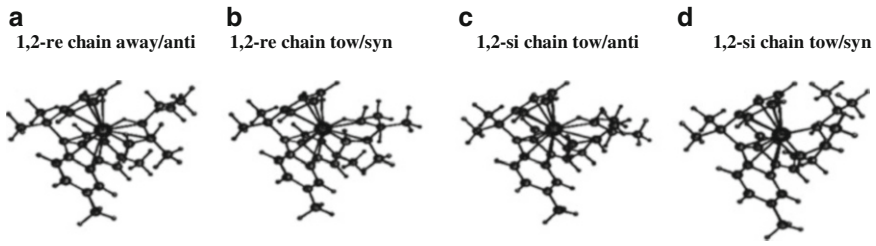

Fig. 16 Gas-phase optimized transition states for the insertion of propylene into the Zr–C bond of system 2: (**a**) 1,2-*re* chain away/*anti*; (**b**) 1,2-re chain toward/*syn*; (**c**) 1,2-si chain toward/*anti*; (**d**) 1,2-*si* chain toward/*syn*

conformation "chain-toward/*anti*," Fig. 16d). The situation in which the polymer chain points toward the fluorenyl ligand and is in a "syn" relationship with the methyl group of propylene (conformation "chain-toward/*syn*," Fig. 16b) would lead to 1,2-*re* insertion with the "correct" enantio-face, but it is expected to be the highest in energy; it is the least preferred stereochemical event due to two unfavorable steric interactions.

The gas-phase energies for propylene π-complexes and of the resulting insertion transition states (TSs) have been computed for all four possible diastereomeric conformations mentioned (chain-away/*anti*, chain-toward/*anti*, chain-toward/*syn*, chain-away/*syn*) for systems 1–3; the structures are shown in Scheme 1 and can be found in reference [146]. As expected, for all three ligand systems the lowest energy conformation is the one in which the alkyl chain points away from the fluorenyl moiety (chain-away/*anti* conformation) and the spatial relationship between the chain and the methyl group of propylene is *anti*. This corresponds to a 1,2-*re* approach (since the *R* chirality has been arbitrary chosen for the Zr metal center). The 1,2-*si* insertions are energetically slightly less favorable because one of the two interactions (either alkyl chain–monomer or alkyl chain–catalyst) is not energy-minimized. When both interactions are unfavorable, there is a dramatic increase in the relative energy for the remaining channel, ch-tow/syn, following a 1,2-*re* approach considerably higher in energy than all the others.

The substitution pattern on the fluorenyl moiety of the ligand plays an important role in the enantioselectivity. Adding bulky groups to the 3,6-positions strengthens repulsive interactions and increases the energy gap between the four conformations, as can be seen in the series 1–3. The calculated selectivity for system 1 is 2.0 kcal/mol [145, 147], for system 2 it increases and reaches the value of 2.4 kcal/mol, and for system 3 it is 2.6 kcal/mol. Because of its bulk, the *tert*-butyl substituent exerts the greatest conformational constraints on the growing polymer chain and consequently exhibits the highest enantio-facial selectivity. The increased selectivity comes only at a marginal expense of reactivity. In fact, in the gas phase the energy of the most favorable transition state for the hypothetical system 2, the dimethyl-substituted ligand system, (TS2 away/*anti*) is 7.4 kcal/mol below the reference energy point (zirconocenium isobutyl complex + propylene), whereas that of the

most favorable transition state for system 3 (TS3 away/*anti*) is 5.0 kcal/mol below the reference energy point. It should be noted that when the counter-ion is taken into account, both transition states would be destabilized because in the reference state the anion and cation interact closely.

Due to the different bulks of the substituents, it is likely that the ion-pair energy is, however, weaker in system 3. On the other hand, the anion does not play any important role in stabilizing one particular conformation of the diastereomeric cations versus the other. Therefore, enantio-face selectivity is hardly affected by including the anion in the picture and the anion can be disregarded in the calculations. The influence of toluene solvation, mimicking the polymerization medium, has been estimated by calculating the solvation energies of the gas-phase optimized geometries. The relative energies of the species involved in the insertion process are reported in [146]. Unsurprisingly, for all the different ligand systems, solvation effects are comparable for the four competing conformational channels. $\Delta\Delta E$ ranges between 0.1 and 0.2 kcal/mol. Thus, differential solvation plays a minimal role.

From the above calculation and discussion, two conclusions can be drawn regarding the origin and factors impacting the enantioselectivity of the syndiospecific catalyst systems:

1. The enantioselectivity does not emanate from a particular molecular symmetry of the catalyst structure but is tightly related to the steric arrangement of the organic ligand that engulfs the transition metal and its direct interaction with the growing polymer chain, which dictates its conformation and final spatial orientation (further ensured through a-H–Zr agnostic interaction). The combination of the steric arrangement of the ligand and the particular spatial orientation of the polymer chain (directing the coordination mode of the propylene) creates an overall repulsive steric force that "blocks" a large space in and around the coordination sphere of the transition metal center. The remaining "free" and accessible space forms a shape-selective "chiral pocket" that can only accept monomers of a certain shape, i.e., unique π-face that fits in that pocket easily without much repulsive interaction.
2. Any new substituent(s) at proper position(s) that could enhance the shape-selectivity of the chiral pocket via enforcing and stabilizing the spatial orientation of the growing polymer chain, regardless of its impact on the symmetry, would enhance the enantioselectivity of the final catalyst, be it of C_s or C_1 symmetry (see below). The substitution(s) at position 3(6) or 3,6 of the fluorenyl group, just beneath the growing polymer chain, provide exactly that enhancing effect.

4.3 Importance of the Frontal Substituents

To emphasize the importance of fluorenyl's frontal substituents at positions 3 and 6 and to confirm the findings of the computational calculations presented in Sect. 3.2, two new syndioselective catalysts systems are introduced whose ligands

Table 9 Polymerization conditions and results for μ-(Me_2Si)(3,6-di-^{t}BuFlu)(^{t}BuN)$TiCl_2$/MAO system

Temperature (°C)	Activity (kg/g)	M_W (×1,000)	rrrr (%)	Melting point (°C)
40	222	703	81.6	123.0
60	371	351	75.8	105.1
80	226	226	60.1	–

Table 10 Presentation of ^{13}C NMR spectroscopic stereosequence distributions (%) for syndiotactic polypropylene samples produced with **10**/MAO at different polymerization temperatures

Temperature (°C)	rrrr (%)	rmmr (%)	rrmr (%)
40	81.6	1.6	3.6
60	75.8	1.7	6.5
80	60.1	2.2	10.60

differ completely from the ligands of complexes **1**, **5**, **6**, and **9** by lacking a cyclopentadienyl ring. Let us start first with the complex η^1,η^5-*tert*-butyl (3,6-bis-*tert*-butylfluorenyl-dimethylsilyl)amido$TiCl_2$, the half-sandwich complex **10**. After activation with MAO, complex **10** very efficiently polymerizes propylene to high molecular weight s-PP chains [32].

Tables 9 and 10 presents the polymerization conditions, results, and polymer analyses of syndiotactic polymers produced with the **10**/MAO catalyst system. The degree of the syndiotacticity of the polypropylene polymer that it produces at 40°C (measured as the concentration of *racemic* pentads rrrr) is higher than 81%. The s-PP polymers that are produced at higher polymerization temperatures have lower stereoregularity but still high enough (74.00% at 60°C and 69.40% at 70°C) to impart to the resulting polymers measurable crystallinity and melting points (see Table 9). Only for polymers produced at 80°C is the crystallinity lost and no melting point observed.

The microstructure . . .rrrrmmrrrrmrrrr. . . of the s-PP polymers that are produced with **10** MAO includes the two characteristic types of stereodefects and is similar in nature to the microstructure of the s-PP polymers produced with other syndiotactic-specific metallocene catalysts (**1**, **5**, **6** and **9**)/MAO. From these results it can be concluded that the η^1,η^5-bonded dimethylsilyl-bridged amido-fluorenyl-based ligand is perfectly capable of imparting the needed stereorigidity and steric environment prerequisite for syndioselectivity of the transition metal active site. Additionally, the microstructural similarity between the s-PP polymers produced with **1**, **5**, **6**, **9**, and **10** indicate clearly that the formation of the s-PP polymers with **10** also proceeds according to the chain migratory insertion mechanism operating on enantiomorphic coordination sites.[4] Table 10 lists the variation in the relevant

[4] Due to the presence of a high number of site epimerization errors, the microstructure of the syndiotactic polypropylene polymers prepared with the catalyst system **10**/MAO looks deceptively similar to the microstructure of the syndiotactic polypropylene polymers prepared via chain-end control mechanisms; cf. [29] on syndiotactic polypropylene from [Me_2Si(3,6-^{t}Bu$_2$-9-fluorenyl)(N-^{t}Bu]$TiCl_2$-based catalysts.

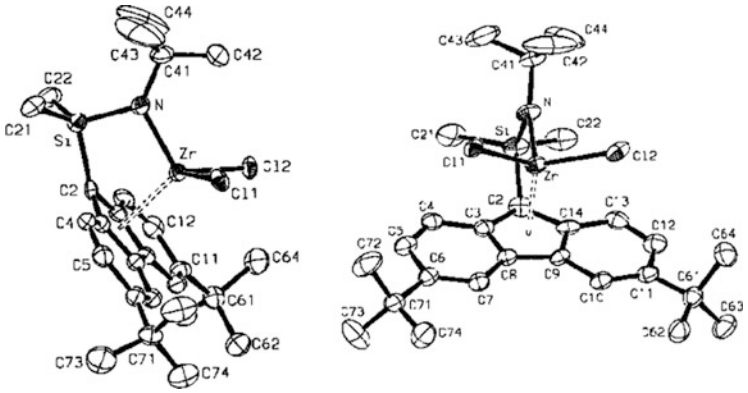

Fig. 17 Side and front view of the molecular structure of the complex η^1,η^5-*tert*-butyl(3,6-bis-*tert*-butylfluorenyl-dimethylsilyl)amidodichlorozirconium, **10**

stereopentad intensities with polymerization temperature. The data indicate that the syndiotacticity of the polymers produced with the **10**/MAO catalyst system at different polymerization temperatures, measured as the concentration of *racemic* pentads rrrr, are relatively high. The catalysts' enantioselectivity, judged by the concentration of the rmmr pentad sequences, are also very high and close to the enantioselectivities measured as rmmr pentads for the catalyst systems consisting of (**1**, **5**, **6** and **9**)/MAO.

The overall stereoregularity and melting points of the polymer are, however, lower for the syndiotactic polymers produced with the **10**/MAO catalyst system due to the presence of high concentration of site epimerization related stereo-errors (rrmr pentads). A rather frequent or fast site epimerization rate at higher polymerization temperatures is probably facilitated by the flexibility of the molecular structure of **10** (dynamic umbrella-type reversible inversion at the amido-nitrogen center see: [148]) and the rapid "same site" contact ion-pairing.

The single-crystal X-ray molecular structure of the complex μ-(Me_2Si)(3,6di-^{t}BuFlu)(^{t}BuN)$TiCl_2$ **10**, is depicted in Fig. 17. It shows a striking similarity to crystal structure of complex **9** with respect to its overall symmetry, despite the exchange of one of the aromatic rings, the cyclopentadienyl, in the molecule and its replacement with an amido group. Complex **10** exemplifies one of the rare examples of a titanium-based syndiotactic-specific metallocene catalyst systems.

It is in many other aspects different from all the catalyst systems t discussed in previous sections. It is based on a half-sandwich metallocene molecule that contains an amido-type N–Ti bond and is a 12-electron system (14-electron system at the most if one considers the contribution of the nitrogen's lone pair of electrons to the overall N–Ti bonding) leaving a cationic 10-electron (maximum 12 including the lone pair electrons of N) electron configuration active site.[5]

[5] As a comparison group, 4B neutral metallocenes have a 16-electron configuration and 14-electron configuration in their monoalkyl-cationic forms.

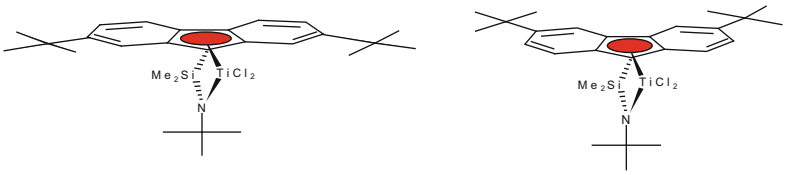

Fig. 18 Computer drawn structure of the complex η^1,η^5-*tert*-butyl(2,7-bis-*tert*-butylfluorenyl-dimethylsilyl)amidodichlorotitanium, **11** (*left*). On the *right*, the structure of **10** is shown for comparison

Table 11 Polymerization conditions and results for μ-(Me_2Si)(2,7-di-^{t}BuFlu)(^{t}BuN)$TiCl_2$/MAO system

Temperature (°C)	Activity (kg/g)	M_W (×1,000)	MWD	rrrr (%)	Melting point (°C)
40	27	605	2.6	75.74	111
60	160	506	3.2	63.92	–
80	75	367	3.1	55.89	–

Table 12 Presentation of ^{13}C NMR spectroscopic stereosequence distributions (%) for syndiotactic polypropylene samples produced with **5**/MAO at different polymerization temperatures

Temperature (°C)	rrrr (%)	rmmr (%)	rrmr (%)
40	75.74	3.15	4.72
60	69.05	3.03	8.55
80	55.89	3.46	11.23

The fact that the catalyst system **10**/MAO owes its high enantioselectivity mainly to the presence and the steric bulk of the *tert*-butyl substituents implanted at positions 3 and 6 of the fluorenyl moiety of its ligand can be demonstrated by reviewing the polymerization behavior of a similar complex, namely η^1,η^5-*tert*-butyl(2,7-bis-*tert*-butyl-fluorenyl-dimethylsilyl)amido-$TiCl_2$, **11** [29]. The only difference between the structures of complexes **11** and **10** lies in the different positions of the fluorenyl moiety where the *tert*-butyl substituents have been introduced. Complex **11** is prepared according to known synthetic procedures developed for constrained geometry, half-sandwich-type metallocene complexes. Its computer-drawn structure is shown in Fig. 18.

A glance at the molecular structure of **11** shown in Fig. 18 reveals again that from a molecular symmetry point of view complex **11** (like complex **10**) has all the structural and symmetry characteristics required to be classified as a syndiotactic-specific catalyst system after its activation. In practice, after activation with MAO, complex **11** does polymerize propylene to a high molecular weight s-PP very efficiently [29]. Tables 11 and 12 present the polymerization conditions, results and polymer analyses for **11**/MAO and the syndiotactic polymers it produces. According to these data, only the syndiotacticity of the polymers produced at and below 40°C (measured as the concentration of *racemic* pentads rrrr; about 75%) are

high enough to generate measurable crystallinity and melting points. The syndiotactic polymers that were produced at higher polymerization temperatures have much lower stereoregularity and exhibit no crystallinity and/or melting points.

Here again, like in the case of s-PP polymers produced with the **10**/MAO catalyst system, the main reason for lower stereoregularity is the rapidly increasing concentration of the site epimerization related (rrmr pentad) stereodefects. They double in size by increasing the polymerization temperature from 40°C to 60°C and reach values of over 10% at a polymerization temperature of 80°C and above for the very same reasons explained for syndiotactic polymers produced with the **10**/MAO catalyst system. The enantiomorphic site control related stereo-errors (rmmr pentads) are high but remain almost unchanged (as for **10**/MAO-produced polymers) over the entire measured temperature range.

The large enantioselectivity difference between the two catalyst systems involving complexes **10** and **11** (with rmmr pentad concentration of over 3% for **11**/MAO and about 1.7% for **10**/MAO) demonstrate the crucial role of the positions 3,6 for introducing the substitutions in the fluorenyl moiety of the ligand.

The syndiospecific catalysts systems (**10** and **11**)/MAO in which one of the ligand's main ingredients, an η^5-bonded cyclopentadienyl moiety, is exchanged for an η^1-bonded amido group with respect to the parent syndiospecific system made with complex **1**, are convincing examples for the validity of the fact that the proper steric balance between the three participants (ligand, polymer chain, and propylene) in the active transition state structure and the preference for one of the two monomer enantio-faces at each of the two enantiotopic coordination positions rather than for any particular geometry or symmetry, are the origin of syndiospecificity.

The polymerization behavior of (**10** and **11**)/MAO catalyst systems also demonstrates nicely that no matter what the chemical makeup of the metallocene precursor, composition of the ligand, or nature of the transition metal, the resulting catalysts (once their structure fulfills the prerequisites discussed based on the model given in Sect. 3.2) will act in a syndiotactic-specific manner and produce crystalline s-PP. The overall stereoselectivity is, however, determined by the frequency and rate of the site epimerization process. The lower stereoregularity of the new syndiotactic chains is probably the related to higher flexibility of the structures of complexes **10**/**11** in solution due to the absence of one of the η^5-bonded aromatic ring systems and the dynamic environment of a reversibly inverting amido group (dynamic umbrella-type reversible inversion at the amido-nitrogen center see: [148]) imparting a high degree of flexibility to the structure and/or facilitating fluorenyl ring slippage (see Sect. 4), leading occasionally to the dissymmetry of the site and the formation of lop-sided tight contact ion-pairing and short *meso* dyad units/sequences.

It is worth mentioning that the zirconium analogue of **10** produces only oligomeric materials.

5 Stereorigidity of Bridged Metallocenes and Stereoselectivity of the Catalysts

The lower stereorigidity and structural flexibility in complexes **5**, **10**, and **11** were associated with the more frequent occurrence of site epimerization and the lower stereospecificity of the resulting catalyst systems. In complex **5**, the conformational interconversion due to the fluxional behavior of the ethano-bridge, and in complexes **10** and **11**, the highly flexible structure as a result of the replacement of a strongly η^5-bonded ligand moiety (an aromatic ring) by a single atom η^1-bonded –N–R amido group (and the resulting amine-type umbrella interconversion[6] were considered to be the underlying reasons for lower skeletal rigidity and a probable source for higher site epimerization rate. However, one should be aware that even for bridged metallocene structures that have doubly η^5-bonded ligand systems such as in complexes **1** (**2**), **6** (**7**), and **9** the idea of high rigidity conveyed from solid state, X-ray images are somehow deceptive and should be taken as relative. The images extracted from X-ray crystal structural analysis project molecules contained in the unit cells in the solid state under the crystal packing effects. These rigid and static images reflect only a snapshot of the constantly vibrating, bending, and "breathing" molecules (the inward/outward movement of the two centroids towards and from the transition metal). In solution, the individual molecules freely float in the solvent and interact with the solvent molecules (the medium); they are much more mobile and dynamic than one would imagine.

Thus the question arises as to how rigid the stereorigid metallocene structures are in solution. In this context, it is important to be aware of at least two dynamic phenomena regarding the fluxional behavior of metallocene molecules in solution, namely, the phenomena of haptotropy [149–156] and ring slippage. The haptotropy and ring slippage [157–160, 161, and references therein] [162, 163], depicted schematically in Fig. 19, could influence the electronic properties of the active site and the steric environment surrounding it, particularly in the cationic state and in the presence of a counter-ion.

In Sect. 2.3 it was shown by the example of complexes **1** (**2**) and **6** (7), that the phenomenon of hapticity change or bond order variation between the transition metal and the aromatic ligands can change the kinetic pathways of the polymerization process and its outcome dramatically. The haptotropic behavior of metallocenes is a known phenomenon in transition organometallic chemistry and homogeneous catalysis [149–156].

The hapto-flexible aromatic ligands bonded to the transition metal can facilitate the ligand exchange reaction by "temporarily" lowering the hapticity in the transition state and permitting the increase in the formal coordination number without breaking the canonic electronic rules [157–160, 161, and references therein; 162, 163]. As a general rule, the hapticity change should be considered to be involved in almost all

[6] See footnote 5.

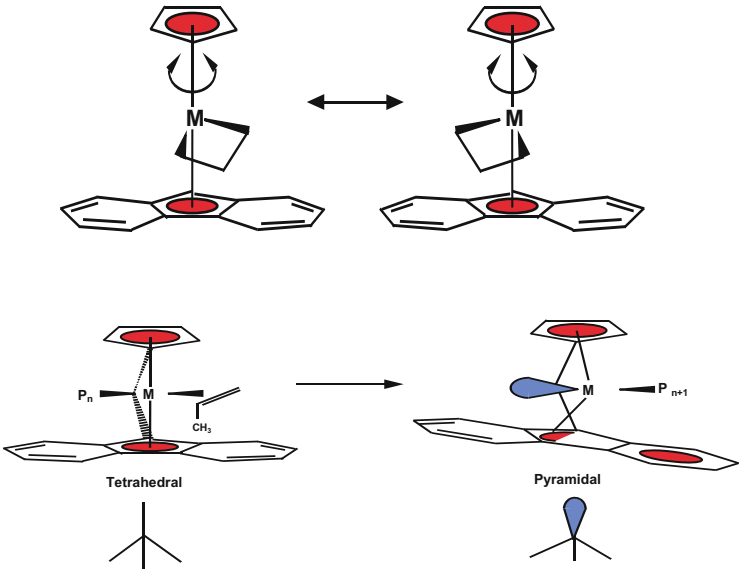

Fig. 19 *Top*: Lateral displacement of ligand system around the centroid–Zr bond axis (the bridge is omitted for the sake of clarity). *Bottom*: Geometry change

metallocenes catalyses particularly those comprising at least a fluorenyl and an indenyl, and possibly those with substituted cyclopentadienyl ring system(s). Whether or not any change in hapticity influences the polymerization behavior of the catalysts depends on the individual case and particularities of the catalysts/polymerization processes under discussion.

In this context, it is also noteworthy to mention another ligand/transition metal related, dynamic behavior, namely, the lateral displacement of the whole ligand system around the imaginary axis connecting the transition metal bonds to the centroids, which was first described by Petersen [164]. This movement can be described as a kind of windshield wiper-type oscillation of the MCl_2 moiety within the fixed ligand framework and could facilitate or influence the steps involved in the counter-ion-assisted site epimerization and chain migratory insertion processes (Fig. 19, top).

Finally, it is important to be aware of another, but slightly different, phenomenon that is related to the geometry change in the catalyst structure during the coordination and insertion steps. The pseudo-tetrahedral geometry, which is assumed for the tetra-coordinated transition metal site in the transition state, cannot be further extended to the step just after insertion. At this stage, the tetra-coordinated structure collapses due to the disappearance of one of the ligands, the monomer/counter-ion, leaving a tri-coordinated species behind in which the repulsive forces acting upon the bonding electron pairs are different and require a new geometry. The most logical structure that can be suggested for this step is a pyramidal structure and an empty fragment orbital. After the next monomer coordination (or the anion

association) the structure will again adopt the tetrahedral geometry (Fig. 19, bottom). This counter-ion-assisted change in geometry operates on all metallocenic catalyst systems, but is probably more crucial for the syndiotactic-specific catalyst systems and syndiospecific polymerization where dynamic processes such as chain migration and, particularly, site epimerization are vital or fatal for its existence. In this aspect, the syndiospecific polymerization process resembles a poly-insertion reaction following at each step the mechanism of a SN2-type reaction. For the isospecific system, the reagent propylene "always" attacks the tri-coordinated intermediate from the same side with the same face because of its homotopicity. For the syndiospecific case, the stereochemistry is determined by the reagent, propylene, attacking the tri-coordinated intermediate form on the opposite side with different faces because of the enantiotopic nature of the active site.

5.1 Catalysts Stereorigidity and Site Epimerization

In the preceding sections, the term "site epimerization" was frequently used as the phenomenon responsible for the formation of the *meso* dyad (m) stereodefects and the lower stereoregularity and crystallinity of the s-PP polymers. To increase the stereoregularity and melting point of these polymers, obviously, the concentration of the rrmr pentads must be suppressed in the polymer chain's backbone by devising means that enable circumventing their formation during syndiospecific polymerization of propylene.

The occurrence of site epimerization is generally explained [165–172] in the following manner: The *R* and *S* configured active sites that are formed during the initial stages of the activation are equi-energetic and can interconvert (epimerize) during the polymerization, particularly in the absence of a coordinating monomer or a stabilizing solvent molecule, particularly at higher polymerization temperatures. The interconversion occurs when occasionally the polymer chain swings back ("back-skip") to its initial coordination position after an insertion before the coordination of the next monomer (Fig. 6). Under these conditions, two (and more than two in the case of Hf-based catalyst **2**) consecutive insertions will take place at the same enantiomorphic coordination position, resulting in enchainment of two monomer units with the same prochiral face and insertion of two units with same stereogenic center. This leads to the formation of *meso* dyad, m-type, stereodefects in the s-PP polymer chains (and/or short isotactic blocks for the Hf analogue).

Little was known initially about the driving forces underlying the phenomenon of site epimerization. Empirically, it has been observed that (in addition to low monomer concentration and higher polymerization temperature dependency) the catalysts formed with metallocene structures with inherently lower stereorigidity or higher flexibility (such as structures **5**, **10**, and **11**) tend to undergo a more frequent site epimerization than those known to be less flexible, as can be seen from data presented in Table 13. Additionally, it was shown that the frontal substituents in more stereorigid catalysts systems impact the site epimerization rate (see **9**/MAO rrmr in

Table 13 Comparison of ^{13}C NMR stereo-error-related normalized spectroscopic stereosequence distributions (%) for syndiotactic polypropylene samples produced with **1**, **5**, **6**, **9**, **10** and **11**/MAO at polymerization temperatures of 40, 60, and 80°C

	Pentad rmmr (%)			Pentad rrmr (%)		
Catalyst	40°C	60°C	80°C	40°C	60°C	80°C
1	1.55	1.65	2.20	1.15	2.70	04.82
5	1.98	2.48	2.91	5.95	8.94	13.49
6	2.08	2.40	–	1.21	1.95	–
9	0.73	0.83	1.63	0.93	1.65	03.79
10	1.60	1.70	2.20	6.50	8.30	10.60
11	3.15	3.03	3.46	4.72	8.55	11.23

Table 13). Section 4.2 describes how computational calculations can be applied for different catalysts systems in the gas phase and solution phase in an attempt to pinpoint the origin(s) of site epimerization and possible ways to circumvent it.

5.2 *The Origin of Site Epimerization: Computational Investigation*

In order for site epimerization to occur during the syndiospecific polymerization of propylene with metallocene-based catalysts, two different mechanisms can be envisaged. Either the site epimerization occurs without inclusion of the counter-ion or it relies on its assistance.

5.3 *Site Epimerization in the "Absence" of the Counter-Ion*

The first and simplest mechanism starts with the naked anion and does not take into account the presence of a counter-ion, the anion (Fig. 6). It was originally presented as the mechanism responsible for the formation of the *meso* dyad (m) stereodefects based on the fact that the transition state geometries before and after a site epimerization are equi-energetic and therefore the assumption is that the activation energy barrier for the site epimerization is be very high.

However, the calculations performed by Angermund et al. [145] on a simple zirconocene complex catalyst model demonstrated that these assumptions do not corroborate with the energy barriers to be surmounted during the site epimerization process. According to the authors, the nonbonded repulsive interaction exerted between the polymer chain and different parts of the ligand, during its insertion-less migration from one coordination position to other, implicates several agostic bond making and breaking transition states, requiring large activation energies (in the order of more than 10 kcal/mol). According to our calculations for the

parent syndiospecific catalyst system **1**/MAO, the energy barrier for the site epimerization is even higher and reaches above 13 kcal/mol [146].

The polymer chain's passage between the two available coordination sites involves many nonbonded repulsive steric interactions with different parts of the ligand and the transformation of the β-agostic resting state into a symmetrical β′-agostic state, via a symmetric transition state in which the alkyl chain rests approximately in the plane formed by the metal and the ligands' centroids, half way between the two coordination positions. During the transformation, on either side of the reaction energy profile, other intermediates with α- and α′-agostic bonds are also formed [170]. Overall, the site epimerization mechanism that does not take into account the role of the counter-anion in the process has a very large activation energy compared to the propagation activation energy. Such a mechanism does not agree with the experimental results, which show that the pentad distributions are in reality influenced by a rather frequent site epimerization.

5.4 Counter-Ion-Assisted Site Epimerization

In the regular and real olefin polymerization processes with metallocene catalysts, the anion is an ever-present participant and an integral part of the functioning catalyst system. It is systematically displaced and moves (in and) out of the coordination sphere in a concerted action, while the monomer units approach for coordination to be paired again with the cation after the insertion process is complete. Assuming that the monomer approach proceeds along the most favorable path (i.e., via a *cis* approach with respect to the anion), immediately after the monomer insertion the anion is positioned at the outer coordination sphere, on the side of the polymer chain (Fig. 20a).

The resulting metalloocenium–polymeryl cation has an empty coordination site available for the re-formation of a close-contact ion pair with the anion. To avoid unnecessary steric interaction with the alky group (polymer chain), the anion can first undergo a spatial reorganization in the outer coordination sphere and then approach the free coordination site unhindered (Fig. 20b) [168, 169]. Alternatively, it can approach the cation directly, forcing in the process the polymer chain to move to the empty coordination site. The first process is what normally occurs during a syndiospecific propagation step (Fig. 20c), while the second process leads to the site epimerization since the immediate ion pairing and the simultaneous displacement of the polymer chain, results in a complex in which the polymer chain occupies the same coordination site as in the previous catalytic cycle (Fig. 20d).

Intuitively, it can be reasonably assumed that the anion reorganization in the outer coordination sphere is spontaneous and occurs freely; its rearrangement is governed purely by diffusion. Indeed, our gas-phase calculations [146] show that for the cation/anion model system, $Me_2C(CpFlu)ZrMe\text{-}Me\text{-}B(C_6F_5)_3$, the energy barrier is about 0.5 kcal/mol, and well within the error associated with the computational method. On the other hand, the formation of the close-contact ion pair is also an exothermic and

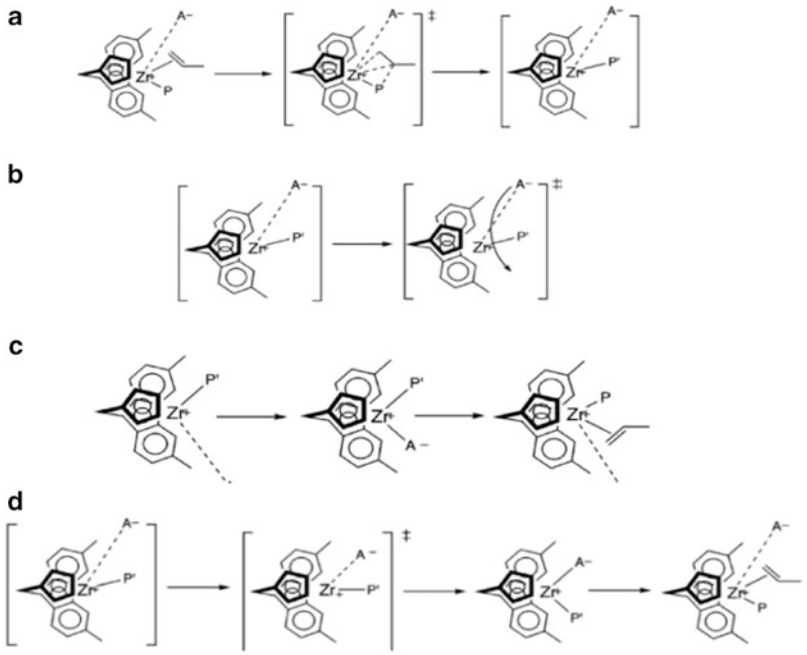

Fig. 20 Cation/anion (A^-) dynamics in the normal propagation process and in site epimerization. (**a**) The concerted process of monomer coordination and anion dissociation. (**b**) Diffusion-controlled process of anion rearrangement. (**c**) Normal chain migratory insertion/propagation. (**d**) Site epimerization

spontaneous process on the potential energy surface, as can be seen from the reaction coordinate shown in Fig. 21, which depicts the re-association of the $MeB(C_6F_5)_3^-$ anion to the metallocenium cation. The exothermicity of the ion pairing is so high (~20 kcal/mol) that the process is irreversible [146].

Ion pairing without previous anion reorganization has an activation barrier due to the fact that the agostic metal–alkyl interaction must be weakened, while repulsive interactions increase as the anion pushes the polymer chain to the other coordination site. During site epimerization, the β-agostic interaction is, however, maintained. The agostic interaction is only lost past the transition state, at a point where the energetic cost of its loss is overcompensated by the gain from the exothermic ion pairing reaction. The extent of the energy barrier depends on the overall charge distribution of the anion and on the substitution pattern of the ligand system.

The computed barriers to the site epimerization with the set of ligands selected for systems 1, 2, and 3 (shown in Scheme 1; see Sect. 3.2) in the gas phase and in toluene solution are given in Table 14. The counter-ion used for all these calculations is the $MeB(C_6F_5)_3^-$ anion. The calculated site epimerization energy barrier seems to decrease from system 1 (barrier of 3.3 kcal/mol) to system 2 (barrier of 2.6 kcal/mol). Only when the substituents are large enough, as is the case for system 3, are repulsive steric interactions increased and the barrier to site epimerization reaches its maximum (5.3 kcal/mol in the gas phase [146]).

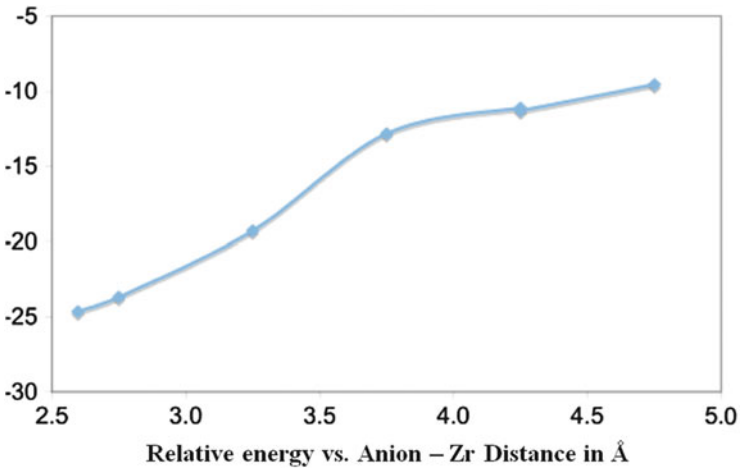

Fig. 21 Ion pairing in the regular polymerization mechanism in system 2, after the diffusion-controlled anion reorganization. Plot shows relative energy (in kcal/mol) versus anion–Zr distance (in Å)

Table 14 Dependence of the relative energies of the species involved in the site epimerization on the nature of the ligand system

	Gas phase			Solution (toluene)		
Catalyst	β-Agostic product	TS_{SE}	Ion pair	β-Agostic product	TS_{SE}	Ion pair
1	−5.3	−2.0	−23.9	−9.9	−5.9	−25.6
2	−4.3	−1.7	−23.0	−9.9	−6.5	−25.5
3	−5.9	−0.6	−22.9	−11.3	−4.8	−20.9

The counter-anion is $MeB(C_6F_5)_3^-$. All energies are relative to the respective parent close-contact ion-pair precursor and propylene. Relative energies in kcal/mol

As can be seen from Table 14, for all three systems, in general, the effect of solvation is to stabilize the transition state species involved, relative to the reactants, i.e., the $L_2Zr\text{-}iBu^+$ $MeB(C_6F_5)_3^-$ close-contact ion pair plus propylene.

To estimate the importance of the anion's charge distribution in the differential solvation of the species involved, the site epimerization of system 2 in the presence of three different anions was investigated. In addition to the already mentioned $MeB(C_6F_5)_3^-$, the site epimerization was studied with an anion developed by Marks, the fluoro-tris-perfluoro-biphenylaluminate, $FAl(Bif_f)_3^-$ anion [168, 169], and also with a model representing methylated MAO, MAO-Me^- [171, 172]. The reaction profiles in the gas phase and in toluene (marked COSMO) are shown in Fig. 22. The energies of the species are reported in Table 15. Marks' anion is much bulkier than $MeB(C_6F_5)_3^-$ and its negative charge is more concentrated on the fluorine, which bridges with the zirconocenium cation. The model for the methylated MAO also has the negative charge more concentrated in the part that interacts with the cation, compared to $MeB(C_6F_5)_3^-$, while its steric bulk is lower

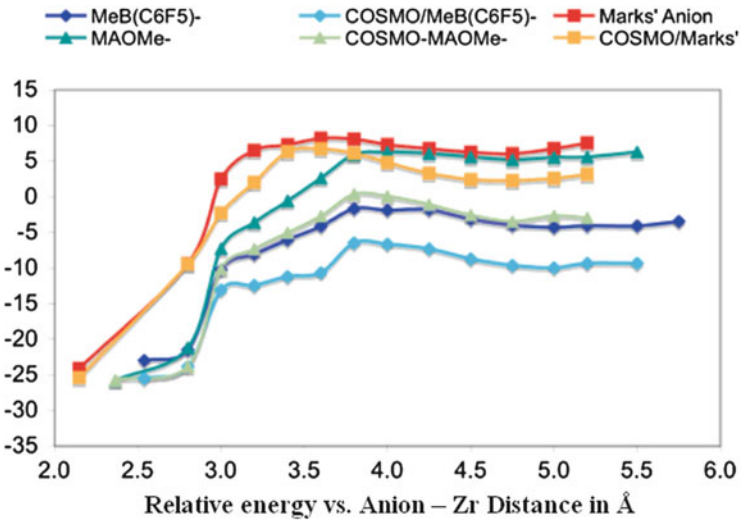

Fig. 22 Influence of the counter-ion on the site epimerization reaction profile in the gas phase and in toluene solution. The anions studied are $MeB(C_6F_5)_3^-$, $FAl(Bif_f)_3^-$ (Marks' anion), and a model for MAO-Me^-. Energies are relative to the respective parent ion pairs plus propylene of system 2. Plot shows relative energy (in kcal/mol) versus anion–Zr distance (in Å). *COSMO* (conductor-like screening model) relates to calculation in the solution phase, toluene [146]

Table 15 Dependence of the relative energies of the species involved in the site epimerization on the nature of the counter-anion

	Gas phase			Solution (toluene)		
Anion	β-Agostic product	TS_{SE}	Ion pair	β-Agostic product	TS_{SE}	Ion pair
$MeB(Ph_f)_3$	−4.3	−1.7	−23.0	−9.9	−6.5	−25.5
MAO	5.2	6.3	−25.8	−3.4	0.4	−25.7
$FAl(Bip_f)_3$	6.1	8.2	−24.1	2.3	6.7	−25.4

The ligand system is 2. All energies are relative to the respective parent close-contact ion-pair precursor and propylene. Relative energies in kcal/mol
TS_{SE} transition state for site epimerization

than that of $FAl(Bif_f)_3^-$ and comparable to $MeB(C_6F_5)_3^-$. The results obtained from gas-phase calculations suggest that site epimerization should occur most easily with a catalyst system that employs the MAO-Me^- anion ($\Delta E = 1.1$ kcal/mol) than with the catalysts formed with Marks' anion ($\Delta E = 2.1$ kcal/mol). The $MeB(C_6F_5)_3^-$ should be the best anion for suppressing the site epimerization to a minimum ($\Delta E = 2.6$ kcal/mol) [146].

However, when the solvation effects are considered, the correct qualitative trend is obtained: Marks' anion is the most effective in reducing the site epimerization ($\Delta E = 4.4$ kcal/mol), with the likelihood of site epimerization increasing when methylated MAO or $MeB(C_6F_5)_3$ are used to activate the Zr–Me bond of the precatalyst ($\Delta E = 3.8$ and 3.4 kcal/mol, respectively). The reason for this behavior

is twofold. First, Marks' anion interacts more strongly with the solvent than the other anions because its charge is the most localized. Therefore, solvent destabilization of the transition state with respect to the reactant is highest for Marks' anion. Second, the steric bulk makes it more difficult for the fluoroaluminate to get close to the zirconocenium cation. The MAO-Me^- model also has a more concentrated charge than $MeB(C_6F_5)_3^-$, which in solution has an effect similar to that found for Marks' anion but it is smaller and therefore the steric effects do not contribute as much to the barrier. The two effects combined are capable of explaining the experimental results.

It seems that the site epimerization mechanism, complex as it is, can be related to three main factors. Optimization of each would contribute to the lowering of its frequency of occurrence and to improvement in the stereoregularity and physical properties of the produced s-PP. Whereas a direct link could be establish between site epimerization and the ligand substituents' bulkiness and positions on one hand, and the anion's size and charge distribution on the other hand, the connection between structural flexibility and site epimerization, though proven empirically, is not very clear.

However, although optimization of the stereorigidity and substitutional factors are, more or less, controllable and within practical grasp, the anion–cation interaction, although very well understood, is in practice very difficult to implement in a large-scale catalyst manufacturing plant for commercial purposes. Understanding the effect of anion size, charge, and charge distribution on the site epimerization transition energy barrier in particular and controlling site epimerization in general, is of utmost importance not just for academic reasons but also for the commercialization of s-PP using large-scale supported catalysts.

6 Metallocene Molecular Symmetry and the Catalyst's Syndiotactic Specificity

In the previous sections, various factors affecting the stereospecificity of the syndiotactic-specific catalysts systems were discussed. A final topic that should be covered to complete these discussions is the relevance of the symmetry of the metallocene molecules and its role in the tactic behavior of the final catalyst. As shown in previous sections, for many different reasons the perfect bilateral symmetry of the original metallocene structure is most likely not maintained in the solution phase. The enantioselectivity calculations with model catalysts have also revealed that the catalyst system will behave in a syndioselective way as long as the conditions for the proper arrangement of ligand, polymer chain and minimum energy monomer coordination mode is provided at each coordination position. Thus, the legitimate question to be answered is whether the C_s or bilateral symmetry of a metallocene molecule is a good indicator for the syndiospecificity of the final catalyst.

All syndiotactic-specific catalysts that have been discussed so far had one principal element in common: their precatalyst's metallocene molecules in solid phase all presented bilateral molecular symmetry or a vertical plane of symmetry (σ_v) in the solid state. However, from the discussions in Sect. 4.3 it is clear that the whole notion of a "perfect" molecular symmetry, bilateral or otherwise, in the solution phase should be handled with caution and not t taken very literally. We saw that even with initially "perfect" bilateral symmetric metallocene molecules like **1** (**2**) and **6** (**7**), the perfect symmetry may be lost, at least in part, in solution and during different stages of the polymerization due to incessant η^5, η^3, and possibly η^1 reversible hapticity change or occasional ring slippage [149–160, 161, and references therein; 162, 163]. Thus, the question to be answered is whether or not the bilateral symmetry embodies the necessary and/or sufficient condition(s) for syndiotactic specificity of a catalyst system. It is apparent that a catalyst's syndiospecificity, as defined in preceding sections, is the result of the combined actions of several factors, the absence of any one of which could lead to the malfunctioning of the catalyst and destruction of the whole syndiospecificity process. The delicate steric balance between the three main participants (ligand, polymer chain, and monomer) as well as the interaction of cation with the counter-ion and proper functioning of the dynamic processes are all essential for its existence. Therefore, it should not be surprising if, occasionally, catalysts prepared with structurally "acceptable" metallocenes and with perfect bilateral symmetry do not function accordingly.

6.1 *Syndio- and Nonsyndiospecific Catalyst Systems with C_s Symmetric Metallocene Structures*

A disappointing example of this kind is the performance of the bilaterally symmetric complex dimethysilyl-(cyclopentadienyl-tetramethyl-cyclopentadienyl)$ZrCl_2$. After its activation with MAO and exposure to propylene, the resulting enantiotopic catalyst system does not function in a syndiotactic-specific manner and the polypropylene polymers that it produces are completely atactic. Here, obviously the presence of constantly rotating, relatively voluminous methyl groups, particularly those two placed in the distal positions (with respect to the bridge-head carbon of the substituted cyclopentadienyl group), blocks the central free space in front of the active site and interferes vigorously with the proper "head-down" coordination mode of propylene and disrupts completely the enantio-face selective process of the system.

Another example demonstrating the determining role of the molecular bilateral symmetry versus the (delicate and fragile) steric balance between the chain, monomer, and ligand substituents for the syndiospecificity process is the polymerization behavior of the metallocene complex diphenylmethylidene-(cyclopentadienyl-octahydrofluorenyl)$ZrCl_2$, with the chemical formula (η^5-C_5H_4-μ-CPh_2-η^5-$C_{13}H_{16}$)$ZrCl_2$, **8**.

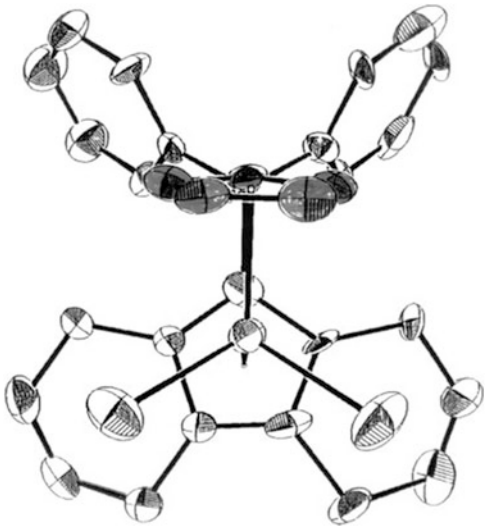

Fig. 23 Single-crystal X-ray-determined molecular structure of (η^5-C_5H_4-μ-CPh_2-η^5-$C_{13}H_{16}$)$ZrCl_2$, **8**

As mentioned in Sect. 2.4, complex **8** is prepared by selective hydrogenation of the fluorenyl moiety of the parent highly syndiotactic-specific metallocene molecule **6**. Its crystal structure is presented in Fig. 23. Complex **8** fulfills all symmetry requirements that one would expect a priori from a would-be syndiotactic-specific precatalyst molecule, nevertheless, after its activation with MAO and its exposure to propylene, complex **8** produces polypropylene chains with perfectly atactic microstructure [28, 30].

At a first glance, one could imagine that the minor changes in the size of the "substituents" resulting upon transformation of benzenic CH groups to slightly larger cyclohexylic CH_2 groups in the distal cyclic positions would be tolerated by the system and would not disturb the proper chain orientation and monomer coordination mode essential for the syndiospecific polymerization process. Closer look at the metallocene molecule **8** reveals that the change in substituent size from CH to CH_2, even though negligible, is concomitant with a dynamic phenomenon that might be the real disturbing factor. Hydrogenation of the six-membered rings transforms a flat "cyclohexatrien"-like cyclic system to a sterically more demanding, cyclohexene/cyclohexane-like aliphatic ring system involving dynamic boat/chair conformation interconversion. The flexible pseudo-cyclohexylic rings of the hydrogenated fluorenyl ligand moiety probably interfere more with proper chain orientation and the face-selective coordination mode of the monomer than the slight increase in the size of the substituents. This situation does not favor systematic and consecutive face-selective enchainment of the propylene monomers in an enantioselective manner conducive to formation of a stereoregular polymer chain.

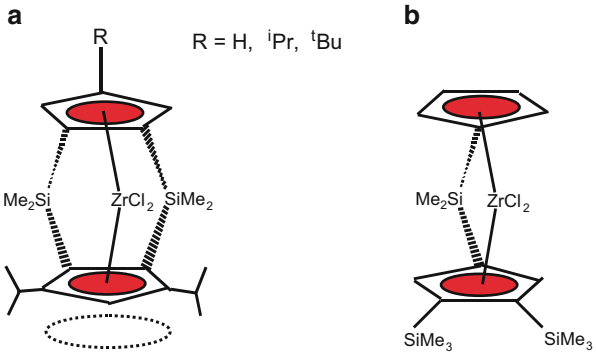

Fig. 24 Double-bridged syndiospecific (**a**) and nonsyndiospecific (**b**) structures [173–175]. *Dotted circle* indicates free space in the central position in front of the active site

6.2 *Other Types of C_s Symmetric Metallocene Catalysts with Syndio- and Nonsyndiospecific Behavior*

The double-bridged bis-cyclopentadienyl-based metallocene catalyst systems developed by Bercaw et al. [173–175] are excellent examples that can be employed to test further the universality of the syndiospecificity requirements for an independent check and verification by a new catalysts system with different ligand settings. The double-bridged zirconocene molecules shown in Fig. 24 do not contain any fluorenyl groups and yet they fulfill all structural and symmetry prerequisites for a potentially syndiotactic-selective metallocene catalyst. They resemble in their general molecular structure the molecules shown in Fig. 2 in that they have a bilateral symmetry and an unsubstituted cyclopentadienyl ring linked to a symmetrically substituted cyclopentadienyl ring (replacing fluorenyl) via a structural bridge.

Of these two structures, only the structure depicted in Fig. 24a acts in a syndiotactic-specific manner and, after activation with MAO, produces s-PP polymers. The structure depicted in Fig. 24b, despite its bilateral symmetry, behaves completely in a nonstereospecific way and, after activation with MAO and exposure to propylene monomer, produces atactic polypropylene. What makes the difference for these two systems is the fact that in the structure shown in Fig. 24a, the free space in the central position in front of the active site is maintained by the substituted cyclopentadienyl group and can accommodate the "head-down" oriented propylene's methyl group with respect to the growing polymer chain. This arrangement cannot be accommodated by the catalyst resulting from the metallocene structure presented in Fig. 24b. The two sterically encumbering germinal tri-methylsilyl groups entirely "fill" the central space and block the space needed for the methyl group "head-down" coordination mode of propylene (see Fig. 25). According to the authors, the double-bridge system exhibits very high stereospecificity (high stereorigidity!) and some of the doubly silylene-bridged zirconocene catalysts investigated by them have shown very high enantioselectivity (rrrr >99.5%) for insertion of α-olefins into zirconium–polymeryl bonds. Loss of stereospecificity in these catalysts occurs mainly by stereochemical inversion at the metal center, i.e., by site epimerization.

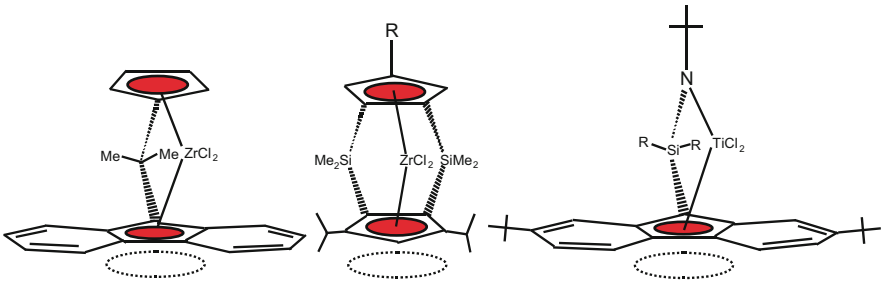

Fig. 25 Presentation of the central free space (*dotted circles*) and its importance for active site syndiospecificity

6.3 C_1 Symmetric Structures: Syndio- and Nonsyndiospecific Catalyst Systems

In the preceding section, the lack of syndiospecificity in certain catalyst systems prepared with bilaterally symmetric, prochiral metallocene molecules was discussed. On the other side of the spectrum, there are reports supporting the existence of many examples of syndiotactic-selective catalyst systems that are produced with metallocene molecules lacking any symmetry. These C_1 symmetric metallocene molecule precursors are capable of producing highly syndiotactic polypropylene [132, 133, 176, 177]. Several syndiotactic-specific catalysts produced with a C_1 symmetric metallocene precursor have been reported by several groups [132, 133, 176]. In these systems, the fluorenyl moiety of the ligand in complexes **1** and **6** is expanded via substitution, in a lop-sided manner, e.g., by fusing another aliphatic or aromatic six-membered ring to it. In these reported cases, the lack of C_s symmetry does not perturb the enantioselectivity of the resulting catalysts and even leads to a slight improvement in their enantioselectivity with respect to the parent catalysts made from complex **1**/MAO.

The most striking example for a C_1 symmetric syndiotactic-specific case is, however, the catalysts prepared with metallocene molecule, diphenylmethylidene-(cyclopentadienyl-3-*tert*-butyl-fluorenyl)zirconium dichloride **12**, with chemical formula (η^5-C_5H_4-μ-CPh_2-η^5-3-^{t}Bu-$C_{13}H_6$)$ZrCl_2$. Complex **12** is clearly a C_1 symmetric molecule, as can be seen from its single-crystal X-ray molecular structure depicted in Fig. 26 (right) [132, 133, 176, 177]. The symmetry-breaking substituent, a large *tert*-butyl group, is positioned at close proximity to the active transitional metal coordination sphere and one of its coordination positions; it interferes strongly with the growing polymer chain in a nonbonded steric manner. Nonetheless, after its activation with MAO, metallocene complex **12** polymerizes propylene to highly stereoregular s-PP chains. The syndiotacticities of the polymers produced with the **12**/MAO catalyst system are higher than of all the syndiotactic polymers produced with **1**/MAO, **5**/MAO, and **6**/MAO catalyst systems and ranks only below polymers produced with the **9**/MAO catalyst system. The s-PP produced

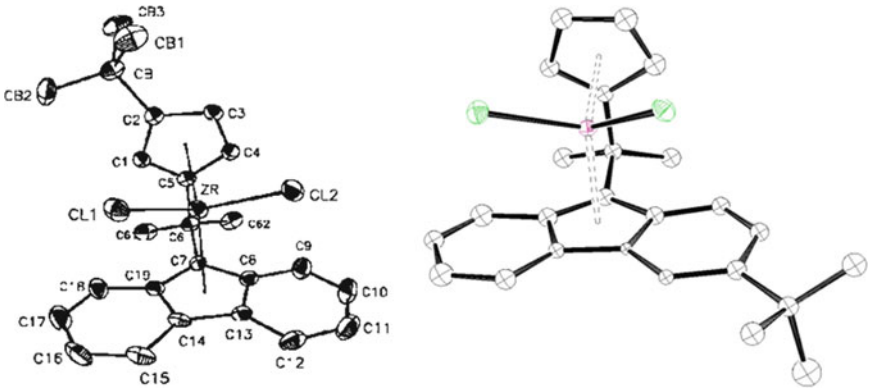

Fig. 26 Single-crystal X-ray molecular structures of (η^5-C_5H_4-μ-CPh_2-η^5-3-^{t}Bu-$C_{13}H_6$)$ZrCl_2$, **12** (*right*) and (η^5-3-^{t}Bu-C_5H_3-μ-CPh_2-η^5-$C_{13}H_7$)$ZrCl_2$, **13** (*left*)

with **11**/MAO at 60°C shows a stereoregularity-related rrrr pentad distribution of higher than 88% and a melting point of 143°C, with a molecular weight of 240 kDa [177].

The polymerization behavior of **12**/MAO might appear at first very surprising; however, a quick review of the principles discussed in previous sections discloses that the catalyst's performance is perfectly in line with all the principal elements, cited as prerequisites for having a high catalyst syndiotactic specificity. The *tert*-butyl group, located at position 3 of the fluorenyl moiety of the ligand, not only does not perturb the delicate balance described for catalyst systems **1** (and **6**)/MAO but also further enhances some of the steps involved in the enantioselective process. The bulky *tert*-butyl group is positioned just below one of the two coordination positions of the active site and interacts with the growing polymer chain strongly, in a "constructive" way, whenever it occupies this position. It reinforces the fluorenyl's role in pushing the polymer chain to move away from it and to adopt the mentioned "upward" chain conformation (this chiral chain conformation is conducive to a proper α-agostic interaction with the active site in the transition state). By doing so, it stabilizes further the enantioselective diastereomeric conformer's transition state and reduces the probability of occasional mis-insertion. The symmetry-breaking *tert*-butyl group makes this coordination position even more enantioselective and renders the catalyst **12**/MAO more enantioselective than the corresponding catalyst **1** (or **6**)/MAO. In this respect, catalyst **12**/MAO can be considered as having an intermediate enantioselectivity state between catalysts **6**/MAO and **9**/MAO.

The catalytic behavior of **12**/MAO is in direct contrast to another, structurally similar, C_1 symmetric catalyst system also prepared via modification of complex **1** with a *tert*-butyl group. However, in this case the *tert*-butyl group is placed at position 3 of the cyclopentadienyl moiety of its ligand. The metallocene molecule isopropylidene-(3-*tert*-butyl-cyclopentadienyl-fluorenyl)$ZrCl_2$, **13**, is prepared according to procedures described in Sect. 8. After its activation with MAO, the catalyst system becomes highly active for polymerization of propylene to

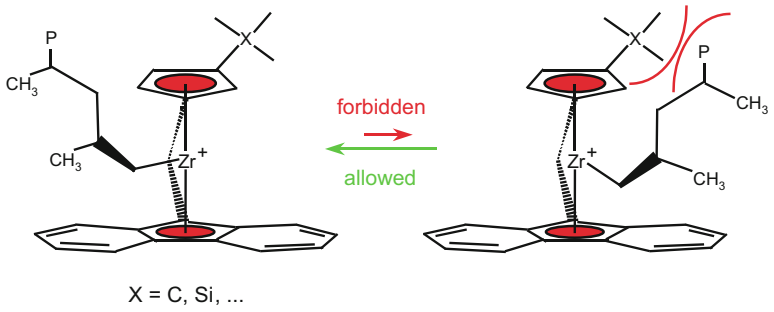

Fig. 27 Nonbonded steric repulsion between polymer chain and β-substituent provoking the systematic and predominant site epimerization

crystalline i-PP. In contrast to complex **12**, the bulky *tert*-butyl group in position 3 of the cyclopentadienyl in complex **13** poses a huge steric challenge to the polymer chain conformational orientation and blocks its systematic migration practically to a halt. Instead of the familiar chain migratory insertion, the polymerization process is dominated by systematic site epimerization, via forcing the growing polymer chain to return to its previous position after each insertion, effectively depriving the originally enantiotopic active site of one of its coordination positions. The overall effect of this *tert*-butyl substitution is the transformation of an originally syndiotactic-specific catalyst system to an isotactic-specific catalyst system. The molecular structure of complex **13** is depicted in Fig. 26 left. Figure 27 demonstrates schematically the ligand-induced site epimerization with the **13**/MAO catalyst system. Metallocene molecule **13** is the first example in a series of C_1 symmetric molecules that form the basis for a new important class of highly isospecific metallocene catalysts [32, 178–185].

6.4 *Other C_1 Symmetric but Syndiospecific Catalyst Systems*

Finally, to close this section, other examples of C_1 symmetric syndiospecific metallocene catalysts system that were reported by Waymouth et al. [186] are presented here briefly. Systematic investigations of the stereoselectivity of metallocene catalysts by these authors revealed that *ansa*-(3-*R*-indenyl)(Cp) zirconocene dichloride complexes whose representative example is depicted in Fig. 28 can generate, after their activation with MAO and exposure to propylene, s-PPs of low to intermediate stereoregularity. The authors report that the introduction of a substituent at position 3 of the indenyl moiety of the ligand will render the second coordination sites of these metallocene catalysts, initially nonstereoselective, stereoselective. Additionally, each of the coordination sites in these catalyst systems is selective and discriminatory with respect to the opposite "enantio"-faces of the propylene molecule. On the basis of the propylene concentration dependency of the

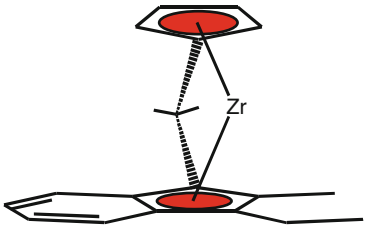

Fig. 28 Generic structure of syndiotactic-specific C_1 symmetric metallocene reported by Waymouth [186]

stereochemistry and an investigation of statistical modeling they implicate site epimerization or "back-skip" as the predominant contributor to the low stereospecificity of these metallocene catalysts. They claim that the indenyl's 2-substituent (the bridge-head position being position 1) in these catalyst systems helps to decrease their tendency to undergo site epimerization [186].

6.5 Industrial Production of Syndiotactic Polypropylene

In 1993, just about 5 years after the initial discovery of the metallocene-based syndiospecific catalyst systems and crystalline s-PP, the large scale commercial production of s-PP was announced by Fina Oil & Chemicals, at the time a subsidiary of Petrofina Belgium now itself an integrated part of the Total Petrochemical company. To reach this stage, 5 years of intensive preparatory work was needed by research groups and engineering teams from three companies: Fina Oil & Chemicals USA, Fina Research/Petrofina Belgium, and Mitsui Toatsu Japan (Mitsui Chemicals Inc). The preparations for the first industrial run with a supported metallocene catalysts focused mainly on challenges that were expected to be encountered during the following stages:

1. Pre-production phase: Large scale production, storage, and safe transportation of the supported metallocene catalyst to the production site.
2. Production phase: Employment of the Phillips loop reactor technology for the large-scale production of polypropylene with a supported metallocene catalyst for the first time ever.
3. Post-production phase: The processing conditions (addition, extrusion, pelletization, etc.) and product handling.

The general efforts to meet these challenges are described in the rest of this section, without the details and specifics that are given in the corresponding patents. These measures are common to all supported metallocene catalysts in commercial runs employing loop bulk or slurry processes.

6.6 Optimization of the Procedure for Synthesis of the Metallocene Molecule

The initial synthetic procedure developed for the synthesis and isolation of the pure metallocene dichloride samples included steps that required subambient reaction temperatures and chlorinated solvents such as methylene chloride [19, 20]. The recipe, though very convenient at smaller scales, was not very practical for the preparation of large quantities of, e.g., structures **1** or **6**. A new synthetic procedure that did not require the application of sub-zero temperatures and also eliminated the methylene chloride as solvent by replacing it with pentane resolved this issue [187, 188]. In the new procedure for the preparation of the metallocene molecule, the exact stoichiometric amount of the ligand's di-anion and $ZrCl_4$ are suspended in pentane and are reacted together. The procedure is effective in such a way that it does not necessitate any purification steps if the starting reagents are reacted together in stoichiometrically exact molar ratios. In this new "pentane procedure" the yield is practically quantitative.

6.7 Proper Choice of the Silica and MAO

For the industrial preparation of supported metallocene catalysts, selection of the inorganic support, generally a type of silica, is very important. There are many varieties of silica available in the market and each has different specifications with respect to the particle surface area, pore size (diameter, volume), bulk density, and mechanical properties [189–194]. The silica pore diameter and volume must be chosen bearing in mind that these pores will be partially filled with MAO.

Once the silica with desired properties is selected, the physically absorbed and chemically bonded (OH groups) excess water molecules have to be removed to reduce the number of OH groups and adjust their concentration to the selected MAO type and concentration in order to minimize excess usage the of MAO. The amount of fines formation during the polymerization, the bulk density of the polymer particles, and even the morphology of the final polymer particles depend, aside from the initial silica type, largely on the silica heat treatment regime and proper MAO treatment [189–194]. The heat treatment of the silica is also essential in ensuring optimum catalyst activity and, as mentioned, reducing the amount of MAO needed. It helps to reduce the amount of catalyst required and consequently the overall production cost. In contrast to silica, there are only a few known sources of MAO available commercially, with more or less similar compositions but different tri-methyl aluminum contents. No matter which of these MAO types is chosen, care must be taken to ensure the freshness and constancy of the product in each delivered batch to maintain the consistency of the resulting catalyst properties and of polymer production in the plant.

6.8 Large-Scale Preparation of the Supported Metallocene Catalysts

There are many different ways to combine the three main ingredients (metallocene molecule(s), MAO, and the silica) chemically to obtain the final supported metallocene catalysts. One of the most recommended procedures in the patent literature is to first treat the silica with MAO and then combine it with metallocene molecules. No matter which procedure is used, one must be aware that the resulting final heterogeneous metallocene catalyst is very reactive towards moisture, leading to its destruction, and to polar molecules that act as a very effective poison and deactivate the catalyst in an irreversible manner. The "long-term" storage of different batches of supported catalyst under inert atmosphere, in a temperate environment that excludes excessive heat, and with no exposure to light is essential for its constant activity and reliability.

6.9 Large-Scale Production of Syndiotactic Polypropylene

The Phillips process technology involving loop reactors, using liquid propylene both as the reaction medium and monomer, requires like any other continuous process meticulous control of polymerization conditions. Any deviations in temperature, pressure, liquid circulation velocity, etc. must be maintained within a very narrow range during the entire period of production. The process is very sensitive to formation of fines (very fine polymer particles), which are formed gradually during the polymerization and adhere to the reactor walls if the catalyst composition is not well defined or the set polymerization conditions not respected. With time, under the influence of the reactor wall temperature, these fines are transformed into a thin layer of polymer film that can act as an insulator and interfere with the reactor's temperature control system, leading to temperature and pressure fluctuations in the reactor. In severe cases, this phenomenon can lead to reactor fouling and shut down. The build-up of fines is generally avoided by the proper choice of silica particles, adjustment of the heat treatment regime, and the reaction conditions between silica support and MAO. The use of an antistatic agent is also not uncommon in moderate cases.

The polymer particle size, morphology, and bulk density are other important parameters for the maximum efficiency of the loop bulk process. Spherical or semi-spherical polymer particles of an average size of about 50–100 μm, with narrow particle size distribution and bulk densities close to or higher than 4 g/ml are generally desired. This is achieved primarily by the proper choice of silica particle morphology and the catalyst preparation conditions but also by adding a pre-polymerization step to the process during which the catalyst is first contacted with propylene, or other polymerizable monomers, at low concentration and moderate temperatures, before entering the main reactor.

6.10 Processing of Syndiotactic Polypropylene Polymers

Highly stereoselective metallocene catalysts, undergoing few site epimerization errors, that produce high crystallinity s-PP with melting points close to or higher than 160°C and fast crystallization rates are available for homogeneous polymerization [195–197]. The very same catalysts systems, however, when supported on a silica carrier, produce s-PP polymers with much lower melting points and crystallinities. Consequently, the crystallinities and crystallization rates decrease in heterogeneously produced s-PP polymer samples. For example, the same MAO-activated metallocene structure, in homogeneous and heterogeneous polymerization reactions, would produce two s-PP polymers whose melting points could differ by 5–20°C. Strangely, the higher the stereospecificity of the metallocene precatalyst and the higher the melting point of the homogeneous s-PP polymer, the lower is the melting point of the heterogeneously produced s-PP polymer counterpart, e.g., a metallocene structure providing s-PP polymers with a melting points around 132°C in homogeneous polymerization, produces s-PP polymers having melting points of about 127°C in heterogeneous polymerization under the same conditions. However, if the improved metallocene catalyst produces a s-PP polymer with a melting point of 160°C in a homogeneous polymerization [195–197, 198–202], the same structure under the same polymerization conditions produces a s-PP polymer with a melting point of only 140°C in heterogeneous polymerization. The analysis of the two polymers reveals that the heterogeneously produced polymer samples contain a much larger number of site epimerization-related errors, whereas the *meso* triad-related errors remain basically unchanged and almost equal for both polymer samples.

Therefore, and inadvertently, the s-PP resins that are produced industrially with supported metallocene catalysts have lower crystallinity and relatively low crystallization rates, which makes their processing challenging. The s-PP polymer melt that exits the extruder does not solidify quickly enough to proceed effectively with the pelletization process. In practice, one can mitigate the problem by addition of a nucleating agent or by cooling the extrudate. Another side-effect of the low crystallinity is that the commercially produced s-PP resins, with melting points below 130°C, contain a substantial amount of absorbed propylene monomer, which is released with time and necessitates vigorous aeration of the storage hanger. These handicaps hamper the fast and efficient extrusion and pelletization of very large quantities of commercially produced s-PP and have so far prevented its vast market penetration as a commodity product compared to other olefin-based thermoplastics.

7 Properties of Syndiotactic Polypropylene Polymers

7.1 Polymorphism of Syndiotactic Polypropylene

Syndiotactic polypropylene (s-PP) presents a very complex polymorphic behavior (the first part of this section on s-PP modifications is reported in the publication [203–212]). s-PP chains crystallize to various polymorphic crystalline phases and,

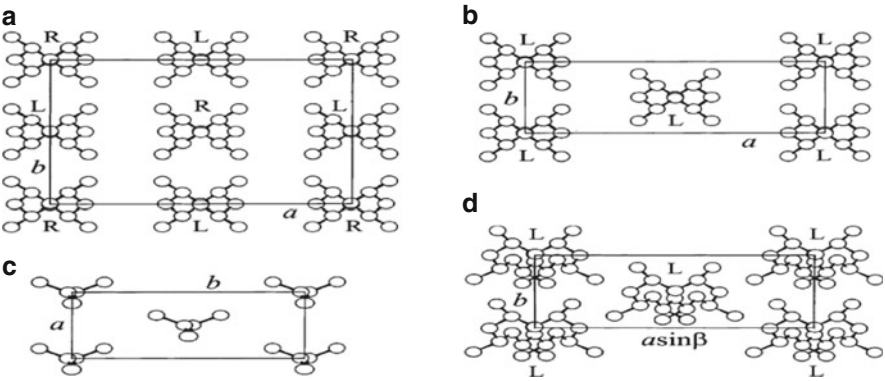

Fig. 29 Models of packing of the limit ordered (**a**) form I (axes $a = 14.5$ Å, $b = 11.2$ Å, $c = 7.4$ Å), (**b**) form II ($a = 14.5$ Å, $b = 5.6$ Å, $c = 7.4$ Å), (**c**) form III ($a = 5.22$ Å, $b = 11.7$ Å, $c = 5.06$ Å), and (**d**) form IV ($a = 14.17$ Å, $b = 5.72$ Å, $c = 11.6$ Å, $\beta = 108.8°$) of s-PP. *R* right-handed helix, *L* left-handed helix

depending on the degree of stereoregularity and the mechanical and thermal history, different degrees of statistical disorder are present in the crystal packing. Four crystalline forms (I–IV) have been described so far and are shown in Fig. 29. The most stable modification, which crystallizes under high crystallization temperature ($T_c > 130°C$) from melt or solution is defined as form I (Fig. 29a) and belongs to the space group Ibca. It is characterized by chains in the s(2/1)2 helical conformation packed in orthorhombic unit cells with axes $a = 14.5$ Å, $b = 11.2$ Å, and $c = 7.4$ Å. The axes of the helices are in the positions (0, 0, *z*) and (1/2, 0, *z*) of the unit cell, and the main X-ray peak in the powder spectrum appear at $d = 7.25$, 5.60, 4.70, and 4.31 Å ($2\theta = 12.2$, 15.8, 18.8, and 20.6°, Cu Kα). In an ideal lattice of form I, right handed (TTG^+G^+) and left handed (G^-G^-TT) helices alternate along the *a* and *b* axes, as imposed by the presence of the (211) reflection. Form II (Fig. 29b), was discovered during investigation of the X-ray diffraction spectra of drawn fibers of s-PP, and is characterized by chains in s(2/1)2 helical conformation packed in orthorhombic unit cells with axes $a = 14.5$ Å, $b = 5.60$ Å, and $c = 7.4$ Å. The axes of the helices are at $d = 7.25$, 5.22, and 4.31 Å ($2\theta = 12.2$, 17.0, and 20.6°, Cu Kα). The space group proposed for form II modification is $C222_1$, for which helices of the same chirality are included in the unit cell. The two metastable modifications, form III (Fig. 29c) and form IV (Fig. 29d), present chains in *trans*-planar and (T6G2T2G2) *n* helical conformations, respectively, and can be obtained only in oriented fibers. Form III is obtained by stretching at room temperature the compression-molded samples, as found by Natta et al. It is characterized by chains in zigzag *trans*-planar conformation. Its crystal structure has been reported recently [203–212] and belongs to the space group $P2_{1cn}$. In this form, the *trans*-planar chains are packed in orthorhombic unit cells with axes $a = 5.22$ Å, $b = 11.17$ Å, and $c = 5.06$ Å. The *trans*-planar form III has been, indeed, obtained by cold drawing procedures of low stereoregular s-PP samples or by stretching at room

temperature highly stereoregular samples prepared with metallocene catalysts. Finally, a form IV was obtained by exposing fiber specimens in the zigzag *trans*-planar form to various organic solvents (e.g., benzene, toluene) at room temperature. This form is characterized by helices with $(T_6G_2T_2G_2)_n$ conformation. A monoclinic unit cell has been proposed for this modification with $a = 5.72$ Å, $b = 7.64$ Å, and $c = 11.6$ Å (chain axis), $\alpha = 73.1°$, $\beta = 88.8°$, and $\Upsilon = 112.0°$. The hypothetical X-ray diffraction powder spectrum of this form would present main peaks at $d = 6.84$, 5.26, and 4.46 Å ($2\theta = 29°$, 16.8°, and 19.9°, Cu Kα).

The formation of the four crystalline modifications depends, as mentioned above, on the conditions of crystallization and the stereoregularity of the polymer sample. Form I, the thermodynamically stable form of s-PP is obtained under the most common conditions of crystallization, from the melt and/or precipitation from solution, in powder samples and single-crystals of s-PP. Form II is a metastable polymorph of s-PP and has been obtained only in oriented fibers of s-PP and, recently, by melt-crystallization at elevated pressure [203–212]. It can be also obtained by room temperature stretching of compression-molded specimens of low stereoregular s-PP samples prepared with vanadium-based Ziegler–Natta catalysts [10–17] or upon releasing the tension in stretched fibers of highly stereoregular s-PP samples initially in form III.

In fact, when highly stereoregular samples, prepared with homogeneous metallocene catalysts, are stretched at room temperature, the *trans*-planar form III is obtained, which transforms into the isochiral helical form II by releasing the tension. In powder of unoriented s-PP samples, only disordered modifications of form II, characterized by conformationally disordered chains containing *trans*-planar sequences (kink band defects) [213–215], can be obtained at atmospheric pressure, for instance, by precipitation from solutions of low stereoregular samples and in copolymers of s-PP with ethylene as the co-monomeric units. The metastable polymorphic forms II, III, and IV generally transform into the stable form I by annealing.

The complex polymorphic behavior of s-PP influences its macroscopic properties. For instance, oriented fibers of s-PP show an elastic behavior that is related to the structural organization. Unoriented compression-molded samples of s-PP behave like a typical highly crystalline material showing a plastic deformation upon stretching at room temperature. The crystalline domains, with chains in helical conformation, tend to assume a preferred orientation along the stretching direction to originate a plastic, irreversible, deformation. High orientation of the crystalline phase is generally achieved. Along with this plastic deformation, a phase transition from the most stable helical form into form III, with chains in the *trans*-planar conformation, gradually occurs. The phase transition is reversible: after release of the tension, the crystalline domains remain nearly oriented with the *c*-axis parallel to the preferred (stretching) direction, and the *trans*-planar form III transforms again into the more stable helical form. As a result, for previously unoriented material, a partial recovery of the macroscopic dimensions of the sample is attained. Therefore, unoriented samples show only fair or poor elastic properties. Stress-relaxed fibers show instead very good elastic behavior upon successive

stretching and relaxation; the helical form transforms by stretching into the *trans*-planar form, which transforms again into the helical form by releasing the tension, and a nearly total recovery of the initial dimensions of the fiber samples is observed. When the crystalline domains are already oriented along the stretching direction, i.e., when the sample has already undergone the plastic deformation, the fibers show good elastic properties. Of course, during the mechanical cycles the chains in the amorphous regions are also subjected to a reversible conformational transition from the "random coils" into extended conformations, and vice versa.

This reversibility of the transition is possibly assisted and is, somehow, favored by the polymorphic transition occurring in the crystalline regions. It has been suggested that although the driving force that induces the recovery of the initial dimensions in common elastomers upon release of the stress is mainly entropic, in the case of s-PP it is basically linked to the enthalpy gain achieved when the sample is relaxed due to the metastability of the *trans*-planar form III. On the other hand, it has been also hypothesized that the elastic behavior is mainly due to the conformational transition occurring in the amorphous phase for chains connecting the crystalline domains.

7.2 *Thermal Properties and the Origin of Multiple Melting Behavior of s-PP*

Differential scanning calorimetry (DSC) studies that were performed on the isothermal bulk crystallization and subsequent melting behavior of various s-PP resins from laboratory and commercially produced samples, indicate that most DSC endothermic traces exhibited two (or three) distinct melting endotherms, depending on the temperature at which the samples were crystallized. The DSC scans performed at different heating rates on as-polymerized or melt-crystallized forms of such samples generally present endotherms with a double peak shape. The increase in the enthalpy of the high-melting peak with decreasing heating rate is indicative of the occurrence of a recrystallization phenomenon during the heating process, whereby the less-ordered form II is partially transformed to the more ordered form I. This observation was made mainly for s-PP samples with stereoregularity lower than 90% (rrrr $< 90\%$); disordered modifications of form I are always obtained by melt crystallization. For highly stereoregular samples (rrrr $> 93\%$), only a single endothermic peak is observed, independent of the crystallization temperature of the isothermally melt-crystallized samples and the heating rate. The equilibrium melting temperature, T_m of the fully s-PP estimated to be 182°C, which is close to the value of 186°C found for i-PP [128]. Multiple melting behavior is not an exclusive phenomenon for s-PP. In fact, similar observations have been made on a number of other semicrystalline polymers, including some flexible polymers and some semi-stiff polymers.

Supaphol et al. [216–218] reviewed a number of hypotheses that have been proposed to explain the occurrence of multiple melting endotherm phenomena. In the studies on isothermal crystallization under quiescent conditions (i.e., crystallization is only a function of temperature), the multiple melting behavior of these semicrystalline polymers have been attributed to the following four phenomena: (1) the presence of two (or more) crystal modifications in the sample; (2) the presence of two (or more) crystalline morphologies; (3) the presence of two populations of crystal lamellae of different thicknesses; and (4) the simultaneous melting, recrystallization, and re-melting of the lamellae initially formed at the crystallization conditions.

7.3 *Syndiotactic Polypropylene: Physical and Mechanical Properties*

Compared to conventional i-PP produced with ZN catalysts, the s-PP produced commercially with supported metallocene catalyst has, due to its relatively low crystallinity, on the one hand, lower density, hardness, tensile strength, and flexural modulus and, on the other hand, higher clarity or transparency, impact strength, toughness (or elasticity), and stiffness. The melting point, density, hardness, crystallization temperature, heat of fusion, tensile strength at break, flexural modulus, and percent haze of s-PP all increase with increasing syndiotacticity of the polymer. The crystallization rate (defined customarily as the inverse of the time needed to attain one half of the final crystallinity multiplied by 100), crystallization temperature, and melting point are also all affected by the degree of stereoregularity of the polymer chains. The low temperature impact strength of s-PP decreases with decreasing temperature, but at 0°C it has still about two to three times higher impact strength than that of i-PP. Syndiotactic polypropylene also has different thermal properties to conventional i-PP and its glass transition temperature and heat of fusion are lower than those of i-PP. Unique properties of s-PP include good γ-ray internal stability and very low melting point for heat sealing. s-PP has also different thermal properties than the conventional i-PP. Its heat of fusion is lower than that of i-PP. Syndiotactic polypropylene also has different rheological behavior to i-PP; for example, regardless of the degree of its tacticity, s-PP has a much smaller melt flow than i-PP with comparable molecular weight. The rheological behavior of s-PP seems to indicate that, owing to its more flexible chain backbone structure, it contains a significantly higher number of molecular entanglements per unit volume than i-PP (see following section).

7.4 Syndiotactic Polypropylene: Processing and Rheology

Syndiotactic polypropylene has proven to process very differently from conventional i-PP, both in melt-phase processes and in solid-phase processes. At high shear rates, s-PP is more viscous and has higher elastic modulus than conventional i-PP, regardless of the degree of the tacticity. s-PP, has also a much smaller melt flow than that of the corresponding i-PP with the same molecular weight. s-PP has a lower crystallization rate than i-PP, and minor modifications are necessary when existing processing equipment designed for conventional i-PP is used for s-PP, e.g., s-PP needs a longer cycle time.

With a melting point of approximately 130°C (versus 160°C for i-PP) and crystallinity of approximately 30% (versus 55% for i-PP) for commercially produced s-PP, the discrepancies and the differences in solid-phase properties and processing seem obvious. As for the melt phase, the narrow molecular weight distribution of 2 for metallocene catalyst-based s-PP provides only part of the explanation for the observed differences in melt-phase properties. A cursory comparison with controlled-rheology i-PP (an ex-situ, extruder tailormade i-PP of very narrow MWD) makes one realize that must still be other reason(s), for the observed melt behavior. Polymer microtacticity could be one parameter to considered. When considering the molecular networks in high molecular weight polymer melts, the molecular weight and MWD are usually the only parameters compared at length for such linear polymers (long-chain branching does not usually exist in ZN polypropylenes). The effects of polymer chain tacticity are widely ignored in these rheological treatments. One reason is probably that it does not seem obvious why there should be a difference between amorphous polymer melts of i-PP and s-PP, each containing freely rotating molecules of similar chemistry (equal monomer units) in motion. However, polymer microtacticity appears to be the only other parameter that could provide the necessary explanations for the observed melt property differences for s-PP and i-PP.

Rheological studies have confirmed [219–221] that s-PP forms significantly more entanglements in the melt than its isotactic counterpart. Melt property effects are thus justified with this inherent difference in molecular chain flexibility and entanglement in mind. It is generally accepted that above a minimum (critical) molecular weight for each polymer type, there exists an equilibrium level (or distribution) of molecular entanglements in the molten phase. These chain entanglements contribute in expected ways to the observed rheological behaviors. In particular, they are imagined to act as minor "crosslinks," providing resistance to flow beyond the normal friction of molecule against molecule. In addition, each polymer backbone defines a characteristic flexibility (or rigidity) for interaction with its neighboring molecules. This also contributes to a polymer molecule's ability to move and fold around and amongst other like molecules in the melt. These two properties are obviously related.

The calculations performed by Wheat [220] for i-PP and s-PP also give surprising differences in these quantities. Essentially, based on this study, s-PP is

predicted to contain nearly three times the number of entanglements as i-PP, due primarily to tacticity differences alone! This would begin to explain many of the effects observed.

7.5 Market Applications

Although s-PP resins were originally designed for specialty markets, not yet served by conventional i-PP, it has the potential to compete against conventional i-PP, low density polyethylene (LDPE), linear low-density polyethylene (LLDPE), and polyvinyl chloride (PVC) in certain markets because of its toughness, impact strength, transparency, and low heat-seal temperature. As pure polymer, s-PP has found new applications and as a blend with i-PP it yields new properties that can be exploited in existing applications as a substitute for other polymers. Potential application areas include: (1) adhesives such as hot melt and functional grafting-type adhesives; (2) clear containers for sub-zero temperature usages; (3) preparation of color and/or additive concentrates; (4) elastomers; (5) extrusion products, especially those that must be sterilized by radiation, such as flexible bags and tubing; (6) fibers; (7) films, especially those requiring high clarity, toughness, and a low heat-sealing temperature, such as for snack food packaging; (8) injection molded products, especially those that must be sterilized by radiation, such as containers, rigid bottles, and syringes for medical use; (9) modifier and/or clarifier for resins such as i-PP; (10) modifier for polypropylene film; and (11) transparent sheets. A few important applications are reviewed below.

7.5.1 Injection Molding

The cycle time in injection molding with s-PP is significantly increased compared to that for i-PP. Because s-PP polymer thins less than i i-PP under shear, s-PP requires a longer boost time in injection molding and has a lower die swell than i-PP. Injection-molded s-PP samples and articles have lower haze, higher gloss, much higher notched Izod impact strength, lower flexural modulus (thus higher flexibility), lower Vicat softening temperature, and lower heat distortion temperature than similarly molded i-PP and copolymer containing 2% ethylbenzene. Their tensile properties are lower than that of i-PP and are comparable to that of the copolymer. s-PP homopolymer and clear impact resin also have higher Gardner impact at room temperature, higher light transmittance, and lower flexural modulus and haze than i-PP, i-PP copolymer, and s-PP-modified i-PP copolymer. After aging at room temperature, the tensile properties and flexural modulus of s-PP increases during the first 48 h, then the tensile properties begin to decrease and the flexural modulus begins to level off. s-PP also has a higher percentage decrease in elongation with time than i-PP homo- and copolymer at room temperature, probably due to the more pronounced secondary crystallization effect. The elongation at break of s-PP remains relatively stable at 130°C up to about 1,000 h. Injection-molded s-PP

samples were found to break up like a flexible polymer when exposed to 500 h of UV radiation, and the reduction in its intrinsic viscosity (or molecular weight) due to γ-ray irradiation is lower than that for i-PP.

7.5.2 Injection Blow Molding

Syndiotactic polypropylene resins allow the production of small flexible containers with very good γ-radiation resistance and a degree of transparency never achieved before with any polypropylene. Moreover, the final objects transmit a feeling by contact that has been qualified as "soft and warm." Only some highly expensive specialty and engineered polymers can achieve the same combination of properties, but require a significantly longer cycle time.

7.5.3 Films

Syndiotactic polypropylene can be heat-sealed at a lower temperature than conventional i-PP copolymers containing high levels of ethylene (sealing initiation temperature of around 100°C versus 110–120°C). s-PP films can be heat-sealed at a lower temperature than conventional ethylene/propylene copolymers containing 6% ethylene, e. g., $<$113°C versus $>\sim$119°C to develop a seal strength of 500 g/in., When compared with conventional i-PP, cast and blown films extruded from s-PP have much lower haze, much higher gloss, slightly higher elongation at yield, and comparable tensile strength at yield. Bi-axially oriented polypropylene (BOPP) films with improved shrink versus conventional BOPP films are obtained by blending a few wt% of s-PP into i-PP. The tensile, elongation, and optical properties and the impact strength of s-PP cast films are influenced by the melt temperature and chill roll temperature. Lowering the chill roll temperature leads to production of films with slightly higher tensile strength and elongation. Film extruded from an s-PP-modified random propylene copolymer has much lower haze, much higher gloss, slightly higher elongation at yield, comparable tensile strength at yield, slightly lower Elmendorf tear strength, and much lower Dart drop impact than that extruded from a ultra-low-density polyethylene (ULDPE)-modified random copolymer. It also has higher haze, gloss, Elmendorf tear strength, Dart drop impact, and elongation, and lower tensile strength at yield than films extruded from a propylene copolymer containing 2% ethylene and a conventional homopolypropylene.

7.5.4 Fibers

Addition of a few wt% of s-PP to i-PP before spinning dramatically improves the bulk and the softness of spun laid or staple nonwovens, two important techniques in fiber application. Moreover, the thermal bonding temperature is lowered by about 5–10°C, whereas the mechanical properties of the nonwovens are retained or slightly improved.

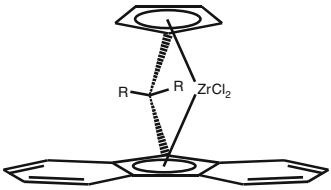

R = methyl (**1**), R = phenyl (**6**)

1

Fig. 30 Generic structure representing the simplest members of bridged cyclopentadienyl-fluorenyl zirconocenes (**1**)

7.5.5 Additive, s-PP/i-PP Blends

Syndiotactic polypropylene can be used as an impact modifier. Indeed, the addition of s-PP to i-PP can improve impact characteristics over pure i-PP [222–225]. When s-PP is blended with i-PP, the resulting resin has a processability better than that of i-PP and impact and transparency properties better than those of pure i-PP. As an impact modifier to a controlled rheology i-PP copolymer, s-PP does not crosslink or affect the peroxide efficiency of the copolymer while improving the Izod notched impact and maintaining the similar processability of the copolymer.

8 Experimental Details [187, 188]

8.1 Synthesis of Bridged, Cyclopentadienyl-Fluorenyl Zirconocenes.

The unsubstituted cyclopentadienyl-fluorenyl zirconocenes **1** and **6** (Fig. 30) are synthesized in two steps starting from the respective fulvenes and fluorene. All reactions are performed under inert gas atmosphere. All solvents are dry and free of oxygen.

For synthesis of the ligand, a solution of 150 mmol of fluorene dissolved in 200 mL of THF is cooled to 0°C. At this temperature, 93.75 mL (150 mmol) of a 1.6 M solution of methyllithium in diethylether is added dropwise. After the addition is completed, the resulting orange solution is stirred at room temperature for 4 h. Then, a solution of 150 mol of the respective fulvene in 100 mL of THF is added dropwise. After stirring at room temperature for 16 h, the mixture is hydrolyzed by careful addition of 200 mL of a saturated aqueous solution of ammonium chloride. The product **2** (Fig. 31) is extracted with diethyl ether as a white solid. Recrystallization from methanol:chloroform results in white needle-like crystals. Yield is 80% (R = Ph) to 100% (R = Me).

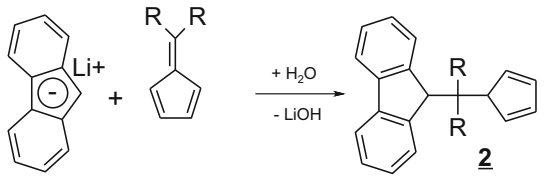

Fig. 31 General synthetic scheme for the preparation of bridged cyclopentadienyl-fluorenyl ligand (**2**)

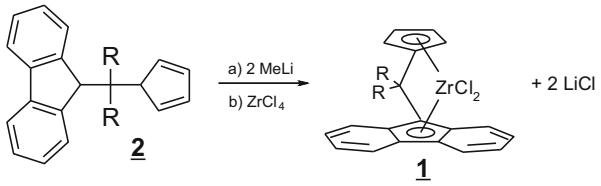

Fig. 32 General synthetic scheme for the preparation of bridged cyclopentadienyl-fluorenyl zirconocenes (**1**)

For synthesis of cyclopentadienyl-fluorenyl zirconocenes (Fig. 32), a solution of 42 mmol of **2** in 300 mL of THF is cooled to −78°C. At this temperature, 56.33 mL (84 mmol) of a 1.6 M solution of methyllithium in diethylether is added dropwise.

After 2 h, the cooling bath is removed and the red solution is stirred at room temperature for 8 h. Then, the solvent is removed in vacuo, resulting in an orange powder. This powder is suspended in 300 mL of pentane. Then 42 mmol of zirconium tetrachloride suspended in 100 mL of pentane is added. The mixture is stirred at room temperature for 6 h. Then, the insoluble red raw product is isolated by filtration. To separate from the lithium chloride, the raw product is taken up in 500 mL of methylene chloride and the turbid solution filtered over dried kieselgur. The resulting clear red solution is slowly evaporated and the product is isolated as a red crystalline precipitate [187, 188].

In Fig. 32, for R = Me the formula is $C_{21}H_{18}Cl_2Zr$. Percentage composition by analysis: C, 58.06; H, 4.14; Cl, 16.34; Zr, 20.99%. Percentage composition by calculation: C, 58.17; H, 4.19; Cl, 16.34; Zr, 20.07%.

For R =Me, results of ^{1}H NMR (CD_2Cl_2) ppm: δ = 8.1 (2H, m, 4,5-Flu), 7.8 (2H, m, 1,8-Flu), 7.5 (2H, m, 3,6-Flu), 7.2 (2H, m, 2,7-Flu), 6. 3 (2H, t, 3,4-Cp), 5.7 (1H, t, 2,5-Cp), 2.3 (6H, s, bridge-CH_3), where m, t and s signify multiplet, triplet and singlet, respectively.

For R = Ph, results of ^{1}H NMR (CD_2Cl_2) ppm: δ = 8.19 (2H, m, 4,5-Flu), 7.95 (2H, m, 2-Ph), 7.88 (2H, m, 5-Ph) 7.56 (2H, m, 3,6-Flu), 7.47 (2H, m, 4-Ph), 7.35 (2H, m, 3-Ph), 6.99 (2H, m, 2,7-Flu), 6.43 (2H, m, 1,8-Flu), 6.37 (2H, t, 3,4-Cp), 5.80 (2H, t, 2,5-Cp).

9 Outlook

The development of syndiospecific metallocene catalyst systems and s-PP from laboratory to commercial production has been one of the most successful projects both from scientific and technological points of view; it was driven mainly by the discovery of a new metallocene structure. During the 5 years of research and development there were many scientific, technical, and technological challenges, for example, regarding optimization of metallocene structure, its large scale production, supported catalyst development, process compatibility issues, polymer processing, and development of new product markets. Although the industrial production of s-PP has been a successful undertaking from both the technical and economic points of view, the production of s-PP has remained limited in volume and s-PP has been introduced to the market as rather a specialty product. There still exist afew handicaps that have hampered its large market penetration despite the attractiveness of its properties, particularly its excellent optical properties and its unusually high radiation resistance. The stumbling block on this road was and still is the slow crystallization rate of industrially manufactured s-PP. This originates from the low crystallinity, which in turn emanates from the presence of high numbers of the site epimerization-dependent *meso* dyad stereodefects in s-PP samples produced with supported catalyst systems.

Despite our good understanding of cation/anion dynamics in solution, our current understanding of the changes that the anionic MAO species undergo upon heterogenization on the silica is still limited and therefore our capability to control and or prevent the site epimerization processes is restricted.

We suspect either that the nature of the anionic species of MAO changes dramatically upon heterogenization to favor site epimerization-related pathway(s) or that, in heterogeneous polymerization, limitations in monomer-to-active site diffusion lower the effective monomer concentration at the active site and change the balance between the propagation rate and site epimerization rate in favor of the latter.[7]

[7] Incidentally, a very similar phenomenon is observed with C_2 symmetric bis-indenyl-based isospecific zirconocene dichloride catalysts. For example, the metallocene dimethylsilyl-bridged 2-methyl-4-phenyl-bisindenylzirconocenedichloride, once activated with MAO, produces an isotactic polypropylene with a melting point close to 160°C in liquid propylene at 60°C. However, the same catalyst, once supported on a silica carrier, produces i-PP polymers that have melting points ranging between 150 and 152°C, at the same polymerization conditions. In this case, the formation of larger amounts of region-irregular units in the heterogeneously produced i-PP is the melting point lowering factor. Interestingly, the bridged cyclopentadienyl-fluorenyl ligand-based C_1 symmetric isospecific catalyst systems are immune to this flaw. The homogeneously and heterogeneously produced isotactic polypropylenes with these catalysts show no or very few regio-irregular errors and their isotactic polypropylene polymer pairs have similar melting points that reach, for polymers produced with highly selective C_1 symmetric catalyst systems, values close to or even higher than 160°C.

No matter what the real causes behind the increased site epimerization rate in heterogeneous polymerization might be, the major challenge to s-PP resins becoming commodity products is the development of a heterogeneous catalyst system that does not trigger the mechanisms responsible for the acceleration of site epimerization processes. While waiting for this development, there exist two options for circumventing this dilemma in the short- or medium-term. Either operate the plant at lower temperatures and/or select the solution process as the technology of choice for the production of s-PP so that the heterogenization step becomes redundant. The first option will lead naturally to higher production costs and the second requires complete revision of the process conditions for the companies owning the technology.

References

1. Natta G, Pasquon I, Zambelli A (1962) J Am Chem Soc 84:1488
2. Natta G (1956) Chim Ind 38:751–765 (Chem. Abstr. 1957, 57, 11063)
3. Natta G (1960) Macromol Chem 35:94–131
4. Natta G, Pino P, Mazzanti G (1957) Gazz Chem Ital 87:528–548 (Chem. Abstr. 57, 88347)
5. Natta G, Corradini P, Ganis P (1960) Makromol Chem 39:238
6. Natta G, Pasquon I, Corradini P, Peraldo M, Pegoraro M, Zambelli (1960) A Atti Accad Nazl Lincei Rend Classe Sci Fis Mat Nat 28:539
7. Natta G, Pasquon I, Corradini P, Peraldo M, Pegoraro M, Zambelli A (1961) Rend Acc Naz Lincei 8(28): 539
8. Corradini P, Natta G, Ganis P, Temussi PA (1967) J Polym Sci C 16:2477
9. Natta G, Peraldo M, Allegra G (1964) Makromol Chem 75:215
10. Zambelli A, Gatti G, Sacchi C, Crain WO Jr, Roberts JD (1971) Macromolecules 4:45–477
11. Bovey FA, Sacchi MC, Zambelli A (1974) Macromolecules 7:752–754
12. Zambelli A, Tosi C, Sacchi C (1972) Macromolecules 5:649–654
13. Zambelli A, Wlofsgruber C, Zannoni G, Bovey FA (1974) Macromolecules 7:750–752
14. Zambelli A, Natta G, Pasquon I (1964) J Polym Sci 4:411
15. Zambelli A, Longo P, Terenghi S, Recupero D, Zannoni G (2000) J Mol Catal A 152:25–31
16. Lehr MH (1967) Macromolecules 1:178–184
17. Zambelli A, Sessa I, Grisi F, Fusco R, Accomazzi P (2001) Macromol Rapid Commun 22(5):297
18. Ewen JA, Jones LR, Razavi A, Ferrara JJ (1988) J Am Chem Soc 110:6255
19. Razavi A, Ferrara JJ (1992) J Organomet Chem 435:299
20. Razavi A, Atwood JA (1993) J Organomet Chem 459:117
21. Razavi A, Thewalt U (1993) J Organomet Chem 445:111
22. Razavi A, Ewen JA (2001) Syndiotactic polypropylene. Patent US 6,184,326, Fina Technology, Inc
23. Ewen JA, Razavi A (1995) Highly crystalline syndiotactic polypropylene. Patent US 5,476,914, Fina Technology, Inc
24. Razavi A, Ewen JA (1994) Patent US 5,334,677, Fina Technology, Inc
25. Ewen JA, Razavi A (1990) Process and catalyst for producing syndiotactic polyolefins. Patent US 4,892,851, Fina Technology, Inc
26. Elder MJ, Razavi A, Ewen JA (1993) Patent US 5,225,500, Fina Technology, Inc
27. Elder MJ, Razavi A, Ewen JA (1992) Patent US 5,155,080, Fina Technology, Inc

28. Razavi A, Bellia V, De Brauwer Y, Hortmann K, Peters L, Sirol S, Van Belle S, Thewalt U (2004) Macromol Chem Phys 205:347–356
29. Razavi A, Bellia V, De Brauwer Y, Hortmann K, Peters L, Sirol S, Van Belle S, Thewalt U (2004) Macromol Symp 213:157–171
30. Razavi A, Thewalt U (2006) Coord Chem Rev 250:155–169
31. Razavi A, Bellia V, Brauwer Y, Hortmann K, Peters L, Sirol S, Van Belle S, Marin V, Lopez M (2003) J Organomet Chem 684:206–215
32. Razavi A, Thewalt U (2001) J Organomet Chem 621:267–276
33. Razavi A, Vereecke D, Peters L, Den Dauw K, Nafpliotis L, Atwood JL (1995) Homogeneous Ziegler–Natta catalysts. In: Fink G, Muelhaupt R, Brintzinger HH (eds) Ziegler catalysts. Springer, Berlin, pp 112–147
34. Razavi A, Peters L, Nafpliotis L (1997) J Mol Catal A Chem 115:129
35. Sinn H, Kaminsky W, Vollmer HJ, Woldt R (1980) Angew Chem 92:396
36. Sinn H, Kaminsky W, Vollmer HJ, Woldt R (1980) Angew Chem Int Ed 19:390
37. Kaminsky W, Sinn H (1982) Homogeneous and high active Ziegler–Natta catalysts with alumoxane as component. In: Proceedings of the IUPAC 28th macromolecular symposium, Amherst, 1982, p 247
38. Kaminsky W, Miri M, Sinn H, Woldt R (1983) Macromol Rapid Commun 4:417
39. Herwig J, Kaminsky W (1983) Halogen free soluble Ziegler catalysts with methylalumoxane as cocatalyst. Polym Bull 9:464
40. Kaminsky W, Lüker H (1984) Macromol Rapid Commun 5:225
41. Kaminsky W (1984) Naturwissenschaften 71:93
42. Kaminsky W (2004) J Polym Sci A Polym Chem 42:3911–3921
43. Schnutenhaus H, Brintzinger HH (1979) Angew Chem Int Ed Engl 18:777–778
44. Wild FRWP, Zsolnai L, Huttner G, Brintzinger HH (1982) J Organomet Chem 232:233–247
45. Wild FRWP, Wasiucionek M, Huttner G, Brintzinger HH (1985) ansa-Metallocene derivatives. IIV. J Organomet Chem 288:63–67
46. Ewen JA (1984) J Am Chem Soc 106:6355–6364
47. Kaminsky W, Külper K, Brintzinger HH, Wild FRWP (1985) Angew Chem 97:507–508
48. Kaminsky W, Külper K, Brintzinger HH, Wild FRWP (1985) Angew Chem Int Ed Engl 24:507–508
49. Kaminsky W, Miri M (1985) Ethylene propylene diene terpolymers produced with a homogeneous and highly active zirconium catalyst. J Polym Sci A Polym Chem 23:2151
50. Kaminsky W (1985) Polym Prepr 26(2):373
51. Kaminsky W, Külper K, Niedoba S (1986) Macromol Symp 3:377
52. Kaminsky W (1986) Angew Makromol Chem 145/146:149
53. Kaminsky W, Niedoba S (1987) CLB Chemie für Labor und Betrieb 38:398
54. Soga K, Shiono T, Takemura S, Kaminsky W (1987) Macromol Rapid Commun 8:305
55. Werner RW, Brintzinger HH, Rieger B, Zolk R (1990) Angew Chem Int Ed Engl 29(3):279–280
56. Arlman EJ, Cossee P (1964) J Catal 3:99–104
57. Cossee P (1960) Tetrahedron Lett 17:12–16
58. Cossee P (1960) Tetrahedron Lett 17:17–21
59. Cossee P (1964) J Catal 3:80–88
60. Breslow D, Newburg NR (1959) J Am Chem Soc 81:81–86
61. Green MLH (1972) Pure Appl Chem 30:373–388
62. Ivin KJ, Roony JJ, Stewart CD, Green MLH, Mahtab R (1978) J Chem Soc Commun 1978:604–606
63. Brookhart M, Green MLH (1983) J Organomet Chem 205:395–408
64. Corradini P, Barone V, Fusco R, Guerra G (1979) Eur Polym J 15:1133
65. Pino P, Muelhaupt R (1980) Angew Chem 92:869–887
66. Zambelli A, Sacchi MC, Locatelli P, Zannoni G (1982) Macomolecules 15:211–212
67. Zambelli A, Locatelli P, Sacchi MC, Tritto I (1982) Macromolecules 15:831–834

68. Farina M (1987) Top Stereochem 17:1–111
69. Corradini P, Guerra G, Vacatello M, Villani V (1988) Gazz Chem Ital 118:173–177
70. Cheng HN, Ewen JA (1989) Makromol Chem 190:1931–1934
71. Cavallo L, Guerra G, Oliva L, Vacatello M, Corradini P (1989) Polym Commun 30:16–19
72. Cavallo L, Guerra G, Vacatello M, Corradini P (1991) Macromolecules 2:1784–1790
73. Guerra G, Cavallo L, Moscardi G, Vacatello M, Corradini P (1994) J Am Chem Soc 116:2988–2995
74. Zambelli A, Proto A, Longo P (1995) In: Fink G, Mülhaupt R, Brintzinger HH (eds) Zeigler catalysts: recent scientific innovations and technological improvements. Springer, Berlin, pp 217–235
75. Corradini P, Guerra G, Cavallo L, Moscardi G, Vacatello M (1995) In: Fink G, Mülhaupt R, Brintzinger HH (eds) Zeigler catalysts: recent scientific innovations and technological improvements. Springer, Berlin, pp 237–249
76. Toto M, Cavallo L, Corradini P, Moscardi G, Resconi L, Guerra G (1998) Macromolecules 31:3431–3438
77. Dyachkovskii FS, Shilova AK, Shilov AE (1967) J Polym Sci C Polym Symp 16(4):2333–2339
78. Zefirova AK, Shilov AE (1961) Dokl. Akud Nuuk SSSR 136.599; Dokl. Chem (Engl. Translation) p 13677
79. Eisch JJ, Piotrowski AM, Brownstein SK, Gabe EJ, Lee FL (1985) J Am Chem Soc 107:7219
80. Jordan RF, Dasher WE, Echols SF (1986) J Am Chem Soc 108:1718–1719
81. Jordan RF, Echols SF (1987) Inorg Chem 26:383–386
82. Jordan RF, Bajgur CS, Willett R, Scott B (1986) J Am Chem Soc 108:7410–7411
83. Taube R, Krukowka L (1988) J Organomet Chem 347(1–2):C9–C11
84. Hlatky G, Turner H, Eckman R (1989) J Am Chem Soc 111:2728
85. Eshuis JJW, Tan YY, Teuben JH, Renkema J, Evens GG (1992) Organometallics 11:362–369
86. Eshuis JJW, Tan YY, Teuben JH, Renkema J (1990) J Mol Catal 62:277–287
87. Jordan RF (1991) Adv Organomet Chem 32:325–387
88. Borkowsky S, Baenziger NC, Jordan RF (1993) Organometallics 12:486–495
89. Jordan RF, Guram AS (1990) Organometallics 9:2116–2123
90. Hlatky G, Eckman R, Turner H (1992) Organometallics 11:1413
91. Hlatky G (2000) Chem Rev 100:1347
92. Bochmann M (2010) Organometallics 29:4711–4740
93. Bochmann M (1996) J Chem Soc Dalton Trans 1996:255–270
94. Chen EYX, Marks TJ (2000) Chem Rev 100:1391–1434
95. Li H, Marks TJ (2006) Proc Natl Acad Sci 103:15295–15302
96. Ustynyk LY, Fushman EA, Razavi A (2006) Kinet Catal 47(2):213–220
97. Riechert KH (1970) Angew Makromol Chem 12:175
98. Piers WE, Bercaw JE (1990) J Am Chem Soc 112:9406–9407
99. Krauledat H, Brintzinger HH (1990) Angew Chem Int Ed Engl 29:1412–1413
100. Prosenc MH, Janiak C, Brintzinger HH (1992) Organometallics 11(12):4036–4041
101. Leclerc MK, Brintzinger HH (1995) J Am Chem Soc 117:1651–1652
102. Burger BJ, Cotter WD, Coughlin EB, Chacon ST, Hajela S, Herzog TA, Kohn RO, Mitchell JP, Piers WE, Shapiro PJ, Bercaw JE (1995) In: Fink G, Muelhaupt R, Brintzinger HH (eds) Ziegler catalysts. Springer, Berlin
103. Grubbs RH, Coates GW (1996) Acc Chem Res 29:85–95
104. Herzog TA (2007) PhD Thesis, California Institute of Technology, Pasadena
105. Maurice Brookhart M, Malcolm LH, Green MLH, Parkin G (2007) PNAS 104(17):6908–6914
106. Dahlman M, Erker G, Nissinen M, Froehlich R (1999) J Am Chem Soc 121:2820–2828
107. Shapiro PJ (2002) Coord Chem Rev 231:67–81
108. Zachmanoglou CE, Melnick JG, Bridgewater BM, Churchill DG, Parkin G (2005) Organometallics 24:603–611
109. Peifer B, Welch MB, Alt HG (1997) J Organomet Chem 544:115–119
110. Alt HG, Milius W, Palackal SJJ (1994) Organomet Chem 472:113

111. Alt HG, Milius W, Palackal SJJ (1994) J Organomet Chem 472:113–118
112. Schertl P, Alt HG (1999) J Organomet Chem 582:328–337
113. Razavi A, Vereecke D, Peters L, Den Dauw K, Nafpliotis L, Atwood JL (1995) Homogeneous Ziegler–Natta catalysts. In: Fink G, Muelhaupt R, Brintzinger HH (eds) Zeigler catalysts. Springer, Berlin, pp 112–147
114. Kim I, Kim K, Lee MH, Do Y, Won M (1988) J Appl Polym Sci 70:973–983
115. Flory PJ (1953) Principles of polymer chemistry. Cornell University Press, Ithaca
116. Hamilton P, Song H, Luss D (2007) AIChE J 53(3):687–694
117. Liu J, Rytter E (2001) Macromol Rapid Commun 22(12):952–956
118. Razavi A (2008) Patent US 2008/0214759 Al, Total Petrochemicals Inc
119. Razavi A, Debras G (1998) Patent US 005,719,241A, Fina Research, S.A
120. Razavi A (2006) Patent US 2006/0,068,985 Al, Fina Technology Inc
121. Razavi A (2008) Patent US 2008/0,108,766 Al, Fina Technology Inc
122. Lauher JW, Hoffmann R (1967) J Am Chem Soc 98:1729
123. Alt HG, Zenk R, Milus W (1996) J Organomet Chem 514:257–270
124. Yano A, Endo K, Kaneko T, Sone M, Akitomo A (1999) Macromol Chem Phys 200:1542–1553
125. Alt HG, Jung M (1998) J Organomet Chem 568:87–112
126. Razavi A, Vereecke D (1999) Patent US 006,002,033A, Fina Research S. A
127. Resconi L, Cavallo L, Fait A, Piemontesi F (2000) Chem Rev 100:1253–1345
128. Boor J Jr (1979) Ziegler–Natta catalysts for polymerization. Academic, New York
129. Drago D, Pregosin PS, Razavi A (2000) Organometallics 19(9):1802–1805
130. Alt HG, Jung M, Kehr GJ (1998) J Organomet Chem 562:153–181
131. Ewen JA, Elder M, Jones LR, Haspeslagh L, Atwood JL, Bott SG, Robinso K (1991) Makromol Chem Makromol Symp 48/49:253–295
132. Alt HG, Koeppl A (2000) Chem Rev 100:1205–1221
133. Miller SA, Bercaw JE (2004) Organometallics 23:1777–1789
134. Alt HG, Zenk R (1996) J Organomet Chem 526:295–302
135. Alt HG, Zenk R (1996) J Organomet Chem 522:39–54
136. Razavi A, Marin V (2010) Patent US 2010/0,016,528 A1, Fina Technology Inc
137. Zuccaccia C, Stahl NG, Macchioni A, Chen MC, Roberts JA, Marks TJ (2004) J Am Chem Soc 126:1448–1464
138. Chen MC, Roberts JA, Marks TJ (2004) J Am Chem Soc 126:4605
139. Van der Leek V, Angermund K, Reffke M, Kleinschmidt R, Goretzki R, Fink G (1997) Chem Eur 3:585–591
140. Cavallo L, Guerra G, Vacatello M, Corradini P (1991) Macromolecules 24:1784–1790
141. Borreli M, Busico V, Cipullo R, Ronca S, Budzelaar PHM (2003) Macromolecules 36:8171–8177
142. Rappe AK, Polyakov OG, Bormann-Rochette LM (2007). In: Baugh LS, Canich JAM (eds) Stereoselective polymerization with single-site catalysts. CRC, Boca Raton, pp 169–200
143. Guerra G, Longo P, Corradini P, Resconi L (1997) J Am Chem Soc 119:4394–4403
144. Angermund K, Fink G, Jensen VR, Kleinschmidt R (2000) Chem Rev 100:1457–1470
145. Angermund K, Fink G, Jensen VR, Kleinschmidt R (2000) Macromol Rapid Commun 21:91–97
146. Tomasi S, Razavi A, Ziegler T (2007) Organometallics 26:2024–2036
147. Rowley CR, Woo TK (2011) Organometallics 30(8):2071–2074
148. Razavi A, Baekelmans D, Bellia V, De Bauwer Y, Hortmann K, Lambrecht M, Miserque O, Peters L, Van Belle, S (1999) Syndiotactic and isotactic specific metailocene catalysts with hapto-flexible cyclopentadienyl-fluorenyl ligand. In: Kaminsky W (ed) Metalorganic catalysts for synthesis and polymerization. Springer, Berlin, pp 236–247
149. Huttner G, Brintzinger HH, Bell LG, Friedrich P, Bejenke V, Neugebauer D (1978) J Organomet Chem 145:329–333
150. Kowala C, Wunderlich JA (1976) Acta Crystallogr B32:820–823

151. Rerek ME, Basolo F (1983) Organometallics 2:372–376
152. Schonberg PR, Paine RT, Compana DF, Duesler EN (1982) Organometallics 1:799–807
153. Rerek ME, Basolo F (1984) J Am Chem Soc 106:5908–5912
154. Nesmeyanov AN, Ustynyuk NA, Makraova LG, Andrinov VG, Struchkov YT, Andrae S (1978) J Organomet Chem 159:199
155. Basolo F (1986) Isr J Chem 27:233
156. Nesmeyanov NA, Ustynyuk LG, Makraova VG, Andrinov YT, Struchkov S, Andrae J (1978) Organomet Chem 159:199
157. Faller JW, Crabtree RH, Habib A (1985) Organometallics 4:929–935
158. Calhorda MJ, Veiros LF (2003) Inorg Chim Acta 350:547–556
159. Goncalves IS, Ribeiro-Claro P, Romao CC, Royo B, Tavares ZM (2002) J Organomet Chem 648:270–279
160. Calhorda MJ, Felix V, Lu´s F, Veiros LF (2002) Coord Chem Rev 230:49–64
161. Calhorda MJ, Veiros LF (2001) J Organomet Chem 635:197–203
162. Vicente J, Abad JA, Bergs R, Peter G, Jones PG, Carmen M, de Arellano R (1996) Organometallics 15:1422–1426
163. Vicente J, Abad JA, Bergs R, Jones PG, Carmen M, de Arellano R (1996) Organometallics 15:1422–1426
164. Kabi-Satpathy A, Bajgur CS, Reddy KP, Petersen JL (1989) J Organomet Chem 364:105–117
165. Jolly CA, Marynick DS (1989) Inorg Chem 28:2893–2895
166. Castonguay LA, Rappe AK (1992) J Am Chem Soc 114:5832–5842
167. Bierwagen EP, Bercaw JE, Goddard WA (1994) J Am Chem Soc 116:1481–1489
168. Chen MC, Marks TJ (2001) J Am Chem Soc 123:11803–11804
169. Chen EY-C, Marks TJ (2000) Chem Rev 100:1391–1434
170. Graf M, Angermund K, Fink G, Thiel W, Vidar R, Jensen R (2006) J Organomet Chem 691(21):4367–4378
171. Zurek E, Ziegler T (2001) Organometallics 21(1):83–92
172. Zurek E, Ziegler T (2004) Prog Polym Sci 29:107–148
173. Timothy A, Herzog TA, Deanna L, Zubris DL, Bercaw JE (1996) J Am Chem Soc 118:11988–11989
174. Miyake S, Bercaw JE (1998) J Mol Catal A Chem 128:29–39
175. Veghini D, Henling LM, Burkhardt TJ, Bercaw JE (1999) J Am Chem Soc 121:564–573
176. Price CJ, Zeits PD, Reibenspies JH, Miller SA (2008) Organometallics 27:3722–3727
177. Razavi A, Bellia V (2010) Patent US 2010/0,016,528 A1, Fina Technology Inc
178. Razavi A, Atwood JL (1995) J Organomet Chem 497:105–111
179. Razavi A, Vereecke D, Peters LD, Dauw K, Atwood JL (1995) Macromol Symp 89:345
180. Razavi A, Atwood JL (1996) J Organomet Chem 520:115–125
181. Razavi A, Bellia V, Baekelmans D, Slawinsky M, Sirol S, Peters L, Thewalt U (2006) Kinet Catal 47(2):257–267
182. Miller SA (2007) J Organomet Chem 692:4708–4716
183. Tomasi S, Razavi A, Ziegler T (2009) Organometallics 28(8):2609–2618
184. Tomasi S, Razavi A, Wang D, Ziegler T (2008) Organometallics 27(12):2861–2867
185. Min EY-J, Byers JA, Bercaw JE (2008) Organometallics 27(10):2179–2188
186. Gomez FJ, Waymouth RM (2002) Macromolecules 35:3358–3368
187. Razavi A, Hortmann K, Bellia V (2002) In: Hermann WA (ed) Synthetic methods of organometallic and inorganic chemistry, vol 10. Thieme, Stuttgart, pp 185–193
188. Razavi A (1992) Process for the preparation of metallocenes. Patent US 005,117,020A. Fina Research, S.A
189. Razavi A (2006) Catalyst comprising a metallocene with two tetrahydroindenyl ligand for producing a polyolefin. Patent US 007,041,756B2, Total Petrochemicals Research Feluy
190. Razavi A, Debras G (1998) Process for producing polyolefins and polyolefin catalysts. Patent US 005,719,241A, Fina Research, S.A

191. Przybyla C, Zechlin J, Steinmetz B, Tesche B, Fink G (1999) Influence of the particle size of silica support on the kinetics and the resulting polymer properties at the polypropylene polymerization with heterogeneous metallocene catalysts; part I: experimental studies and kinetic analysis. Metalorganic Catal Synth Polymerization 1999:321–332
192. Tisse VF, Prades F, Briquel R, Mckenna TFL (2010) Role of silica properties in the polymerisation of ethylene using supported metallocene catalysts. Macromol Chem Phys 211(1):91–102
193. Tisse VF, Briquel RM, Mckenna TFL (2009) Influence of silica support size on the polymerisation of ethylene using a supported metallocene catalyst. Macromol Symp Spec Issue React Eng Polyolefins 285(1):45–51
194. Bonini F, Fraaije V, Fink G (1995) Propylene polymerization through supported metallocene/MAO catalysts. J Polym Sci A Polym Chem 33(14):2393–2402
195. Marin V, Razavi A (2009) Fluorenyl catalysts composition and olefin polymerization process. Patent US 7,514,510 B2, Fina Technology, Inc
196. Marin V, Razavi A (2009) Syndiotactic polypropylene and methods for preparing the same. Patent US 7,538,167B2, Fina Technology, Inc
197. Marin V, Razavi A (2006) Process for preparation of substituted fluorene. Patent US 7,094,938, Fina Technology, Inc
198. Marin V, Razavi A (2008) Syndiotactic polypropylene and methods of preparing same. Patent US 2008/097,052 A1, Fina Technology Inc
199. Marin V, Razavi A (2008) Stereoregular fluorenyl catalyst compositions for olefin polymerization process gaining polymers with different properties. Patent WO 2008/014,217 A2 2008/0,131, Fina Technology Inc
200. Razavi A (2004) Synthesis of hydrogenated metallocene catalyst for olefin polymerization and polyolefins prepared thereby. Patent WO 2004/078,798 A2 2004/0,916, Fina Technology Inc
201. Razavi A (2002) Production of syndiotactic polyolefins by fluorenyl-containing metallocene catalysts. Patent EP 1,179,553 A1 2002/0,213, Fina Technology Inc
202. Razavi A (2000) Metallocene catalyst technology and environment. CR Acad Sci IIC Chem 3:615–625
203. De Rosa C, Gargiulo MC, Auriemma F, Ruiz de Ballesteros O, Razavi A (2002) Macromolecules 35:9083–9095
204. De Rosa C, de Ballesteros OR, Santoro M, Auriemma F (2003) Polymer 44:6267–6272
205. Stocker W, Schumacher M, Graff S, Lang J, Wittmann JC, Lovinger AJ, Lotz B (1994) Macromolecules 27(23):6948–6955
206. Lotz B, Lovinger AJ, Cais RE (1988) Macromolecules 21:2375
207. Lovinger AJ, Lotz B, Davis DD (1990) Polymer 31:2253
208. Lovinger AJ, Davis DD, Lotz B (1991) Macromolecules 24:552
209. Lovinger AJ, Lotz B, Davis DD, Schumacher M (1994) Morphology and thermal properties of fully syndiotactic polypropylene. Macromolecules 27(22):6603–6611
210. Tsukruk VV, Reneker DH (1995) Macromolecules 28(5):1370–1376
211. Harasawaa J, Ueharaa H, Yamanobea T, Komotoa T, Terano M (2003) Macromolecules 36:6472–6483
212. Thomann R, Wang C, Kressier RJ, Juengling S, Muelhaupt R (1995) Polymer papers. Polymer 36(20):3795–3801
213. Hahn T, Suen W, Kang S, Hsu SL, Stidham HD, Siedle AR (2001) Polymer 42:5813–5822
214. Loos J, Schauwienold A-M, Yan S, Petermann J, Kaminsky W (1997) Polym Bull 38:185–189
215. Lovinger AJ, Lotz B, Davis DD, Padden FJ Jr (1993) Macromolecules 26(14):3494–3503
216. Supaphol P, Spruiell JE, Lin J (2000) Polym Int 49:1473–1482
217. Supaphol P (2001) J Appl Polym Sci 82:1083–1097
218. Supaphol P (2001) J Appl Polym Sci 79:1603–1609

219. Eckstein A, Suhm J, Friedrich C, Maier RD, Sassmannshausen J, Bochmann M, Muelhaupt R (1998) Macromolecules 31:1335–1340
220. Wheat RW (1995) Rheological explanations for syndiotactic polypropylene behaviors. In: Proceedings of the polymers, laminations & coatings conference, TAPPI, Atlanta, pp 407–410
221. Eckstein C, Friedrich A, Lobrecht R, Spitz R, Muelhaup R (1997) Acta Polym 48:41–46
222. Thomann R, Kressler RJ, Setz S, Wang C, MueIhaupt R (1996) Polymer 37(13):2627–2634
223. Thomann R, Kressler RJ, Rudolf B, Muelhaupt R (1996) Polymer 37(13):2635–2640
224. Maier RD, Thomann R, Kressler RJ, Muelhaupt R, Rudolf B (1977) J Polym Sci B Polym Phys 35(7):1135–1144
225. Schardl JM, Sun L, Baumgartner AS, Boyle K (2004) Patent US 2004/0,034,167 A1, Fina Technology Inc